Doctoral Dissertation

Active Power Line Conditioner Topologies and Control Strategies in Electrified Railways and Three-Phase Four-Wire Distribution Feeders

（電気鉄道および三相 4 線式配電用アクティブパワーラインコンディショナトポロジーとその制御法）

March, 2015

TINT SOE WIN

Yamaguchi University

Graduate School of Science and Engineering

Contents

List of Tables

List of Figures

Acknowledgments

First and foremost, I would like to express my deep-felt gratitude to my adviser, Prof. TANAKA Toshihiko of the Department of Electrical and Electronics Engineering at Yamaguchi University, for his acceptance in Power Electronic Laboratory as an international student, his advice, encouragement, enduring patience and constant support. He was never ceasing in his belief in me, although I was unfamiliar with power electronic technology in early time. He always provides excellent ideas, clear explanations, the best approach method to complete research work. This dissertation would not have been possible unless Prof. TANAKA Toshihiko's guidelines. Thank you very much for your precious time, Prof. TANAKA Toshihiko.

I would like to thank Professors on the reviewing committee, Prof. TANAKA Toshihiko, Prof. OGAWARA Kakuji, Prof. HANO Mitsuo, Prof. KUBO Hiroshi, Prof. YAMADA Hiroaki and Prof. Seong Ryong Lee for their valuable comments and encouragement.

I am greatly indebted to Prof. HIRAKI Eiji at the Okayama University, whose encourage me to make the first presentation in the international conference. He taught me not only research areas but also initiative, attitude, and others. He took me deep understanding in my research with his experience. Thank you very much Prof. HIRAKI Eiji, for your valuable comments and suggestions. I would like to thank Professor OKAMOTO Masayuki at the Ube National College of Technology for guiding my research and helping me to develop my background knowledge. I also would like to thank Prof. YAMADA Hiroaki for your kind support in my doctoral assessment preparation.

I would like to special thank to Professor Seong Ryong Lee at the Kunsan National University of Korea for his help in research theme selection, valuable comments and suggestions.

I am grateful to Yusuke Baba and Hidenori Tanaka, who help me in experimental setup and operation of experimental system. Without their help, I would not have been able to finish my experiment in due time. I also wish to thank the other members of Power Electronic Laboratory and I will never forget their support, cooperation and friendship. They made me enjoyable daily life during my stay in Japan.

Additionally, I am very grateful to my parents and my wife for their love and constant under-

standing, encouragement in pursuing this work. They has been my inspiration and motivation for study in Japan and to improve my knowledge and move my career forward.

Finally, I would like to thank Ministry of Education, Culture, Sports, Science and Technology, Japan for the financial support and Ministry of Electric Power, Myanmar for arrangement of my study in Japan.

Chapter 1

Introduction

1.1 Backgrounds

Electric power conditioning have attracted the electrical and electronics engineers because electric power quality direct impacts on efficiency, security and reliability of the power grid and the end user loads. In 2008, Leonardo power quality initiative team conducted a European power quality survey and reported that poor power quality costs European business more then €150 billion a year [1]. This surveys carried out in 8 European countries and it have been reported in the following categories:

- Voltage dips and swells
- Harmonics
- Unbalance, flicker, earthing and EMC problems
- Short interruptions
- Long interruptions
- Surges and transients

This report suggested that power quality improvement in all areas of power generation, transmission and distribution plays an important role for economic operation of power systems and greenhouse gas reduction. Therefore several engineering organizations provide the standards, recommended practices, guidelines and requirements for the power quality improvement issue. Some standards and recommended practices listed below are provided from the Institute of Electrical and Electronic Engineers (IEEE) and International Electrotechnical Commission (IEC) in the areas of power quality:

IEEE 519 Recommended practices and requirements for harmonic control in electrical power systems

IEEE 1159 Recommended practices for monitoring electric power quality

IEEE 141 Recommended practices for electric power distribution for industrial plants

IEEE 241 Recommended practices for electric power systems in commercial buildings

IEC/TR3 61000-2-1 Electromagnetic compatibility - Environments

IEC/TR3 61000-3-6 Electromagnetic compatibility - Limits

EN 50160 Voltage characteristics of electricity supplied by public distribution systems

IEC 61624 Industrial a.c networks affected by harmonics - Application of filters and shunt capacitors

These standards and recommended practices show that both the power utility company and the end users are responsible for the power quality improvement issue for the economic operation of power systems. The utility have to maintain the acceptable margin of voltage, frequency as well as less harmonic supply voltage in the distribution areas. The end users shall ensure that their connection to the distribution systems does not result in limitation level of distortion and fluctuation of supply voltage. However, the heavy nonlinear loads such as large variable frequency drives (VFD), arc furnaces and commercial electrical appliances such as computers, monitors causes harmonic, voltage fluctuation and other power quality problems. Therefore, the power improving devices are used in transmission and distribution areas to meet the recommended practice and limitations.

1.2 Aim of this Research

1.2.1 Single-phase Active Power Line Conditioner for Electrified Railways

The power for ac electrified railways is supplied from the three-phase power grid. The electric locomotive uses single-phase power and requires two single-phase for up and down going locomotives. Therefore, most of the traction substation use the Scott transformer to convert three-phase

system to two single-phase systems as well as to step down appropriate voltage rating. The primary side of the Scott transformer, which is three-phase systems, can get balanced load condition if and only if the two single-phase loads on the secondary-side are balanced. The voltage unbalance ratio at the three-phase grid is limited within 3% in Japan to prevent adverse effects on other consumer loads [2]. Therefore, the load conditions of two single-phase side should be maintained balanced condition. However, different operating plans of the up and down going locomotives cause the unbalanced load conditions on the two single-phase systems. Moreover, the electric locomotives are equipped with the diode or thyristor rectifiers for motor drive. These result in highly distorted load currents in the secondary side of the Scott transformer. These distorted load currents can exceed the acceptable total harmonic distortion (THD) value 5% [3]. Therefore, power conditioning system is necessary for traction substation to balance load condition as well as to reduce the harmonic distortion.

To solve the above power quality problems, Railway Technical Research Institute (RTRI) group has originally proposed a single-phase feeding power conditioner for Shinkansen [4]. The single-phase feeding power conditioner is constructed with parallel connected two single-phase full-bridge inverters with a common DC capacitor. Then, each full-bridge inverter is connected to each single-phase of the secondary side of the Scott transformer. These two single-phase inverters exchange the active power through a common DC capacitor for the secondary side of Scott transformer. The control algorithm was designed to get unity power of source side currents under balanced load condition. Thus balanced active source current are obtained on the two single-phase system of the Scott transformer compensating reactive and negative-sequence currents.

Prof. Zhuo Sun *et al.* has proposed a novel single-phase Active Power Quality Compensator (APQC) topology for the electrified railways [5]. Three-leg inverter with a common DC capacitor is used for the APQC. The proposed three-leg topology based APQC is simple and its compensation characteristic is the same as in [4]. The APQC is operated as a three-phase inverter, and therefore, the Scott connected matching transformer is used to interface the two single-phase electrified railways system. This Scott connected matching transformer can causes design complexity and higher cost as compare to ordinary two single-phase matching transformers. Therefore three-leg topology based APQC with ordinary matching transformer is required

for the practical application.

Our research group have also proposed three-leg inverter based APQC with ordinary two single-phase matching transformers in the electrified railways [6]. The proposed APQC can compensate harmonics, reactive and unbalanced active currents of the loads. In our method, the the three-leg inverter based APQC is operated as two full-bridge inverters. Therefore, the third-leg is used as a common leg for the first- and second-leg of the APQC. As a consequence of using common leg, the third-leg current rating needs $\sqrt{2}$ times as compared to those of other two legs. Therefore, reduction of the third-leg current rating is strongly required for practical applications in the three-leg inverter based APQC.

The aim of this research for single-phase active power line conditioner is to propose a new single-phase active power quality compensator (APQC) topology and control strategy in electrified railways to overcome the drawbacks of the previously proposed APQC systems. The new proposed APQC uses half-bridge inverter topology. The two half-bridge inverters, which use two legs power devices, of APQC compensate harmonics, reactive and unbalanced active currents of the loads. The third-leg power devices is also used in the proposed topology to perform DC voltage balancer of two half-bridge inverters with small output current. The circuit topology of the half-bridge inverter based APQC is discussed in the dissertation. Two different control strategies for the new half-bridge inverter based APQC are also discussed. First, the basic principle of half-bridge inverter based APQC control strategy with DC voltage balancer control is discussed in details and then verify by simulation and experiment. Simulation and experimental results confirm that the proposed half-bridge inverter based APQC can reduce third-leg current rating without changing APQC's performance as previously proposed method in [6]. Then the better control algorithm with a constant DC capacitor control for a half-bridge inverter based APQC is described. The main feature of this control strategy is that it does not need active/reactive calculation blocks of load currents for the APQC operation. A half-bridge inverter based APQC using a constant DC capacitor voltage control strategy is also confirmed by both simulation and experimental verifications. Simulation and experimental results demonstrate that the proposed APQC using constant DC capacitor voltage control can achieve balanced and sinusoidal source currents on the secondary side of Scott transformer in electrified railways.

1.2.2 Three-phase Active Power Line Conditioner in Three-Phase Four-Wire Distribution Systems

A wide variety of distribution systems are used worldwide for residential and commercial power supply. Among them, three-phase four-wire power distribution system can supply both single-phase power and three-phase power simultaneously. However, unbalanced load condition frequently occurs in this distribution systems. This unbalanced load condition causes unbalanced voltage, excessive neutral current and higher loss in the distribution transformer. To solve these power quality problem, three-phase active power line conditioner are proposed in the distribution areas. The active power line conditioner in three-phase four-wire distribution systems are generally constructed with four legs power devices with a common DC capacitor. For the control strategy, different three-phase power theories are used to calculate the effective load condition. Most of the three-phase theories in the control strategies of active power line conditioner are instantaneous reactive power theory, direct-quadrature-zero (dq0) transformation, the instantaneous symmetrical component theory and the sample and hold circuit method [7–12]. These theories based control strategies require a significant number of calculation steps because these methods are based on the three-phase power in $\alpha\beta$ and dq0 coordinates. Therefore, simple control strategy is required for the active power line conditioner in three-phase four-wire distribution systems to reduce size, cost and weight of the systems.

The aim of this research on three-phase active power line conditioner is to propose simple control strategy for the active load balancer (ALB), which is used for power conditioning in three-phase four-wire distribution feeders. A simple constant DC capacitor voltage control based control strategy is proposed in our method. Basic principle of a simple constant DC capacitor voltage control based strategy for the active load balancer (ALB) is discussed in three-phase four-wire distribution systems. The simulation and experimental results demonstrate that the proposed simple constant DC capacitor voltage control based strategy can reduce active/reactive calculation blocks of the load currents. The relative required power rating of the ALB with the distribution system is an important factor for the practical point of view. Therefore, the research's aim is also to reduce the required power rating of the ALB. A simple, efficient reactive power control strategy with DC capacitor voltage control for the ALB is also proposed to reduce the required

power rating of the ALB. The calculated values, simulation and experimental results show that the proposed reactive power control strategy based on DC capacitor voltage control can reduce the power rating of the ALB.

In general, the three-phase active power line conditioner are constructed using three legs inverter for the three-phase three-wire distribution systems. But, in three-phase four-wire distribution systems, the three-leg and four-leg inverters are possible for the construction of the ALB. In this dissertation, the comparison of three legs inverter and four legs inverter based ALB will also be discussed for the three-phase four-wire distribution systems. The simulation results demonstrate that the four-leg inverter based ALB is suitable for the three-phase four-wire distribution systems.

Chapter 2

Power Quality Problems, Their Adverse Effects and Solutions

2.1 Power quality problems

The subject of power quality is very broad and it covers all aspects of generation, transmission, distribution areas as well as the end users loads. Any deviations of voltage, current, frequency and temperature of particular supply systems and their components are regarded as the power quality problems and it affects all connected electrical equipments. The IEC TC77/WG9 task is trying to define measurement parameters of power quality and provide standard measurement methods for characterizing these parameters. The following phenomena play an important roles in power quality problems and power quality controls:

- Voltage dips and swells
- Harmonics
- Unbalance, flicker, earthing and EMC problems
- Short interruptions
- Long interruptions
- Surges and transients

The power quality improving devices also focus on these categories because these phenomena are greatly effects on all electrical generation, transmission, distribution devices and the end users loads. Among these power quality problems, the harmonic and unbalanced phenomena are discussed in this dissertation with the analysis methods and their adverse effects.

2.2 Harmonics

2.2.1 Total Harmonic Distortion

The Fourier series state that, in general, a non sinusoidal waveform $f(t)$ repeating with an angular frequency ω can be expressed as

$$\begin{aligned} f(t) &= F_0 + \sum_{n=1}^{\infty} f_n(t) \\ &= \frac{1}{2}a_0 + \sum_{n=1}^{\infty} \left\{ a_n \cos(n\omega t) + b_n \sin(n\omega t) \right\} \\ &= \frac{1}{2}a_0 + a_1 \cos\omega t + a_2 \cos(2\omega t) + a_3 \cos(3\omega t) + ... \\ &\quad + b_1 \sin\omega t + b_2 \sin(2\omega t) + b_3 \sin(3\omega t) + ... , \end{aligned} \tag{2.1}$$

where,

$$\begin{aligned} a_0 &= \frac{1}{\pi} \int_{-\pi}^{\pi} f(t)\ d(\omega t), \\ a_n &= \frac{1}{\pi} \int_{-\pi}^{\pi} f(t)\ \cos(n\omega t)\ d(\omega t) \quad n = 1, 2, 3, ... , \\ b_n &= \frac{1}{\pi} \int_{-\pi}^{\pi} f(t)\ \sin(n\omega t)\ d(\omega t) \quad n = 1, 2, 3, ... \end{aligned}$$

In this Fourier series, $F_0 = \frac{1}{2}a_0$ is the average value of the function, the component with the frequency corresponding to the original function, $a_1 \cos\omega t$ and $b_1 \sin\omega t$, are called fundamental components and others are called harmonic components. Therefore, the periodic distorted waveform can be decomposed into the combination of the average value, sinusoidal waveform with fundamental frequency and sinusoidal waveforms with harmonic frequencies.

Electrical engineers use the Fourier series to find the harmonic distortion of voltage or current waveforms. Figure 2.1 shows the decomposition of a nonlinear load current i_S into the fundamental current component i_{S1}, and the all harmonic components i_h. Harmonic analysis of nonlinear load current is discussed. Let the utility input voltage v_S be

$$v_S = \sqrt{2} V_S \sin\omega t . \tag{2.2}$$

By using Fourier analysis, nonlinear load current can be expressed as

$$\begin{aligned} i_{\mathrm{S}} &= \sqrt{2}I_{\mathrm{S1}}\sin(\omega t-\phi_1)+\sqrt{2}I_{\mathrm{S2}}\sin(2\omega t-\phi_2)+\sqrt{2}I_{\mathrm{S3}}\sin(3\omega t-\phi_3)+\ldots \\ &= \sqrt{2}I_{\mathrm{S1}}\sin(\omega t-\phi_1)+\sum_{h\neq 1}^{\infty}\sqrt{2}I_h\sin(h\omega t+\phi_h), \end{aligned} \tag{2.3}$$

where ϕ_1 is the phase angle between the sinusoidal input voltage v_{S} and the fundamental load currents i_{S1}.

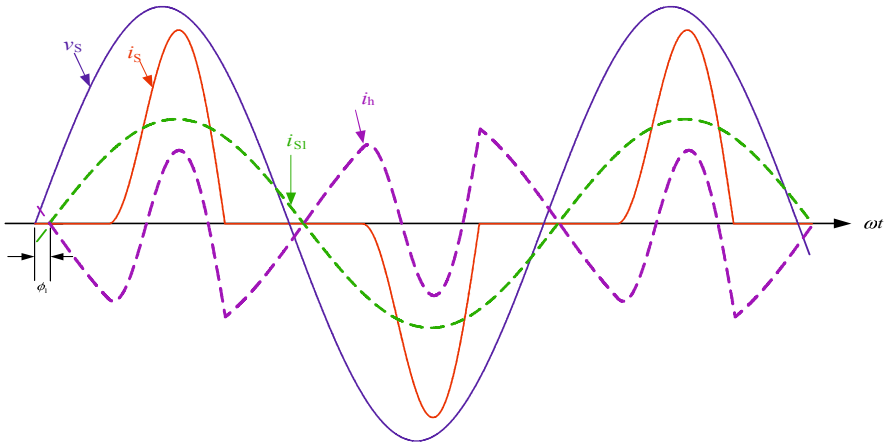

Figure 2.1: Current distortion waveforms.

The root mean square (rms) value of Equation 2.3 can be expressed as

$$\begin{aligned} I_{\mathrm{S}} &= \left\{\frac{1}{T_1}\int_0^{T_1}\left[\sqrt{2}I_{\mathrm{S1}}\sin(\omega t-\phi_1)+\sum_{h\neq 1}^{\infty}\sqrt{2}I_{\mathrm{h}}\sin(h\omega t+\phi_h)\right]^2 dt\right\}^{1/2} \\ &= \sqrt{I_{\mathrm{S1}}^2+\sum I_{\mathrm{h}}^2}\ . \end{aligned} \tag{2.4}$$

where I_{S} is rms value of load currents, I_{S1} is the rms value of the fundamental component and I_{h} is rms value of all harmonic components.

Total harmonic distortion is the contribution of all the harmonic frequency currents to the fundamental. The Total Harmonic Distortion (THD) of the any particular function is defined as the ratio of the amount of all harmonic components to the fundamental component in rms values.

For the current distorted waveform, in example, is expressed as

$$\begin{aligned} \%\text{THD} &= 100 \times \frac{\text{all harmonic components in rms value}}{\text{fundamental component in rms value}} \\ &= 100 \times \sqrt{\frac{\sum_{h\neq 1} I_h^2}{I_{S1}^2}} \\ &= 100 \times \frac{\sqrt{\sum_{h\neq 1} I_h^2}}{I_{S1}} \end{aligned} \tag{2.5}$$

2.2.2 Harmonic Distortions in Power Systems

Nowadays, manufacturers want faster, more productive, more efficient machinery in industrial applications and consumer appliances. However, these equipment uses semiconductor-based devices, and hence suffers common power disruptions. Therefore, many of the loads in present-day power systems are non-linear type and become harmonic current generators. Combined with the impedance of the electrical system, these loads can also be seen harmonic voltages sources. The non-linear loads may therefore be viewed as both harmonic current generators and harmonic voltage generators. The daily life electrical appliances likes fluorescent lighting, power supply of personal computers and laptops and the mobile phone chargers are small power non-linear loads. Adjustable speed control motor drives, inverter type air-conditioners, arc furnaces, traction devices and others similar devices are heavy power non-linear loads. Table 2.1 categorizes the harmonics sources and type of harmonics in terms of their respective frequencies in power systems.

2.2.3 Effects of Harmonics

This section will describe the harmful effects of harmonic in power systems. Harmonics are so insidious that we can know the harmful effects of it until equipment failure occur in the power systems. How harmonics can interact within a power system and how they can affect power system components is important for preventing failures. Therefore, the effect of harmonics on some common power system devices are described.

Table 2.1: Type and Source of Power System Harmonics.

Source	Frequency	Type
Half-wave rectifiers, nonlinear	$n \times f_1(n = odd)$	Odd Harmonics
loads and devices, geomagnetic	$n \times f_1(n = even)$	Even Harmonics
induced currents(GICs)		
Unbalanced three-phase load,	$3h \times f_1(n = 1, 2, 3, ...)$	Triplen Harmonics
electronic switching devices		
Operation of power system with	$n \times f_1(n = 1, 4, 7, ...)$	Positive-sequence Harmonics
nonlinear loads		
Operation of power system with	$n \times f_1(n = 2, 5, 8, ...)$	Negative-sequence Harmonics
nonlinear loads		
Unbalanced operation of power	$n \times f_1(n = 3, 6, 9, ...)$	Zero-sequence Harmonics
system	(same as triplen)	
Induction machines	$n \times f_1(n = an\ integer)$	Spatial Harmonics
Static frequency converters,	$n \times f_1(n = not\ an\ integer)$	Interharmonics
cycloconverters, induction		
machine, arcing devices		

Effects of Harmonics on Transformers

Harmonics can affect transformers primarily in two ways. Voltage harmonics produce additional losses in the transformer core as the higher frequency harmonic voltages set up hysteresis loops, which superimpose on the fundamental loop. Each loop represents higher magnetization power requirements and higher core losses. A second and a more serious effect of harmonics is due to harmonic frequency currents in the transformer windings. The harmonic currents increase the net rms current flowing in the transformer windings which results in additional I^2R losses. Winding eddy current losses are also increased. Moreover, transformers that are required to supply large nonlinear loads must be derated to protect premature failure and overheating. One method by which transformers may be rated for suitability to handle harmonic loads is by K factor rat-

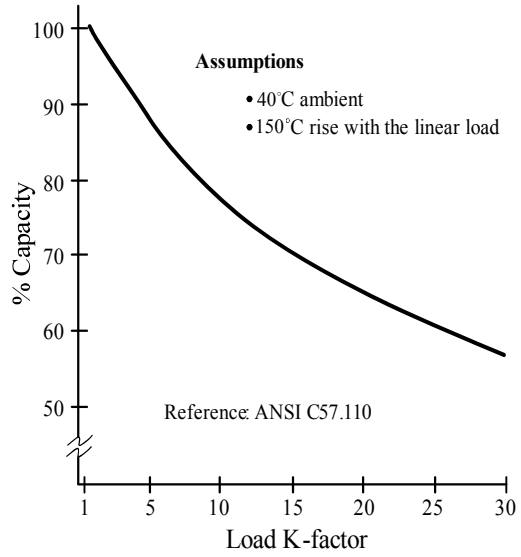

Figure 2.2: Typical transformer derating for non-linear loads.

ings. To calculate the K factor, the distorted current are decomposed into fundamental frequency component and harmonic frequency components. Then, k factor is calculated as follow:

$$\begin{aligned} \mathrm{K} &= \sum I_h^2 \, h^2 \; (h = 1, 2, 3, ..., n) \\ &= I_1^2(1)^2 + I_2^2(2)^2 + I_3^2(3)^2 + ... + I_n^2(n)^2, \end{aligned} \tag{2.6}$$

where,

I_1 is the ratio between the rms value of fundamental current and the total current,

I_2 is the ratio between the rms value of second harmonic current and the total current,

I_3 is the ratio between the rms value of third harmonic current and the total current.

The K factor concept is derived from the ANSI/IEEE C57.110 standard, Recommended Practices for Establishing Transformer Capability When Supplying Non- Sinusoidal Load Currents. From a practical viewpoint, office areas with some non-linear loads and computer rooms normally have observed K-factors of 4 to 9. Fig. 2.2 shows typical transformer derating capacity versus load K-factor graph.

In addition, the three-phase four-wire distribution transformers that supply large harmonic generating loads should have the neutrals over-sized. The triplen harmonic current of the three

phases load is in phase and therefore this triplen current tend to add in the neutral current, which is caused by unbalanced load condition. In theory, the neutral current can be as high as 173% of the phase currents due to triplen harmonic currents.

Effects of Harmonics on Capacitor Banks

Capacitor banks are commonly found in commercial and industrial power systems to improve the low power factor. According to IEC 60831-1 standard, capacitor banks are designed to operate at a maximum of 110% of their rated voltages and at 135% of their rated kVARS. Capacitors are particularly sensitive to harmonic currents since their impedance decreases proportionally to the order of the harmonics present. When large levels of voltage and current harmonics are present, the ratings are quite often exceeded the maximum limits resulting in a capacitor overload, shortening steadily its operating life. A more serious condition for substantial damage occurs due to a phenomenon called harmonic resonance. Resonance conditions are created when the network inductive and capacitive reactances become equal at one of the harmonic frequency. The two types of resonances are series and parallel. In general, series resonance produces voltage amplification and parallel resonance results in current multiplication. In a harmonic-rich environment, both series and parallel resonance may be present. This situation could result in considerable damage to the capacitor bank as well as other power system devices.

Effects of Harmonics on Motors

Supplying the distorted voltage to a motor results in additional losses in the magnetic core of the motor. Hysteresis and eddy current losses in the core increase as higher frequency harmonic voltages are impressed on the motor windings. Hysteresis losses increase with frequency and eddy current losses increase as the square of the frequency. Also, harmonic currents produce additional I^2R losses in the motor windings. Another effect is torsional oscillations due to harmonics in three-phase motor. The fifth and seventh harmonics are more prominent harmonics in a typical power system. The fifth harmonic is a negative sequence harmonic, and the resulting magnetic field revolves in a direction opposite to that of the fundamental field at a speed five times the fundamental. The seventh harmonic is a positive sequence harmonic with a resulting magnetic field revolving in the same direction as the fundamental field at a speed seven times the funda-

mental. The net effect is a magnetic field that revolves at a relative speed of six times the speed of the rotor. This induces currents in the rotor bars at a frequency of six times the fundamental frequency. The resulting interaction between the magnetic fields and the rotor-induced currents produces torsional oscillations of the motor shaft. If the frequency of the oscillation coincides with the natural frequency of the motor rotating bars, damage to the motor can result.

Effects of Harmonics on Cables

Current flowing in a cable produces I^2R losses. When the load current contains harmonic content, additional losses are introduced. The effective resistance of the cable increases with frequency because of the phenomenon known as skin effect. The skin effect causes AC currents to flow only on the outer periphery of the conductor. The higher the frequency of the current, the greater the tendency of the current to crowd at the outer periphery of the conductor and the greater the effective resistance for that frequency. Therefore the harmonic currents result in increasing the resistance of the conductor and causing additional losses.

2.3 Unbalanced Analysis

2.3.1 Concept of Three-phase Systems

Three-phase electric power is a common method of alternating-current electric power generation, transmission, and distribution. It is a type of polyphase system and is the most common method used by electrical grids worldwide to transfer power. A three-phase system is usually more economical than an equivalent single-phase or two-phase system at the same line to ground voltage because it uses less conductor material to transmit electrical power. The three-phase system was invented by Galileo Ferraris, Mikhail Dolivo-Dobrovolsky and Nikola Tesla in the late 1880s.

In a balanced three-phase power system, three conductors each carry an alternating current of the same frequency and voltage amplitude relative to a common reference but with a 120° phase difference to each other. The voltage measured at the terminals of a generator is almost perfectly with equal magnitude and separated by 120°. If the impedances of the various electrical components likes transformers, transmission lines and end user loads are identical for each phase, the

voltage and current would be the balanced conditions. However, many low voltage equipments are single phase and causing unbalanced magnitude and/or phase angle of voltage and current in three-phase powering systems. These unbalanced conditions effect other consumers connected power system devices and end user loads.

2.3.2 Unbalanced Phasor Analysis

Charles LeGeyt Fortescue developed an idea of decomposition of unbalanced three-phase phasors in 1918 to analyze the unbalanced conditions. The unbalanced magnitude and/or phase can be decomposed into balanced three sets of components. Assume that a arbitrary set of three-phase unbalanced currents are I_a, I_b, and I_c. In accordance with Fortescue, these phase currents are resolved into the following three sets of sequence components:

Positive-sequence components, consisting of three phasors with equal magnitudes, 120° phase displacement each other in $I_aI_bI_c$ rotation, as in Figure 2.3(a).

Negative-sequence components, consisting of three phasors with equal magnitudes, 120° phase displacement each other in $I_cI_bI_a$ rotation, as in Figure 2.3(b).

Zero-sequence components, consisting of three phasors with equal magnitudes and with zero phase displacement, as shown in Figure 2.3(c).

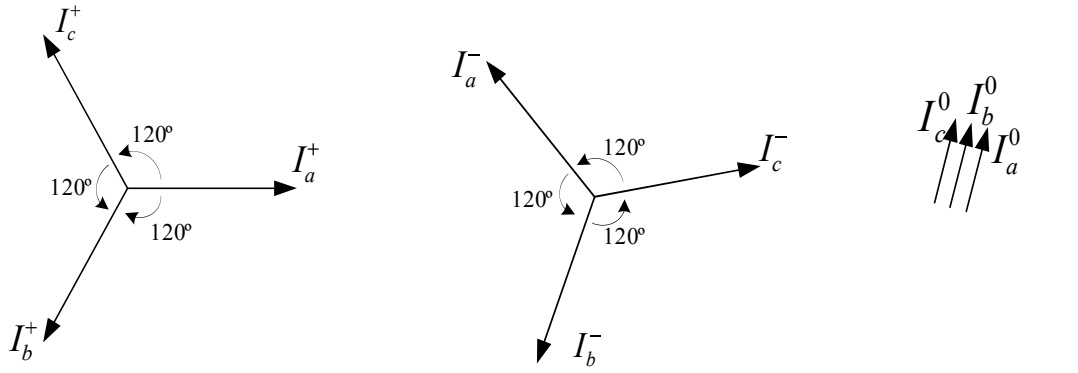

(a) Positive-sequence (b) Negative-sequence (c) Zero-sequence

Figure 2.3: Positive-sequence, Negative-sequence and Zero-sequence components.

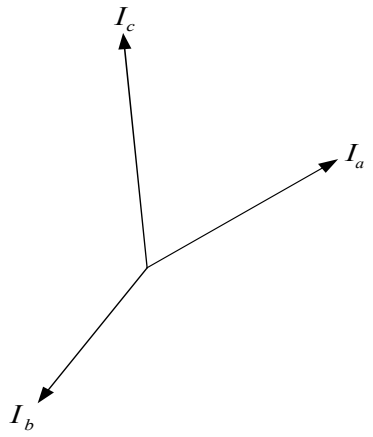

Figure 2.4: Imbalance three-phase system.

Three vectors with a unit magnitude and three different angles of $a = 1\angle 120^\circ$, $a^2 = 1\angle 240^\circ$, and $a^3 = 1\angle 0^\circ$ are used to construct these sequence components. Positive-sequence components are expressed as

$$\begin{aligned} I_a^+ &= I_a^+\angle 0^\circ = I^+ , \\ I_b^+ &= I_b^+\angle 240^\circ = a^2 I^+ , \\ I_c^+ &= I_c^+\angle 120^\circ = aI^+ . \end{aligned} \tag{2.7}$$

Negative-sequence components are expressed as

$$\begin{aligned} I_a^- &= I_a^-\angle 0^\circ = I^- , \\ I_b^- &= I_b^-\angle 120^\circ = aI^- , \\ I_c^- &= I_c^-\angle 240^\circ = a^2 I^- . \end{aligned} \tag{2.8}$$

and zero-sequence components are expressed

$$I_a^0 = I_b^0 = I_c^0 . \tag{2.9}$$

Now, we will decompose three-phase unbalanced currents into positive-sequence, negative-sequence and zero-sequence components. Figure 2.4 shows three-phase unbalanced currents and can be decomposed as:

$$
\begin{aligned}
I_a &= I_a^0 + I_a^+ + I_a^- , \\
I_b &= I_b^0 + I_b^+ + I_b^- , \\
I_c &= I_c^0 + I_c^+ + I_c^- .
\end{aligned} \tag{2.10}
$$

Then these current phasors are rearranged into sequence components as

$$
\begin{aligned}
I_a &= I^0 + I^+ + I^- , \\
I_b &= I^0 + a^2 I^+ + a I^- , \\
I_c &= I^0 + a I^+ + a^2 I^- .
\end{aligned} \tag{2.11}
$$

Using the matrix form, we obtain

$$
\begin{pmatrix} I_a \\ I_b \\ I_c \end{pmatrix} = \begin{pmatrix} 1 & 1 & 1 \\ 1 & a^2 & a \\ 1 & a & a^2 \end{pmatrix} \begin{pmatrix} I^0 \\ I^+ \\ I^- \end{pmatrix} , \tag{2.12}
$$

and simply, we express $I_{abc} = AI^{0+-}$. Matrix A is known as the symmetrical components transformation matrix. Using inverse matrix A, we can also get $I^{0+-} = A^{-1} I_{abc}$. Therefore all sets of sequence components can be obtained by the following matrix.

$$
\begin{pmatrix} I^0 \\ I^+ \\ I^- \end{pmatrix} = \frac{1}{3} \begin{pmatrix} 1 & 1 & 1 \\ 1 & a & a^2 \\ 1 & a^2 & a \end{pmatrix} \begin{pmatrix} I_a \\ I_b \\ I_c \end{pmatrix} \tag{2.13}
$$

Thus, the unbalanced three-phase can be decomposed as a combination of balanced positive-sequence components, negative-sequence components and zero-sequence components. Figure 2.5(a) shows the unbalance three-phase currents and their positive-sequence, negative-sequence and zero-sequence components in phasor diagram. Figure 2.5(b) illustrates the phasor diagram of Figure 2.5(a) into the waveforms diagram.

2.3.3 Effects of Unbalanced Voltages

Unbalanced of voltage or current are regarded as a power quality problem of significant concern at the distribution level. The primary reason of unbalanced voltage is the unbalanced three phases

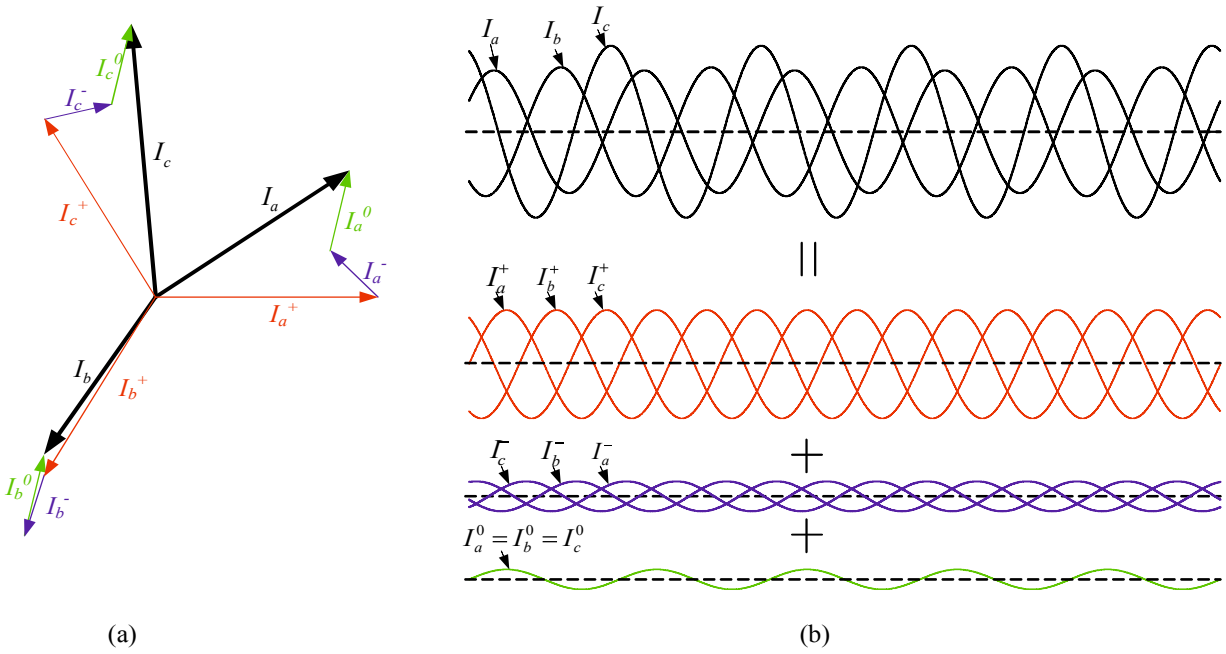

Figure 2.5: Decomposition of unbalanced three-phase currents (not in scale).

current due to unbalanced three-phase load or unbalanced single-phase loads. In addition, the impedance of some system components is not the same in each of the three phases, particularly overhead lines. Hence the current taken by the balanced three-phase load will also produce unbalance which will form part of the background voltage imbalanced. In accordance with the Energy Network Association, the estimation of unbalanced percentage may be evaluated by the following expression [13]

$$\text{Voltage unbalanced (\%)} = \frac{\sqrt{3}\ \text{x}\ \text{negative phase sequence component of the loads (A)}\ \text{x}\ \text{Line voltage}}{\text{three} - \text{phase short circuit level (MVA) at PCC}}\ \text{x}\ 100. \quad (2.14)$$

This estimation is based on negative phase sequence component current. Therefore, the unbalanced voltage condition takes into account the phase angle as well as the magnitude of the each phase current. Another index used in European standards to indicate the degree of unbalance is the voltage unbalance factor (VUF) which is the ratio of the negative sequence voltage to the positive sequence voltage represented as:

$$\text{Voltage unbalanced factor\%} = \frac{\text{negative sequence voltage}}{\text{positive sequence voltage}}\ \text{x}\ 100. \quad (2.15)$$

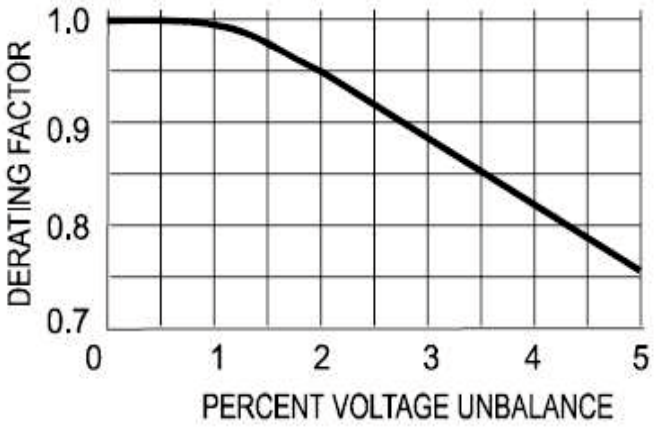

Figure 2.6: Polyphase induction motors derating factor due to unbalanced voltage.

The voltage unbalance in percent is defined by the National Electrical Manufacturers Association (NEMA) is as follow [14]

$$\text{Unbalanced\%} = \frac{\text{Maximum deviation from average}}{\text{Average of three phase} - \text{to} - \text{phase}} \text{ x } 100. \tag{2.16}$$

An excessive level of voltage unbalance can have serious impacts on mains connected induction motors. Although induction motors are designed to tolerate a small level of unbalance they have to be derated if the unbalance is excessive. The unbalanced motor voltage contains positive and negative sequence components which have opposing phase sequences, i.e., ”abc” and ”acb”, respectively. The positive sequence voltage produces the desired positive torque, whereas the negative sequence voltage produces an air gap flux rotating against the rotation of the rotor, thus generating an unwanted negative (reversing) torque. The result is a reduction in the net torque and speed, and the possibility of speed and torque pulsations and increased motor noise. If the motor is operated at the nameplate rated capacity without derating under unbalanced voltage condition, such induction motors can become quite short. Even an induction motor is over-sized to a given application with some level of protection, the motor does not operate at the best efficiency and power factor. Figure 2.6 is the derating graph as in NEMA Standards Publication MG 1-1998 [14]. In general, 2% unbalanced voltage will require 5% lager motor size and 3% unbalanced voltage will require 12% lager motor size. Voltage unbalance also has an impact on ac variable speed drive systems where the front end consist of three-phase rectifier systems.

As mention above, the unbalanced load condition is an primary reason of unbalanced voltage. Another direct impact of the unbalanced load condition is excessive neutral current of distribution transformer in three-phase four-wire system. This excessive neutral current results in transformer overheating, higher transformer losses and lower distribution system efficiency. Therefore, load balancing is one of important issue in the power quality improvement.

2.4 Solutions for Power Quality Problems

The passive power filters, which are constructed with capacitors, inductors and/or resistors, have been broadly used for harmonic compensation and power factor correction in the transmission and distribution areas. These passive power filters principle are based on impedance characteristics of capacitors, inductors and/or resistors on the frequency variation. Thus, they are simple and not expensive. The passive power filters, however, cannot modify their compensation characteristics under dynamic change of loads and they generate series resonances in the system reducing the power system stability. The design of the passive power filters can accept small tolerances in the value of inductors and capacitors [15]. Therefore new power conditioning devices are proposed in the power systems. Active power line conditioner intended for power quality improvement devices are also referred to as active power filter (APF), active power quality compensator (APQC), active load balancer (ALB), static compensator (STATCOM),static var compensator (SVC), etc.

Unlike the traditional passive power filters, modern active power line conditioners (APCs) have the following multiple characteristics; harmonic filtering, reactive power control and voltage regulation, load balancing, voltage flicker reduction, and/or their combinations under different load conditions [16]. The operating principles of APC were firmly established since 1970s [17–19]. Figure 2.7 shows the basic principle of active power line conditioner (APC) application for per phase system. The load drawn the distorted current i_{La} from the source side. But the source side current i_{Sa} is sinusoidal because the APC injects or absorbs the necessary current i_{Ca} so that the desired (standard waveform) current is obtained in the source side. In other words, the APC generate the necessary active, reactive and harmonic currents for the load. Using the various circuit topologies and control strategies, the APC can solve the power quality problems.

The active power line conditioner were less interest in 30 year ago due to their power rating

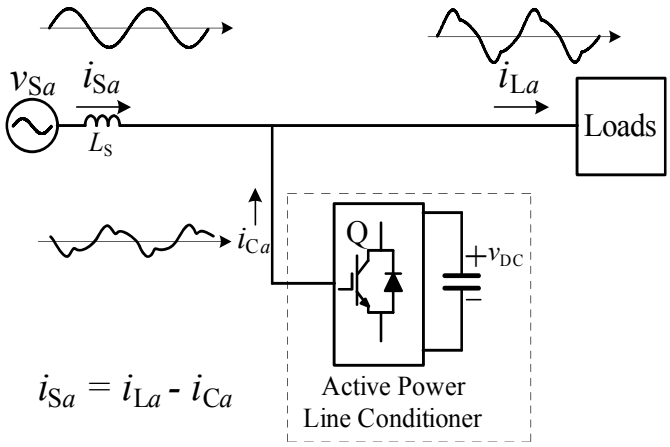

Figure 2.7: Basic principles of active power line conditioner.

limitation and higher cost at that times. Nowadays, semiconductor devices such as insulated-gate bipolar transistors (IGBTs), metal-oxide-semiconductor field-effect transistors (MOS-FET) are characterized by fast switching capability and higher insulated gate structure. Moreover, digital signal processor (DSP), field-programmable gate arrays (FPGA), analog-to-digital converters (A/D), sensors are available at reasonable cost. Therefore, the APC becomes key components in the power transmission and distribution areas. STATic COMpensator (STATCOM), which exchanges reactive power with the host AC system enhancing voltage/angle stability and increases power transmission capacity, are use in transmission system. Thyristor Controlled Rectifier (TCR), active power line filters (APF) are also use in distribution areas.

Active power line conditioner can be divided into series and shunt types based on how to connect the devices with the power systems. The main purpose of the series APC is harmonic isolation between a sub-transmission system and a distribution system. It can also use for voltage flicker compensation and voltage regulation. On the other hand, the shunt APC has the capability of harmonic compensation, load balancing, reactive power and negative-sequence compensation at the utility consumer point of common coupling (PCC) [20]. This dissertation will discuss new topologies and control strategies of shunt APC for both single-phase and three-phase power systems. The single-phase active power quality compensator (APQC) in electrified railways is discussed in the chapters 3 and 4 of the dissertation, and three-phase active load balancer (ALB) in three-phase four-wire distribution systems is discussed in the chapters 5 and 6 of the dissertation.

2.4.1 Half-bridge and Full-bridge Inverters

The purpose of the active power line conditioner (APC) is to inject and absorb the necessary current to/from the power feeders so that the distribution feeders (or transformer) can achieve desired current and/or voltage waveforms. The APC are constructed with the various types of bidirectional inverter. A bidirectional inverter is an electronic device that changes direct current (DC) to alternating current (ac) and vice versa. The output voltage, current, frequency and rated power of the inverter is depend on the design of the specific device. The the basic circuit topology of the inverter is half-bridge type and it serves as a basic building block for the full-bridge and the three-phase inverter.

The half-bridge inverter is composed of two DC sources and two power switching devices Q_1, Q_2 as shown in Fig. 2.8(a). Feedback (freewheeling) diodes D_1, D_2 are required to provide continuity of current for inductive loads. The two switches are turned on and off complementary to each other to generate alternating current on the load. Fig. 2.8(b) shows the simple gate signals generation method for the reference signal v_{ref} using pulse width modulation (PWM) with triangular waveform intercept technique.

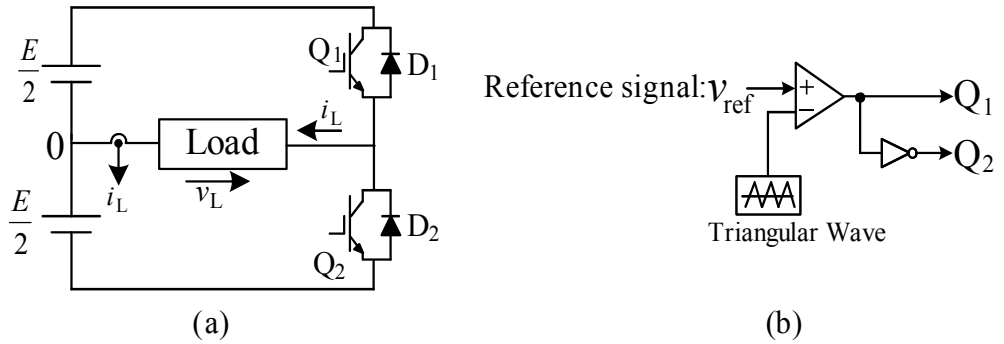

Figure 2.8: Basic half-bridge inverter topology.

Fig. 2.9 shows the reference signal, triangular waveform, and output voltage of the inverter. When the reference signal v_{ref} is greater than or equal to triangular waveform, the switch Q_1 turns on and Q_2 turns off. In this duration, the output voltage v_L is $+\frac{E}{2}$. When the reference signal v_{ref} is less than triangular waveform, the switch Q_2 turns on and Q_1 turns off. In this duration, the output voltage is $-\frac{E}{2}$.

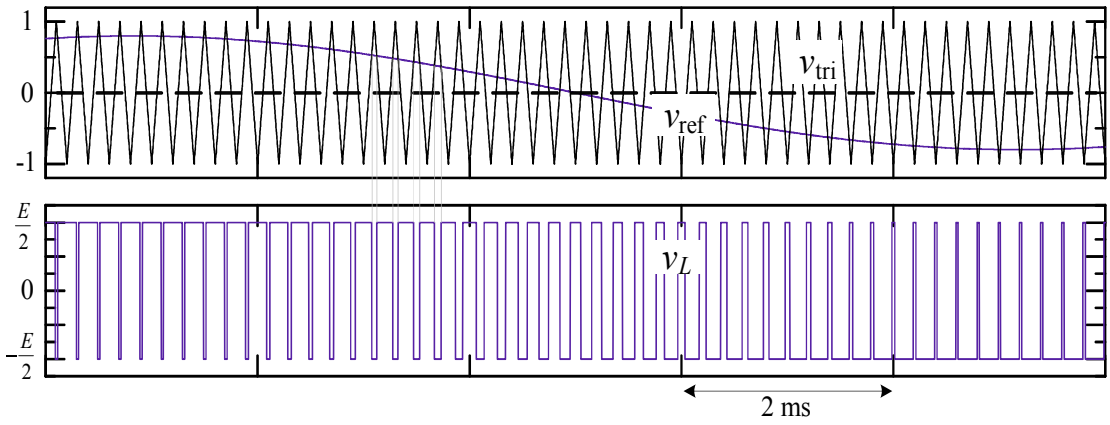

Figure 2.9: Output voltage waveform of half-bridge inverter.

Fig. 2.10(a) shows the basic full-bridge inverter, which includes four power switching devices and four freewheeling diodes with a DC source. Full-bridge inverter is composed of two half-bridge inverters with a common DC source. Therefore, full-bridge inverter needs two reference signals v_{ref1} v_{ref2} as shown in Fig. 2.10(b). The pair switches Q_1 and Q_2, Q_3 and Q_4 are complementary to each other and generate output voltages.

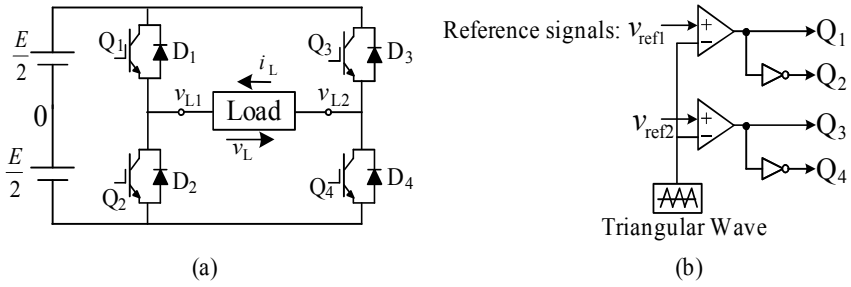

Figure 2.10: Basic full-bridge inverter topology.

Fig. 2.11 shows the voltage output waveforms of the full bridge inverter. v_{ref1} and v_{ref2} are reference signals, v_{L1} is the output waveform for the first half-bridge inverter, v_{L2} is the output waveform for the second half-bridge inverter and v_L is the output waveform of the full-bridge inverter for the load.

Feedback controller, for example a PI controller, is always used in the inverter so that the inverter output follows the reference signal. Figure 2.12 shows the general configuration of the

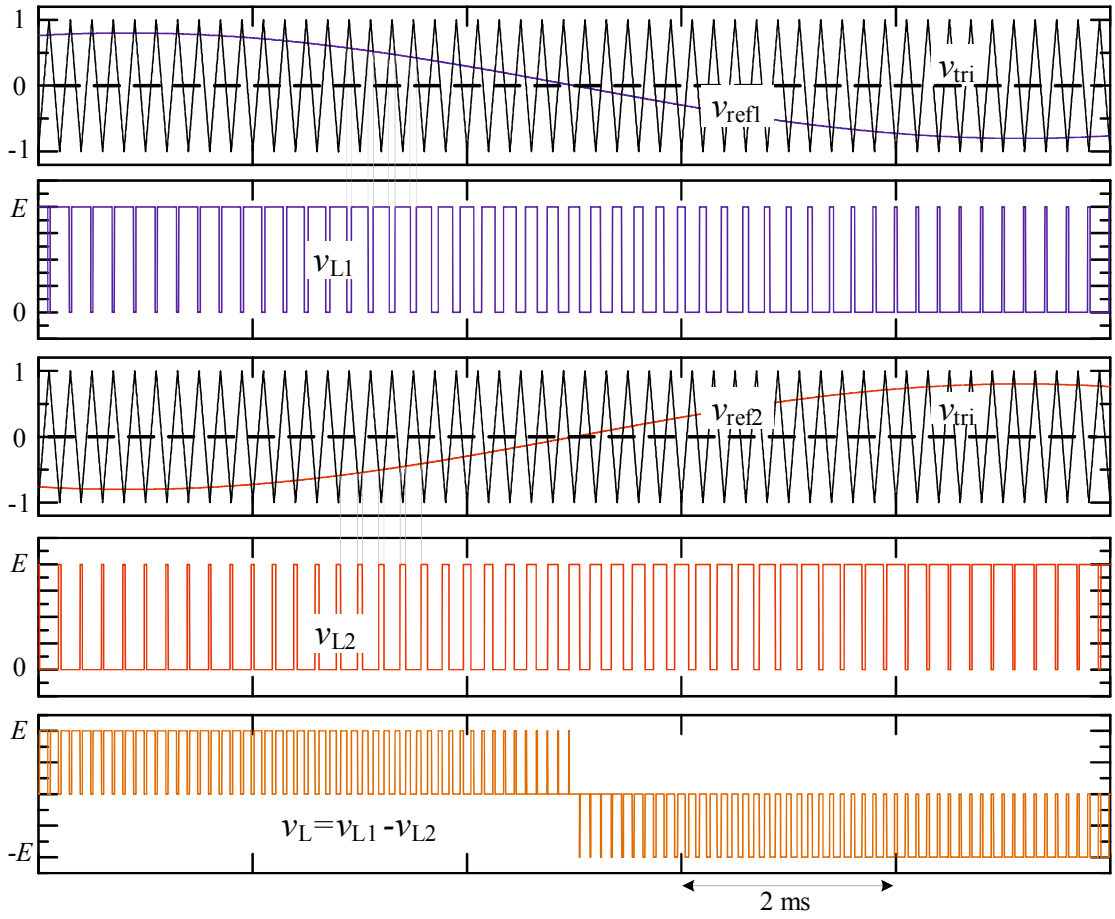

Figure 2.11: Output voltage waveforms of full-bridge inverter.

feedback control system. In the feedback control system, a controller monitors the output of the system and compares it with the reference. The difference between actual output and the reference signal is called the error signal. The controller uses the error signal and generates control signal to the system to bring the actual output closer to the reference.

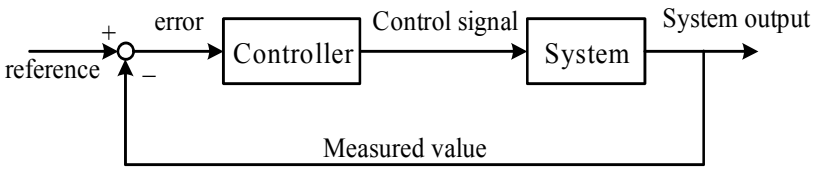

Figure 2.12: General configuration of feedback controller.

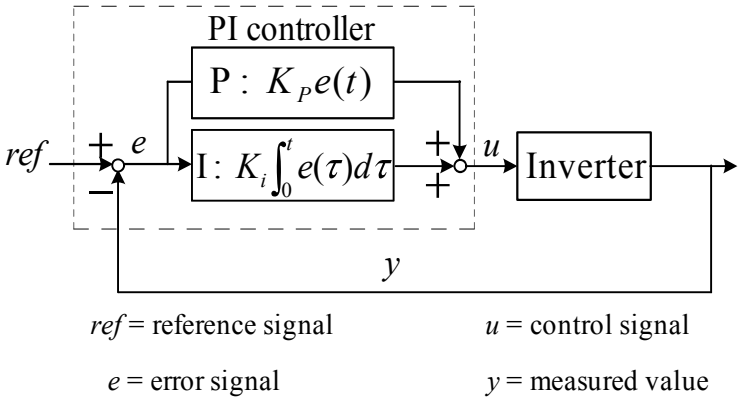

Figure 2.13: PI controller in inverter operation.

Figure 2.13 shows the PI controller in the inverter operation. P is denoted for the proportional control and I is for the integral control. The control output signal of the PI controller is

$$u(t) = K_p e(t) + K_i \int_0^t e(\tau)d\tau. \tag{2.17}$$

where, K_p is the proportional gain, K_i is the integral gain, t is the instantaneous time and τ is the integration variable taken from 0 to the present t. The transfer function of the PI controller is given as

$$G(s) = \frac{U(s)}{E(s)} = K_p\left[1 + \frac{1}{T_I s}\right], \tag{2.18}$$

where, $K_I = \frac{K_p}{K_i}$.

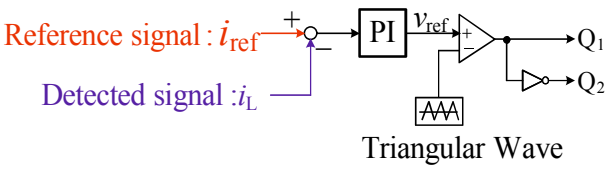

Figure 2.14: Current feedback PI controller in PWM technique.

Figure 2.14 shows the sample PI current feedback controller in the PWM technique. In this control algorithm, the reference current signal i_{ref} is amplified with the PI controller and then the reference voltage signal v_{ref} is compared with the triangular waves.

Figure 2.15 shows the sample inverter output voltage and current using the half-bridge inverter in the Fig. 2.8 (a) and (b) without PI current feedback controller. The upper waveform is the voltage in the load v_L and the lower waveform is the output current of the load i_L. The output load current i_L is depend on the voltage amplitude of the two sources and the load type. Therefore, output current current be controlled to the desired waveform without the current feedback control.

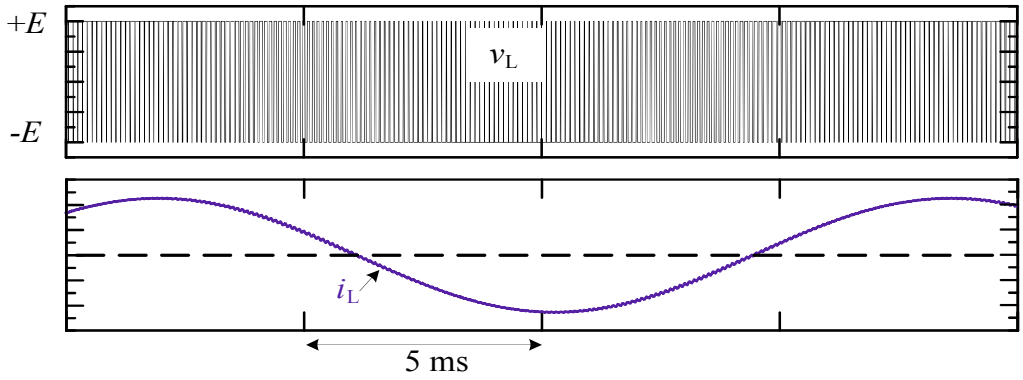

Figure 2.15: Inverter output voltage and current waveforms without PI controller.

Figure 2.16 shows the sample inverter output voltage and current using the half-bridge inverter in the Fig. 2.8 (a) and the PI current feedback controller in Fig. 2.14. The upper waveform is the voltage in the load v_L and the lower waveform is the output current of the load i_L. The output load current i_L is not directly depend on the voltage amplitude of the two sources and the load type but it is controlled by the PI current feedback controller. Therefore, output current closely follows to the reference current i_{ref}.

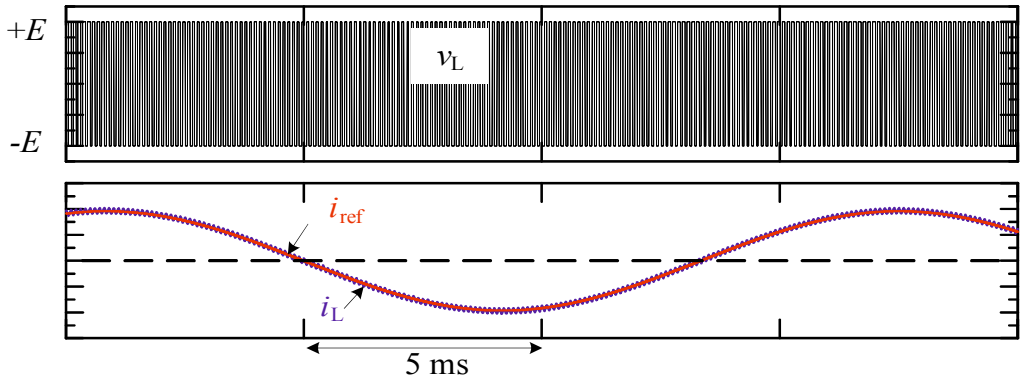

Figure 2.16: Inverter output voltage and current waveforms with PI controller.

Using these half-bridge and full-bridge inverters, the active power line conditioners are constructed to solve the power quality problems.

2.5 Power Quality Problems in Electrified Railways

Electric power of locomotives is supplied from three-phase power grid. In general, the high-speed locomotive are of a large volume and intermittent single-phase loads. They require approximately 2 MVA per train with 10 car at maximum speed of 100 km/h for conventional locomotive and 12 MVA per train for 16 car at maximum speed of 300 km/h for high speed locomotive [21]. To supply required large amount of electric energy, the traction substation use medium voltage level of 25 kV for Shinkansen line and 20 kV for conventional line in Japan. The high voltage systems in Japan are 500 kV, 275 kV and 154 kV. The electric railways company, hence, construct traction substation to step-down the appropriate voltage levels. The electric locomotives use single-phase power and need two power feeders for up and down locomotives. Therefore the main transformer of traction substation must have ability to step-down voltage level as well as to convert three-phase power to two-phase power. Many type of transformers are used in the traction substation such as normal three-phase transformer, single-phase transformer, woodbridge connected transformer. Among many type of transformers, Scott transformer have superior performance for the traction substation providing the above requirements.

2.5.1 Scott Transformer

The Scott transformer is one making the three-phase to two-phase transformation using two transformer windings. The principle of Scott connected transformer is discussed. In Figure 2.17, if A, B and C represent the three terminals of a three-phase system and N represents the neutral point, the primary windings of three single-phase transformers forming a delta-connected three-phase bank may be represented by the lines AB, BC and CA. If it is desired to arrange the primary windings in star, the corresponding lines on the diagram are AN, BN and CN. When AN is continued to the point S, the line AS is perpendicular to the line BC, and it is evident that it would be possible to form a three-phase bank using only two single-phase winding. The first winding is known as the main and the other is known as the teaser, and the ratio of primary turns on teaser

to main transformer can be deduced from an examination of Figure 2.17. ABC is an equilateral triangle for which the ratio of the length of perpendicular AS to side BC is equal to $\frac{\sqrt{3}}{2}$:1.

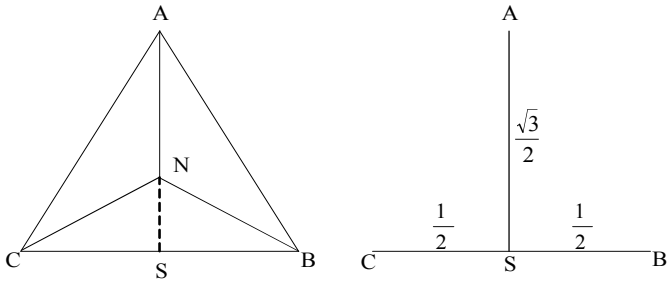

Figure 2.17: Basic principle of the Scott connection.

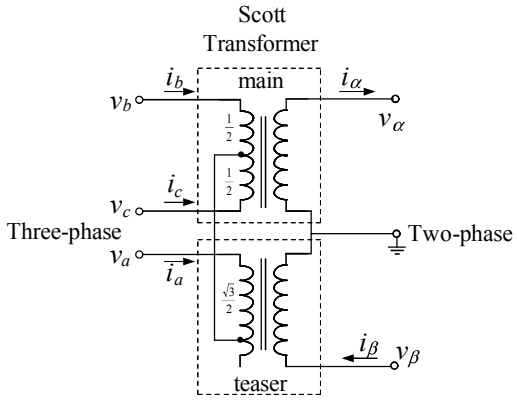

Figure 2.18: Winding diagram of Scott transformer.

Figure 2.18 shows winding diagram of the Scott transformer. The primary-side input is three-phase system (abc) and secondary-side output is two-phase system ($\alpha\beta$) with two windings. Figure 2.19 shows the phasor representation of the Scott transformer

The energy conversion of the Scott transformer between the three-phase side and two-phase side is discussed. Let the three-phase voltages in Figure 2.18 be

$$\begin{aligned} v_a &= \sqrt{2}V\sin\omega t, \\ v_b &= \sqrt{2}V\sin(\omega t - \frac{2}{3}\pi), \\ v_c &= \sqrt{2}V\sin(\omega t + \frac{2}{3}\pi). \end{aligned} \tag{2.19}$$

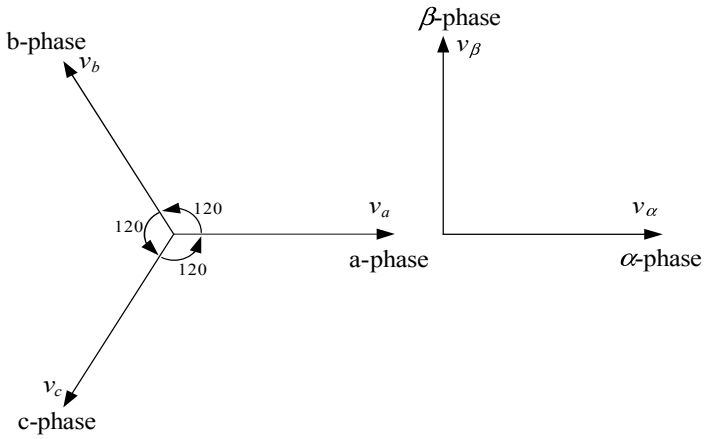

Figure 2.19: Phaser diagram of Scott transformer.

and the currents flowing in each phase are given by

$$\begin{aligned} i_a &= \sqrt{2}I\sin(\omega t - \phi), \\ i_b &= \sqrt{2}I\sin(\omega t - \frac{2}{3}\pi - \phi), \\ i_c &= \sqrt{2}I\sin(\omega t + \frac{2}{3}\pi - \phi). \end{aligned} \tag{2.20}$$

The three-phase to two-phase transformation on $\alpha\beta$ coordinate is given as following matrix

$$\begin{pmatrix} e_\alpha \\ e_\beta \end{pmatrix} = \sqrt{\frac{2}{3}} \begin{pmatrix} 1 & -\frac{1}{2} & -\frac{1}{2} \\ 0 & \frac{\sqrt{3}}{2} & -\frac{\sqrt{3}}{2} \end{pmatrix} \begin{pmatrix} e_a \\ e_b \\ e_c \end{pmatrix}. \tag{2.21}$$

Using above transformation matrix, the two-phase side voltage and current can be obtained.

$$\begin{aligned} v_\alpha &= \sqrt{\frac{2}{3}} \left(v_a - \frac{1}{2}v_b - \frac{1}{2}v_c \right), \\ v_\beta &= \sqrt{\frac{2}{3}} \left(\frac{\sqrt{2}}{3}v_b - \frac{\sqrt{2}}{3}v_c \right), \end{aligned} \tag{2.22}$$

$$\begin{aligned} i_\alpha &= \sqrt{\frac{2}{3}} \left(i_a - \frac{1}{2}i_b - \frac{1}{2}i_c \right), \\ i_\beta &= \sqrt{\frac{2}{3}} \left(\frac{\sqrt{2}}{3}i_b - \frac{\sqrt{2}}{3}i_c \right). \end{aligned} \tag{2.23}$$

The instantaneous power of the Scott transformer for each coordinates can be calculated as

$$\begin{aligned} P_{abc} &= v_a \cdot i_a + v_b \cdot i_b + v_c \cdot i_c \\ &= 3VI\cos\phi\ , \\ P_{\alpha\beta} &= v_\alpha \cdot i_\alpha + v_\beta \cdot i_\beta \\ &= 3VI\cos\phi\ . \end{aligned} \tag{2.24}$$

Therefore the Scott transformer can transfer power equally from primary to secondary side. However, the β-phase voltage and current depend on only b-phase and c-phase while α-phase depend on all three-phase as in (2.22) and (2.23). This indicates that unbalanced load condition in two-phase side greatly affect on three-phase side. So, balancing of loads between α-phase and β-phase is required for the Scott transformer in electrified railways.

2.5.2 Power Quality Problems of Traction Substation

The electric locomotives are single-phase heavy user of electric energy from the traction substation's Scott transformer. It is found that reducing maximum speed and tracefully performed coasting and accelerating operations can reduce energy consumption about 7% to 20% in the literature [22]. Therefore, the train operator uses various operation stratiges which include locomotive movement of accelerating, coasting and regenerative breaking.

The power feeding system for electrified railways and its detected waveforms from three-phase grid is shown in Figures 2.20 and 2.21.

In this power supply system, the primary side of the Scott transformer is connected to the three-phase power grid and the secondary side supply the power to the electric locomotives on the α-phase and β-phase. These α-phase and β-phase locomotives use various operation strategies. Therefore, the two load currents of α-phase and β-phase cause unbalanced load conditions on the secondary side of the Scott transformer. Moreover, the rectifier circuit of the motor drive for the locomotives are nonlinear characteristic. Therefore, the two source currents $i_{S\alpha}$ and $i_{S\beta}$ are unbalanced and distorted as shown in Figure 2.21.

The average power drawn by nonlinear loads will be discussed in more detail using Figures 2.20 and 2.21. The two source voltages are considered as balanced and sinusoidal condition in calculation. Let the α-phase and β-phase voltages in Figure 2.20 be

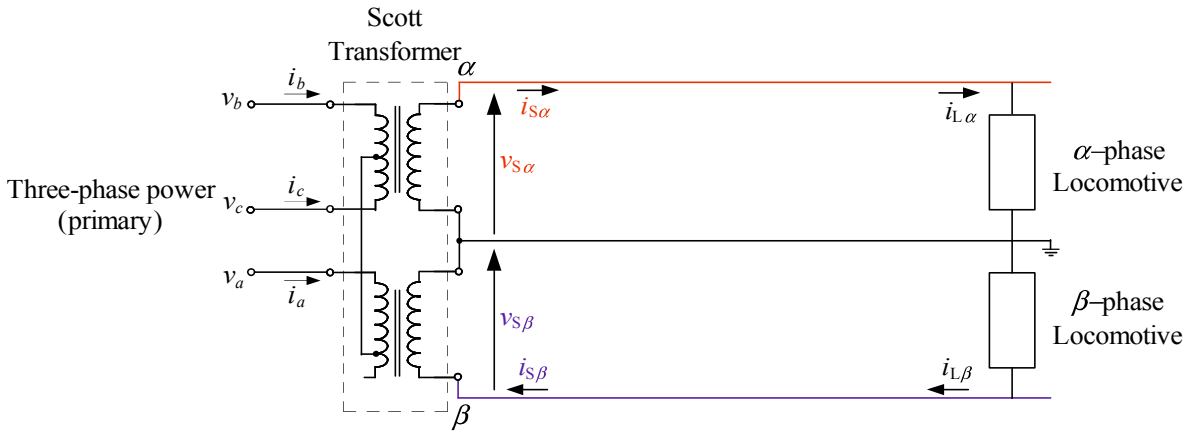

Figure 2.20: Power feeding system for electric locomotive from three-phase power grid through Scott transformer.

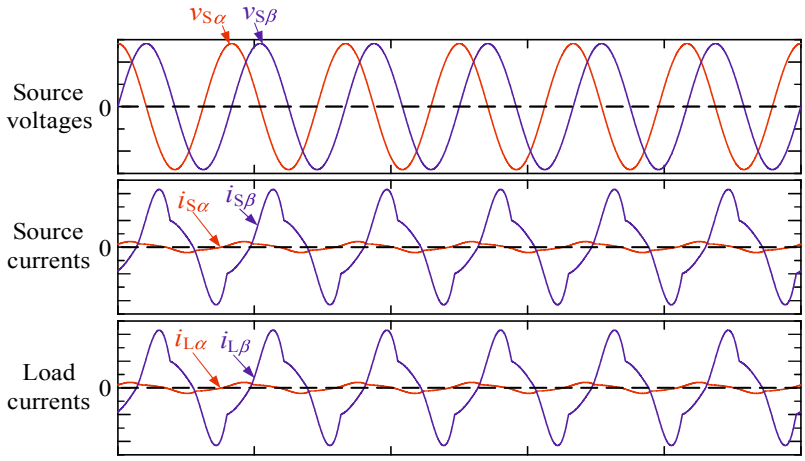

Figure 2.21: Detected waveforms when unbalanced load condition in electrified railways.

$$\begin{aligned} v_{S\alpha} &= \sqrt{2}V_{\alpha}\cos\omega t, \\ v_{S\beta} &= \sqrt{2}V_{\beta}\sin\omega t. \end{aligned} \tag{2.25}$$

and the nonlinear load currents which contains fundamental component and harmonic components are

$$\begin{aligned} i_{L\alpha} &= \sqrt{2}I_{1\alpha}\cos(\omega t + \phi_{1\alpha}) + \sum_{n=2}^{\infty} \sqrt{2}I_{n\alpha}\cos(n\omega t + \phi_{n\alpha}), \\ i_{L\beta} &= \sqrt{2}I_{1\beta}\sin(1\omega t + \phi_{1\beta}) + \sum_{n=2}^{\infty} \sqrt{2}I_{n\beta}\sin(n\omega t + \phi_{n\beta}). \end{aligned} \tag{2.26}$$

From (2.25) and (2.26), the instantaneous power flowing from Scott transformer to the electric locomotive are calculated as

$$\begin{aligned} p_\alpha &= v_{S\alpha} \cdot i_{L\alpha} \\ &= \sum_{n=1}^{\infty} V_\alpha I_{n\alpha} \Big[\cos\{(n+1)\omega t + \phi_{n\alpha}\} + \cos\{(n-1)\omega t + \phi_{n\alpha}\} \Big], \\ p_\beta &= v_{S\beta} \cdot i_{L\beta} \\ &= \sum_{n=1}^{\infty} V_\beta I_{n\beta} \Big[-\cos\{(n+1)\omega t + \phi_{n\beta}\} + \cos\{(n-1)\omega t + \phi_{n\beta}\} \Big]. \end{aligned} \tag{2.27}$$

The average power flowing to the electric locomotives are

$$\begin{aligned} \bar{p}_\alpha &= \frac{1}{T}\int_t^{t+T} p_\alpha \, dt = \frac{1}{T}\int_t^{t+T} v_{S\alpha} i_{L\alpha} \, dt \\ &= V_\alpha I_{1\alpha} \cos\phi_{1\alpha}, \\ \bar{p}_\beta &= \frac{1}{T}\int_t^{t+T} p_\beta \, dt = \frac{1}{T}\int_t^{t+T} v_{S\beta} i_{L\beta} \, dt \\ &= V_\beta I_{1\beta} \cos\phi_{1\beta}. \end{aligned} \tag{2.28}$$

where $T = 2\pi/\omega$. In (2.28), note that the current components at harmonic frequency do not contribute to the average (real) power drawn from the electric locomotives. Therefore, these useless harmonic components cause higher power rating of system, lower power factor and other power quality problems as described in the section 2.2.3. In Figure 2.21, note that, the two source current $i_{S\alpha}$ and $i_{S\beta}$ are unbalanced causing unbalanced load condition on three-phase side. These unbalanced conditions generate negative-sequence current, and cause unbalanced voltage, power loss, lower efficiency and other power quality problems as described in the section 2.3.3. Therefore, compensation of the unbalanced active, reactive and harmonic components of the load currents are required on the secondary side of the Scott transformer in the traction substation.

2.6 Single-Phase Active Power Line Conditioner in Electrified Railways

The passive filters consisting of the capacitors, inductors and/or resistors can suppress harmonic components with the corrected power factor but load balancing are still required to solve in electrified railways traction substation. One of the method to exchange electric energy between dif-

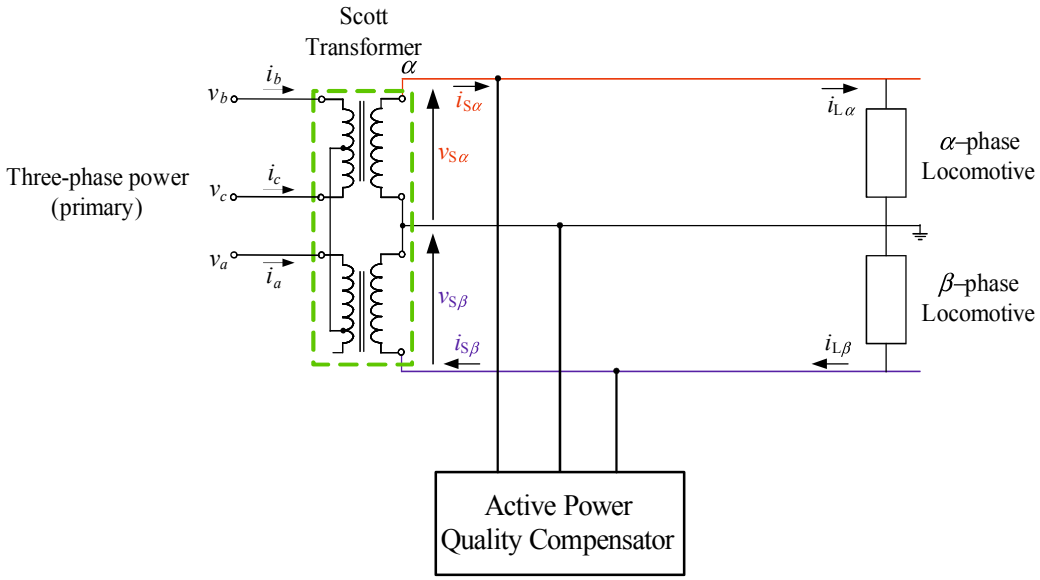

Figure 2.22: Active Power Quality Compensator application in electrified railways.

ferent attributes voltage and/or phase is using power electronic converter. The single-phase PWM inverters, thus, are utilized to compensate harmonic components, reactive and unbalanced active load condition in single-phase power feeding systems. This single-phase PWM inverters, which are used for the power conditioning applications, are called the active power quality compensator.

Figure 2.22 shows an Active Power Quality Compensator (APQC) in electrified railways. This APQC is a kind of single-phase active power filters and it can balance active power, compensate the reactive and harmonic components of the load currents. Figure 2.23 shows the source side currents $i_{S\alpha}$ $i_{S\beta}$ of the transformer and the load currents $i_{L\alpha}$ $i_{L\beta}$ in the electrified railways using the APQC. The source currents are balanced and sinusoidal with a unity power factor although the load currents are unbalanced and distorted. Therefore, many researchers have developed the single-phase Active Power Quality Compensator (APQC) for the electrified railways. This doctoral dissertation will shows various type of existing Active Power Quality Compensator for the electrified railways with their power circuit topologies and the control strategies. Then a newly proposed half-bridge inverter based Active Power Quality Compensator is discussed with the basic principle of the APQC operation and its control strategy.

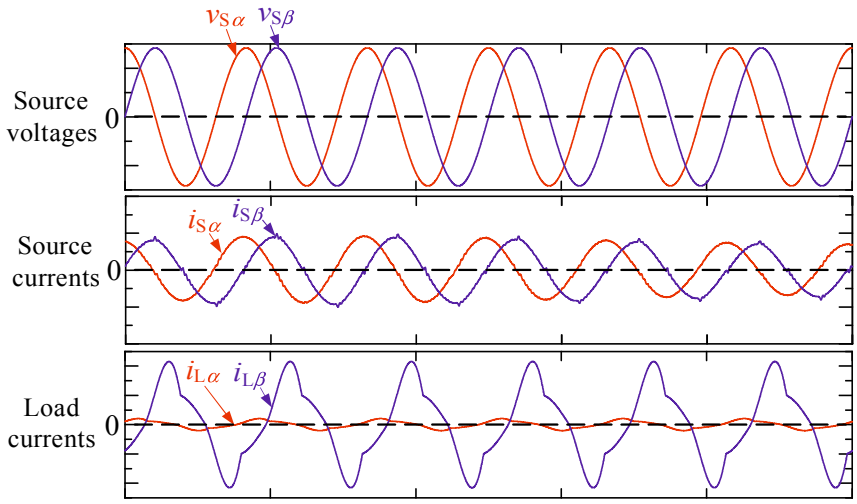

Figure 2.23: Voltage and current waveforms with balanced and sinusoidal source currents.

2.6.1 Full-bridge Inverter Based APQC

Figure 2.24 shows power circuit diagram of a single-phase based Active Power Quality Compensator. The APQC is composed of two single-phase full bridge inverter with a common DC capacitor. Dr. Mochinaga *et al*. has originally proposed this APQC and installed at the traction substation for the Nagano rolling depot in 1997 [4]. In this method, as shown in Figure 2.24,

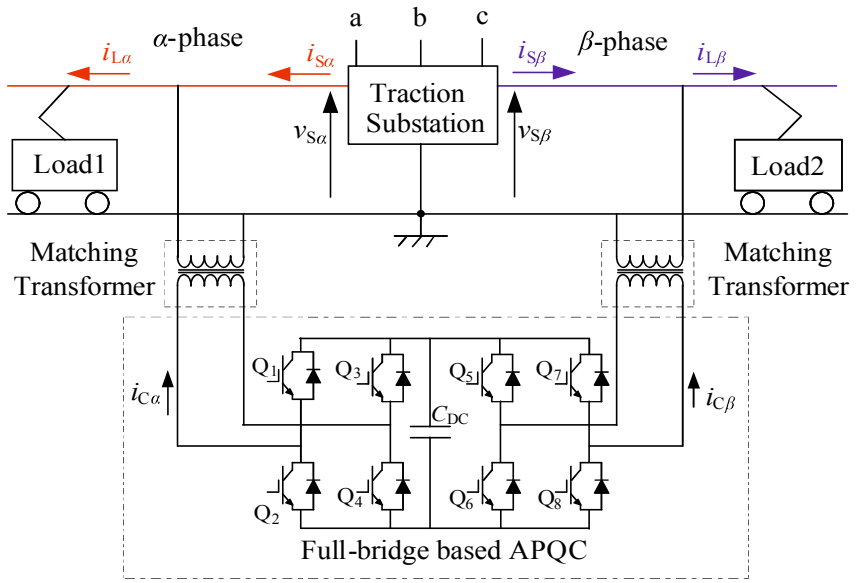

Figure 2.24: The APQC proposed by Dr. Mochinaga.

the first inverter is connected to the α-phase (main-phase) and the second inverter is connected to the β-phase (teaser-phase) of the Scott transformer through an impedance matching transformer.These two inverters exchange active power of α-phase and β-phase through a common DC capacitor. This mean that the active power is delivered from the larger load circuit to the smaller via the common dc capacitor. Therefore, balanced load condition can achieve in the secondary side of the Scott transformer. Moreover, the two inverters control the reactive power to be zero. This APQC, however, require 8 number of switching devices and the control strategy is designed for active power balancing and reactive power compensation. Thus, harmonic components do not compensate in this system.

2.6.2 Three-leg Inverter Based APQC

Prof. Zhuo Sun *et al*. has proposed a novel Active Power Quality Compensator (APQC) topology for the electrified railways [5]. In the proposed method, three-leg inverter with a common DC capacitor is used as shown in Figure 2.25. Therefore, number of switching device was reduced from 8 to 6 as compare to previous proposed APQC [4]. This three leg inverter operates as three-

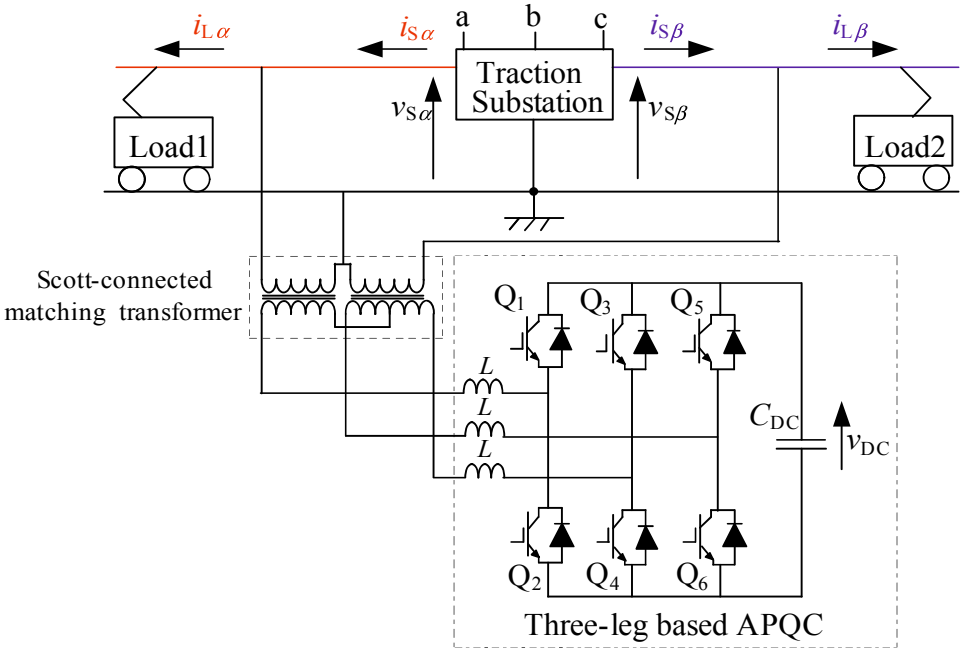

Figure 2.25: Three-leg inverter based APQC proposed by Prof. Zhuo Sun.

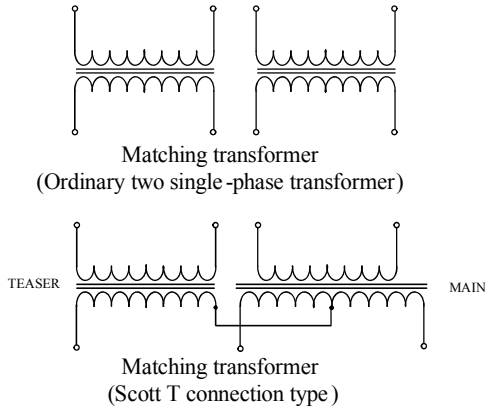

Figure 2.26: Comparison between two single-phase and Scott-connected transformer.

phase inverter even it is used in the single-phase power feeding systems. Thus, Scott-connected matching transformer is used to connect two single-phase electrified railways system with the three-phase APQC. In a Scott-connected matching transformer, the two-phase side windings are equivalent to the windings of two ordinary single-phase windings of the same output, but on the three-phase side the transformer winding is increased by 15.5% above what would be required in a single-phase transformer of the same output as shown in Figure 2.26 [23]. Assuming that the primary and secondary windings of an ordinary single-phase transformer occupies about the same space, then, for a Scott connected group, the main transformer will need to be about 7.75% larger than a single-phase transformer. Therefore, Scott connected matching transformer is more bulky and costly than ordinary two single-phase matching transformer.

Figure 2.27 shows control algorithm of the three-leg inverter based APQC [5]. The Fryze-Buchholz-Depenbrock (FBD) method is used for active power detection of the load currents [24]. In the FBD method, the instantaneous power of the each load current is calculated using detected load currents $i_{L\alpha}$, $i_{L\beta}$ and the electrical angle generated by single-phase phase-locked-loop (PLL). Then, the two instantaneous power are combine and input into low pass filter (LPF) to get the DC component of load current. The filter output value is multiply with cosωt and sinωt for the reference load currents. In Figure 2.27, S is abc/$\alpha\beta$ transformation matrix and S^{-1} is the inverse transformation matrix S. C is the three-phase converter and T is the Scott-connected transformer. These transformation and inverse transformation block are necessary because three-phase inverter is applied to the two single-phase power feeding system.

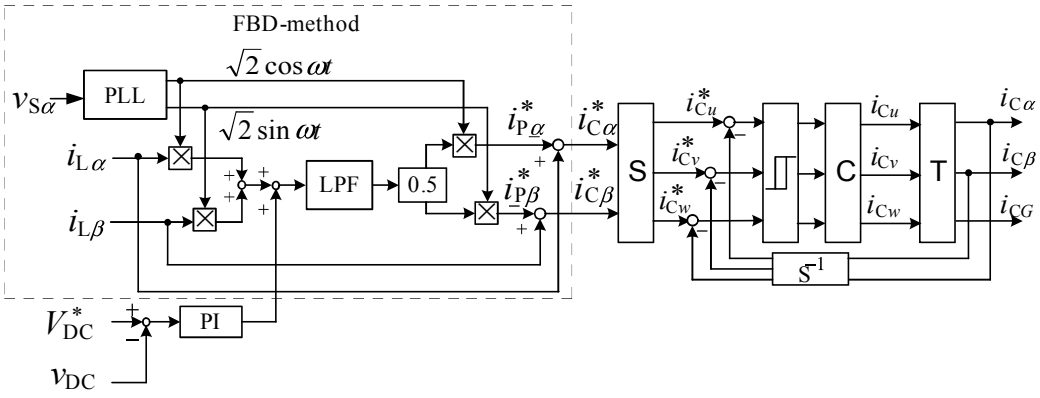

Figure 2.27: Control strategy proposed by Prof. Zhuo Sun.

The power circuit topology of the three-leg based APQC is simple but Scott connected matching transformer is used to interface APQC with electrified railways power supply system. This Scott transformer can causes design complexity in control strategy and higher cost. Therefore simpler control strategy with ordinary matching transformer is required in the three leg inverter based APQC.

Our research group have proposed the three-leg inverter based APQC with two single-phase matching transformer to enhance APQC design and control strategy [6]. Figure 2.28 shows power circuit diagram of the APQC with two single-phase matching transformer.

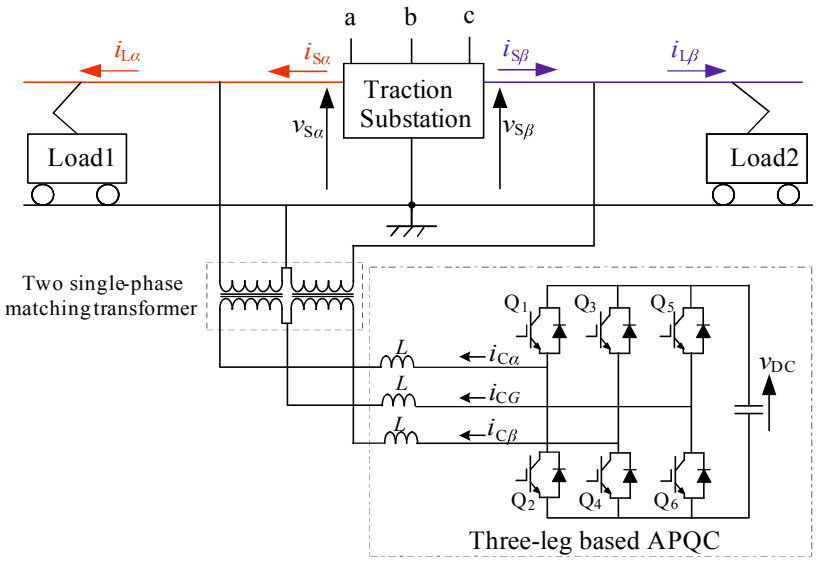

Figure 2.28: Three-leg inverter based APQC proposed by Dr. Ishikura.

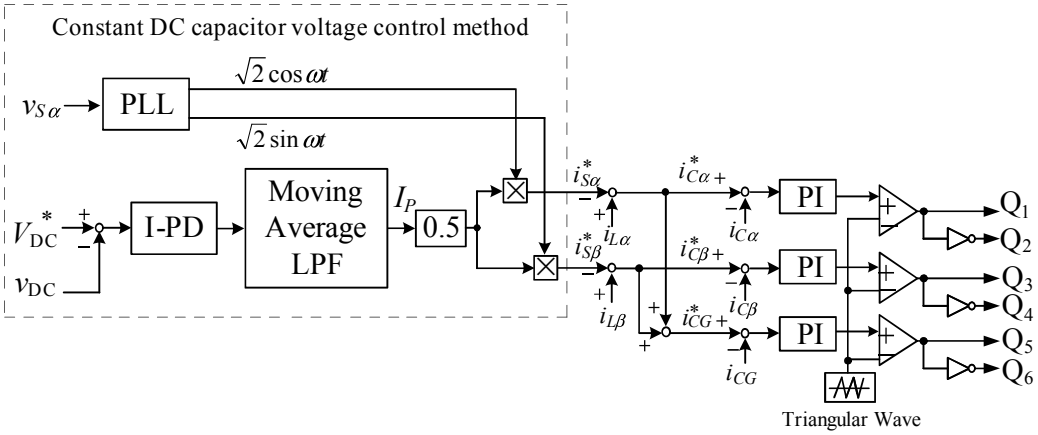

Figure 2.29: Control algorithm proposed by Dr. Ishikura.

The first-leg is connected to the α-phase and the second-leg is connected to the β-phase while the third-leg perform as a common-leg for the first and second. Therefore, the three legs based APQC is operated as two full-bridge converters and ordinary two single-phase matching transformer can be used in this design. Figure 2.29 shows control algorithm for the proposed APQC [6]. We proposed a constant DC capacitor voltage control based control strategy to reduce the instantaneous power calculation blocks of load currents. Therefore, the proposed control strategy is simple and the power circuit configuration is easy to construct. This three-leg inverter based APQC can balance active power on the α-phase and β-phase compensating reactive and harmonic components effectively. However, the third-leg perform as a common-leg for other two legs in our APQC design. As a result, the third-leg current rating requires $\sqrt{2}$ times larger than that of other two legs. To overcome this drawback, we proposed a new half-bridge inverter based APQC topology design. The characteristics and utilization possibilities of newly developed half-bridge inverter based APQC is discussed in the next chapter.

Chapter 3

Half-bridge Inverter Based Active Power Quality Compensator with DC Voltage Balancer for Electrified Railways

3.1 Power Circuit Diagram

Figure 3.1 show a power circuit diagram of the proposed half-bridge inverter based Active Power Quality Compensator (APQC) with DC voltage balancer. The APQC is composed of three-leg power devices with two DC capacitors. The first-leg is connected to α-phase, and second-leg is connected to β-phase of the electrified railways through the two ordinary matching transformers. These two legs perform as two half-bridge inverters with common DC-bus. The two half-bridge inverters exchange and balance the active power for α- and β-phase through two common DC capacitors, compensating reactive and harmonic components of the distorted load currents. The third-leg is used as DC voltage balancer for two DC capacitors with a small amount of output currents. Therefore, a new proposed topology with DC voltage balancer can reduce the third-leg current rating. The half-bridge based APQC, however, needs higher DC capacitor voltage v_{DC}, which is sum of the DC capacitor voltage v_{DC1} and v_{DC2}, than the DC capacitor voltage v_{DC} in Figure 2.28. This problem can be avoided because a matching transformer is still used in the APQC for the electrified railways applications. So the voltage rating can be enhanced without changing the Volt-Ampere rating of the matching transformer. This means that the price of the matching transformer in Figure 3.1 is equal to that in Figure 2.28.

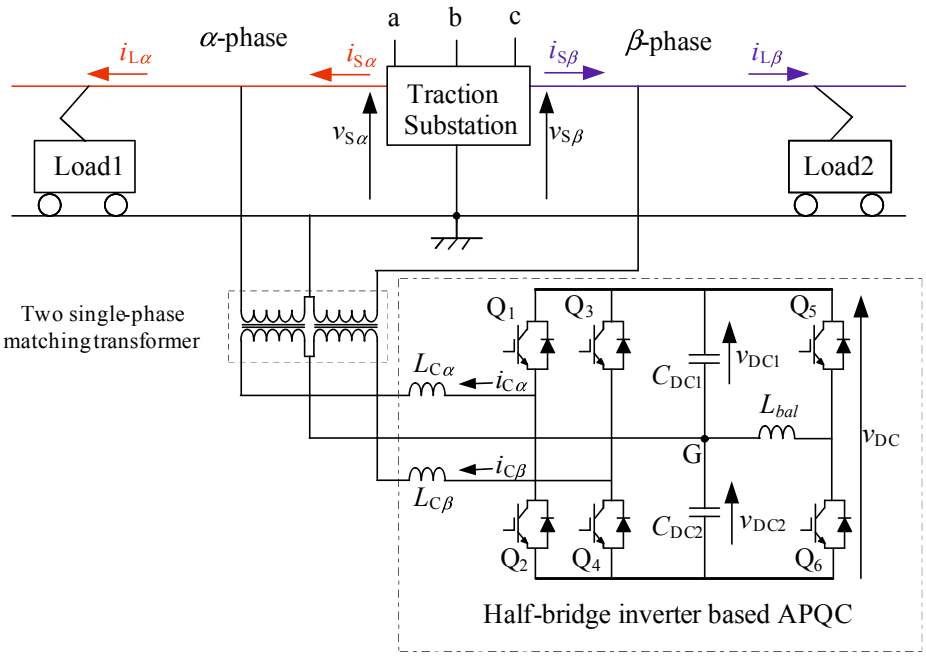

Figure 3.1: Power circuit diagram of half-bridge inverter based APQC with DC voltage balancer.

3.2 Control Strategy

Figure 3.2 shows a control block diagram for the proposed half-bridge inverter based APQC.

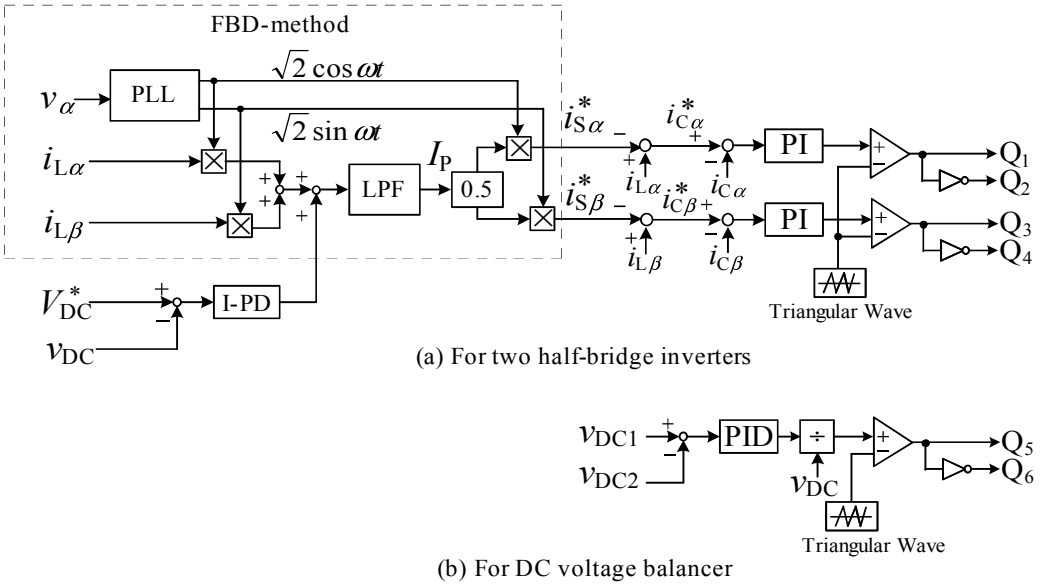

Figure 3.2: Control strategy of the half-bridge inverter based APQC.

The control strategy of the proposed APQC with DC voltage balancer has two parts: for the two half-bridge inverters and the DC voltage balancer. Figure 3.2(a) shows the two half-bridge inverters control strategy. In this control strategy, the PLL control is used for the host system electrical phase angle synchronization [25]. The Fryze-Buchholz-Depenbrock (FBD) method is used for real-time active power detection of α- and β-phase loads. In the FBD method, $\sqrt{2}\cos\omega t$ which is synchronized with electrical angle of $v_{S\alpha}$ and $\sqrt{2}\sin\omega t$ which is synchronized with electrical angle of $v_{S\beta}$ are calculated using electrical angle generated from the single-phase PLL circuit, as shown in Figure 3.2(a). Then two loads currents $i_{L\alpha}$ and $i_{L\beta}$ are detected. The detected load currents $i_{L\alpha}$ and $i_{L\beta}$ are given as

$$\begin{aligned} i_{L\alpha} &= \sqrt{2}I_{1\alpha}\cos(\omega t-\phi_{1\alpha}) + \sqrt{2}I_{h\alpha}\cos(h\omega t-\phi_{h\alpha}) \\ &= \sqrt{2}I_{1\alpha}(\cos\phi_{1\alpha}\cos\omega t+\sin\phi_{1\alpha}\sin\omega t) + \sqrt{2}I_{h\alpha}\cos(h\omega t-\phi_{h\alpha}), \\ i_{L\beta} &= \sqrt{2}I_{1\beta}\sin(\omega t-\phi_{1\beta}) + \sqrt{2}I_{h\beta}\sin(h\omega t-\phi_{h\beta}) \\ &= \sqrt{2}I_{1\beta}(\cos\phi_{1\beta}\sin\omega t-\sin\phi_{1\beta}\cos\omega t) + \sqrt{2}I_{h\beta}\sin(h\omega t-\phi_{h\beta}). \end{aligned} \tag{3.1}$$

The first terms of the right hand side of the (3.1) are the fundamental components and second terms are all harmonic components of the loads. These load currents $i_{L\alpha}$ and $i_{L\beta}$ are multiplied by the generated $\sqrt{2}\cos\omega t$ and $\sqrt{2}\sin\omega t$. This calculation step give the load sides instantaneous power p_C, which is given by

$$\begin{aligned} p_C &= \sqrt{2}\cos\omega t\cdot i_{L\alpha} + \sqrt{2}\sin\omega t\cdot i_{L\beta} \\ &= I_{1\alpha}\cos\phi_{1\alpha} + I_{1\alpha}\cos(2\omega t-\phi_{1\alpha}) \\ &\quad + I_{h\alpha}\Big[\cos\{(h+1)\omega t-\phi_{h\alpha}\}+\cos\{(h-1)\omega t-\phi_{h\alpha}\}\Big] \\ &\quad + I_{1\beta}\cos\phi_{1\beta} - I_{1\beta}\cos(2\omega t-\phi_{1\beta}) \\ &\quad - I_{h\beta}\Big[\cos\{(h+1)\omega t-\phi_{h\beta}\}-\cos\{(h-1)\omega t-\phi_{h\beta}\}\Big]. \end{aligned} \tag{3.2}$$

The instantaneous power p_C contains the active, reactive and harmonic components. Thus the DC component, $\overline{p_C}$, is extracted from (3.2) by a low-pass filter (LPF). The DC component, $\overline{p_C}$, is given by

$$\overline{p_C} = I_{1\alpha}\cos\phi_{1\alpha} + I_{1\beta}\cos\phi_{1\beta}. \tag{3.3}$$

The dc component $\overline{p_C}$ gives the combined fundamental active power on α- and β-phase loads. We need equal load condition on each feeder, and therefore, the reference source currents $i^*_{S\alpha}$ and $i^*_{S\beta}$ in the balanced load condition are expressed as

$$\begin{aligned} i^*_{S\alpha}(t) &= \sqrt{2} I_S \cos\omega t, \\ i^*_{S\beta}(t) &= \sqrt{2} I_S \sin\omega t, \end{aligned} \tag{3.4}$$

where $I_S = (I_{1\alpha}\cos\phi_{1\alpha} + I_{1\beta}\cos\phi_{1\beta})/2$. These above calculation steps are the FBD (Fryze-Buchholz-Depenbrock) method based active power calculation. The constant DC-link voltage control block is commonly added in the (FBD) method, as shown in Figure 3.2(a). In the constant DC-link voltage control, the DC-link voltage v_{DC} is detected and compares with the reference value V^*_{DC}. This difference value is amplified by the I-PD controller, and then the amplified value is added to the instantaneous power p_C. The two half-bridge inverters based APQC compensates the differences between the reference source currents expressed by (3.4) and the detected load currents $i_{L\alpha}$ and $i_{L\beta}$. Therefore, the reference signal $i^*_{C\alpha}$ and $i^*_{C\beta}$ of PWM inverters for the half-bridge inverter based APQC is given by

$$\begin{aligned} i^*_{C\alpha} &= i_{L\alpha} - i^*_{S\alpha} \\ i^*_{C\beta} &= i_{L\beta} - i^*_{S\beta}. \end{aligned} \tag{3.5}$$

Then, using the PI current feedback control and sine-triangle intercept pulse width modulation technique, the control strategy generates four gate signals for the two half-bridge inverter.

DC Voltage Balancer Control Strategy

Figure 3.3 shows a power circuit diagram and control strategy of the DC voltage balancer which are extracted from Figure 3.2. In this control algorithm, the two DC capacitor voltages v_{DC1} and v_{DC2} are detected, and then the difference between v_{DC1} and v_{DC2} is amplified by the PID controller to generate control signal of the switches Q_5 and Q_6. The sine-triangle intercept technique, where the switching frequency is 15 kHz is also used in the DC voltage balancer control.

To confirm the proposed half-bridge inverter based APQC with DC voltage balancer, the simulation was performed using PSIM digital simulation software.

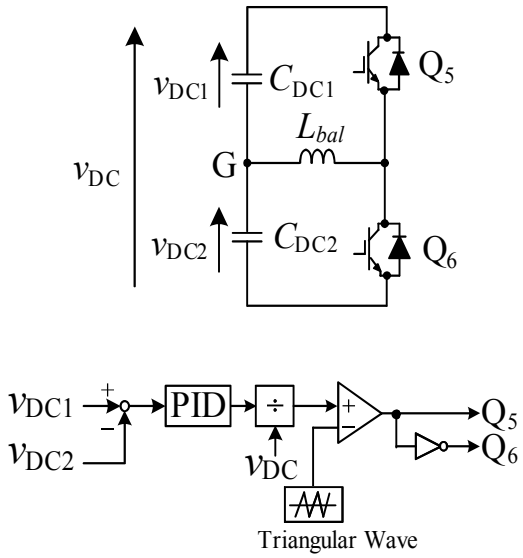

Figure 3.3: Power circuit and control strategy of DC voltage balancer.

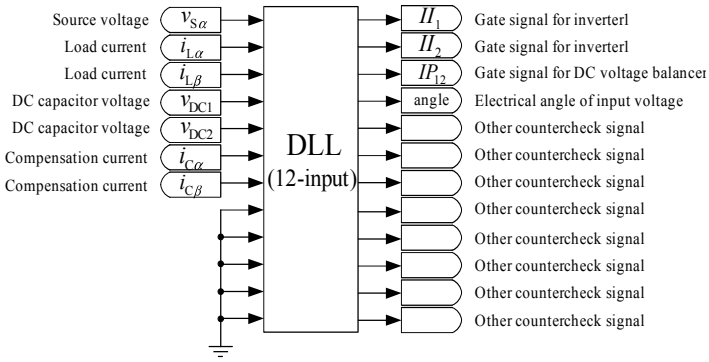

Figure 3.4: Dynamic-link Library in PSIM.

3.3 Simulation Setup

PSIM is a Power electronic circuit SIMulator software specifically designed for power electronics and motor control. The PSIM package consists of three parts: PSIM schematic program, PSIM Simulator, and waveform display program, Simview. This software allows external DLL (Dynamic-link Library) blocks with multiple input/output for desired control strategy. The control strategy of proposed half-bridge inverter based APQC is coded in the Microsoft visual studio, and the DLL block is generated. The input of the DLL block are the source voltage $v_{S\alpha}$, the two

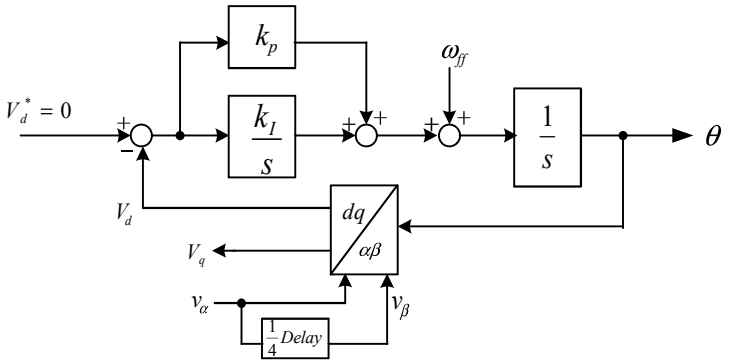

Figure 3.5: Transport Delay-Based PLL structure.

loads currents $i_{L\alpha}$ and $i_{L\beta}$, two DC-capacitor voltages v_{DC1} and v_{DC2}, and the two inverter output currents $i_{C\alpha}$ and $i_{C\beta}$ as shown in Figure 3.4. The output of the DLL block are two gate signals for two half-bridge inverters, one gate signal for DC voltage balancer. Moreover, DLL block can output other signals such as detected electrical phase angle, the calculated load current to check the calculation step of the control strategy.

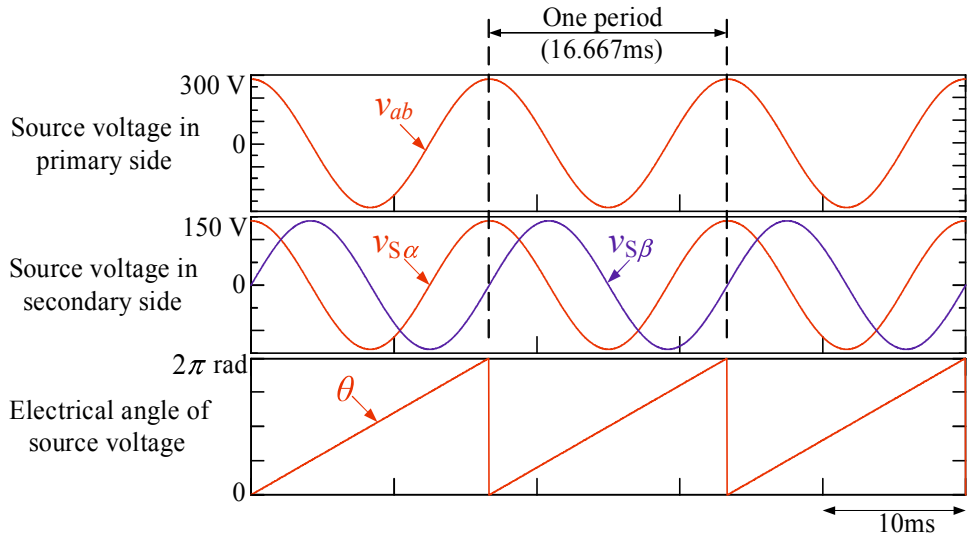

Figure 3.6: Electrical angle of source voltage.

Before performing APQC operation, all detected parameter such as electrical angle of source voltage, unbalanced load conditions, percent THD and reactive components are checked. Fig 3.5 shows constructed PLL structure based on the transport delay block [25] in the DLL block. The

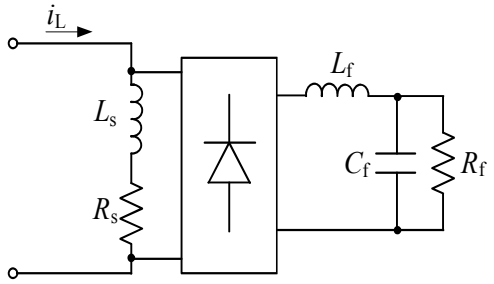

Figure 3.7: Load model of Load1 and Load2 for both simulation and experiment.

transport delay block generate quadrature signal and can phase shift 90° with respect to original input signal for the $\alpha\beta$ axis. The transport delay block is easily implemented through the use of a first-in-first-out (FIFO) buffer, with size set to one-fourth the number of samples contained in one cycle of the fundamental frequency. The advantage of transport delay based PLL is that all harmonic content of the input signal is subjected to the same time delay [26]. Therefore, in our proposed system, we used transport delay-based PLL control algorithm. Figure 3.6 shows the electrical angle generation of the transport delay PLL output. Figure 3.7 shows load model of Load1 and Load2 for simulation and experiment. The most common model for harmonic sources is in the form of a harmonic current source specified by its magnitude and phase spectrum.

Table 3.1: Load conditions for simulation.

	pu	DPF	THD%
Load1	0.05	0.64	21
Load2	0.05	0.64	21
Load2	0.5	0.68	24
3ϕ 200V/ 2ϕ 100V, 2.5kVA, 60Hz			

Table 3.1 shows the details load conditions for Load1 and Load2 in Figure 3.1. The sample load current for time domain is shown in Figures 3.8(a) and frequency domain is shown in 3.8(b) by Fourier analysis. The rating of the Scott transformer is 2.5 kVA, 3ϕ 200V, 60 Hz in the primary

side and 2.5 kVA, 2ϕ 100V, 60 Hz in the secondary side. Load2 includes two conditions, 0.05 per unit (pu) and 0.5 pu, for the load variation and load1 is 0.05 pu only. In the actual electrified railways operation, the load current is rapidly changed to its rated condition. Therefore, 0.5 pu is choose for the accelerating operation. When locomotives reach at sufficient speed, it changes from accelerating to coasting operation causing the load current nearly zero rapidly. Thus, 0.05 pu is used for the coasting operation.

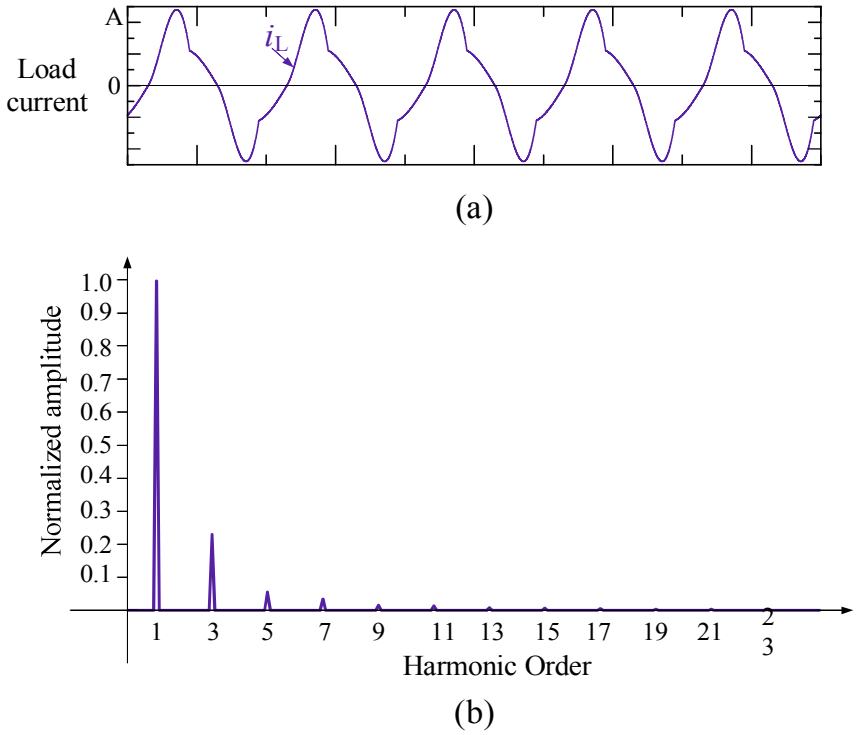

Figure 3.8: Sample load current (a) in time domain and (b) in frequency domain.

Table 3.2 shows the circuit parameters for the proposed APQC. The capacity of two DC capacitor is 3300 μF and the reference DC-link voltage is set to 350 V. The compensation inductor and balancing inductor are 2.14 mH. The switching frequency of all power switching devices is 15 kHz.

Table 3.2: Circuit parameters of APQC.

Item	Symbol	Value
Source voltages	$v_{S\alpha}$, $v_{S\beta}$	100 V
Compensation inductor	$L_{C\alpha}$, $L_{C\beta}$	2.14 mH
Balancing inductor	L_{bal}	2.14 mH
Reference DC-bus voltage	V^{*}_{DC}	350 V
Capacity of capacitors	C_{DC1}, C_{DC2}	3300 μF
Capacitor voltages	v_{DC1}, v_{DC2}	175 V
Switching frequency	f_{sw}	15 kHz

3.4 Simulation Results

3.4.1 Simulation Results for Coasting Operation

Figure 3.9 shows simulation results of proposed half-bridge inverter based APQC, where Load1 0.05 pu was kept constant in α-phase and load2 was changed from 0.5 pu to 0.05 pu in β-phase. This simulation demonstrates that the locomotive is just in the coasting from the accelerating on β-phase. The load variation in the simulation is very fast compare to the actual railways operations. Therefore, this demonstration is enough to examine transient response of the proposed APQC system. $v_{S\alpha}$ and $v_{S\beta}$ show the α-phase and β-phase voltages on the secondary side of the Scott transformer. $i_{S\alpha}$ and $i_{S\beta}$ are the source side currents. $i_{L\alpha}$ and $i_{L\beta}$ are load side currents, which are heavily distorted and unbalanced conditions as shown in Table 3.1. $i_{C\alpha}$ and $i_{C\beta}$ are the output currents of the half-bridge inverter based APQC. i_{bal} shows the output current of the third-leg, which performs DC capacitor voltage balancer. v_{DC1}, v_{DC2} show each DC capacitor voltage and v_{DC} is the sum of v_{DC1} and v_{DC2} voltages. The reference DC-bus voltage V^{*}_{DC} in this simulation is 350 V. Before/ after the Load2 was changed on β-phase, the source side current $i_{S\alpha}$ and $i_{S\beta}$ are also balanced and sinusoidal. Increasing the ripple amount of capacitor voltage should be avoided when loads were changed from the heavy condition to the light one. In Figure 3.9, the DC capacitor voltage fluctuation is less than 5% in both the transient- and steady-state.

3.4.2 Simulation Results for Accelerating Operation

Figure 3.10 shows simulation results in which Load2 was changed from 0.05 pu to 0.5 pu while Load1 was kept at constant 0.05 pu. Although the coasting condition, the electrified railways use service power about 0.05 pu. Therefore, we make the simulation with the worst unbalanced load condition of 0.05 pu and 0.5 pu. This simulation demonstrates that the locomotive on the β-phase is just accelerating from coasting. The load variation in the simulation is very fast compare to the actual railways operations. Therefore, this demonstration is enough to examine transient response of the proposed APQC system when light to heavy load variation. Before/ after the β-phase load was changed, the source side currents, $i_{S\alpha}$ and $i_{S\beta}$, are balanced and sinusoidal. The THD values of the source currents, $i_{S\alpha}$ and $i_{S\beta}$, are 1.7% and 3.0% after load2 was changed. The DC capacitor voltage fluctuation is less than 5% in both the transient- and steady-state.

3.4.3 Simulation Results for Regenerative Breaking Operation

Figure 3.11 shows simulation waveforms, which demonstrate the regenerative breaking operation of electric locomotive. Under regenerative breaking condition, the direction of the load current $i_{L\beta}$ should be opposite to that of load current in normal operation. Therefore, Load2 was changed from 0.05 pu to the rated load currents with the opposite direction of supply current while Load1 was kept constant at 0.05 pu in the normal operation. The source side currents, $i_{S\alpha}$ and $i_{S\beta}$, are also balanced and sinusoidal before and after regenerative load variation. The ripple amount of DC capacitors, v_{DC1} and v_{DC2} are 5.2% in the transient-state and ±2.4% in the steady-state.

The simulation results of three operating patterns were shown using proposed half-bridge inverter based APQC with DC voltage balancer control strategy. In three operating patterns, the two DC capacitor voltages is balanced and ripple amounts are acceptable range because third-leg device control two DC capacitor voltage effectively. Figure 3.12 shows the simulation results of the proposed half-bridge inverter based APQC without DC voltage balancer control. It can be seen that the two DC capacitor voltages are unbalanced and wide range of fluctuation although DC-link voltage is nearly kept constant. Therefore, we can conclude that using DC voltage balancer control in proposed half-bridge inverter based APQC is effective for all mode of half-bridge inverter based APQC operations.

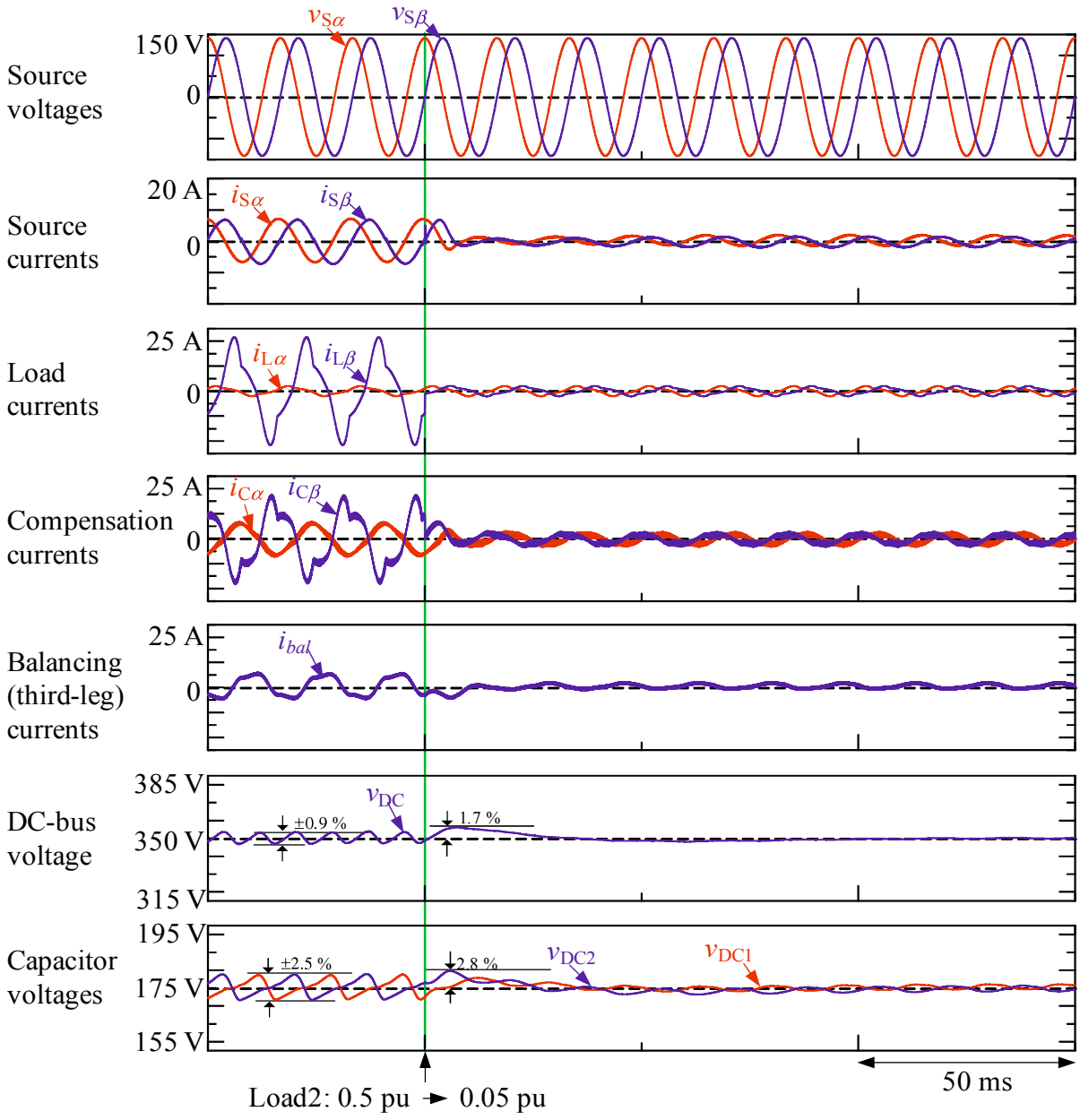

Figure 3.9: Simulation waveforms of proposed APQC with β-phase load variation from 0.5pu to 0.05pu for coasting operation.

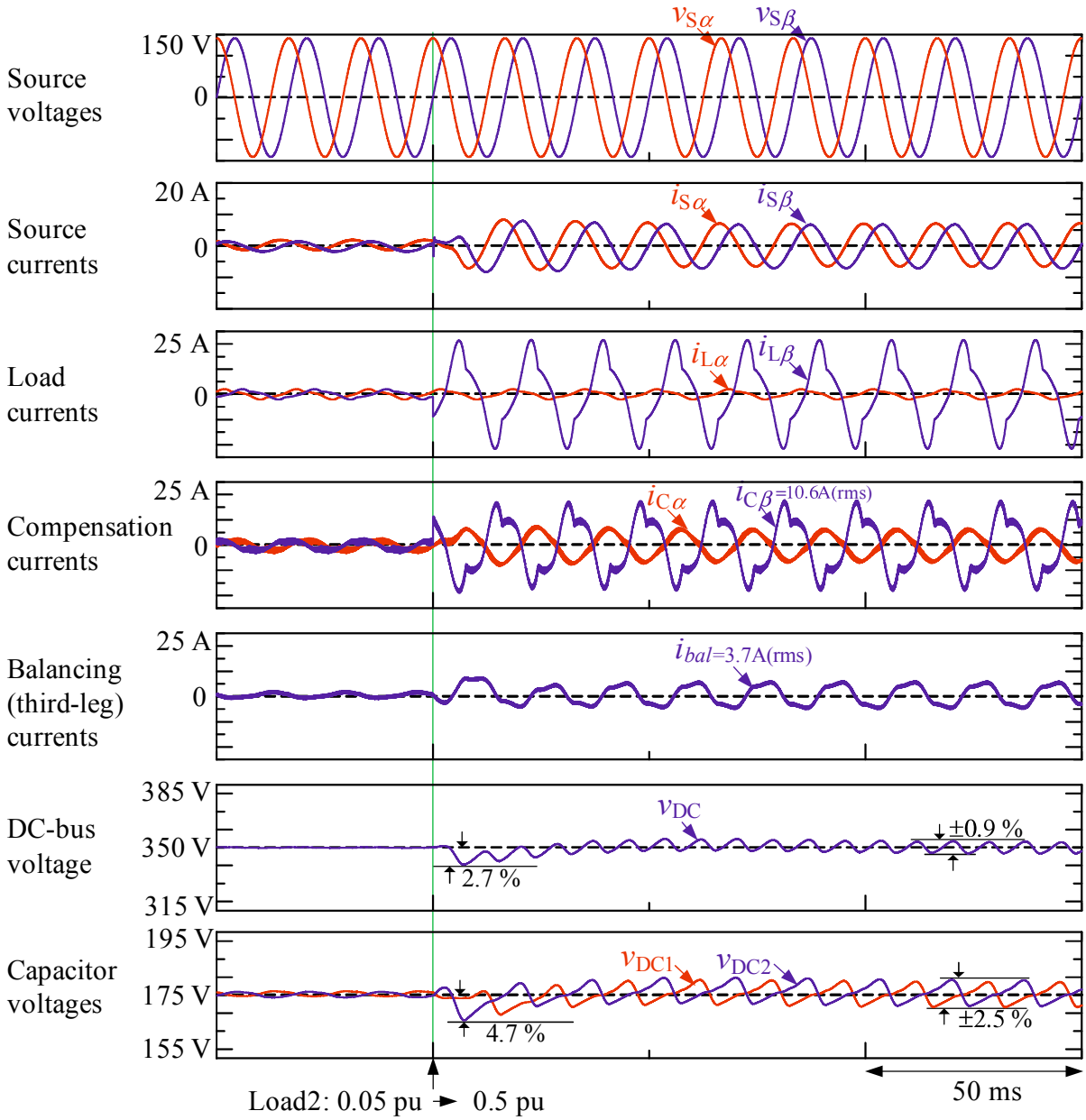

Figure 3.10: Simulation waveforms of proposed APQC with β-phase load variation from 0.05 pu to 0.5 pu for accelerating operation.

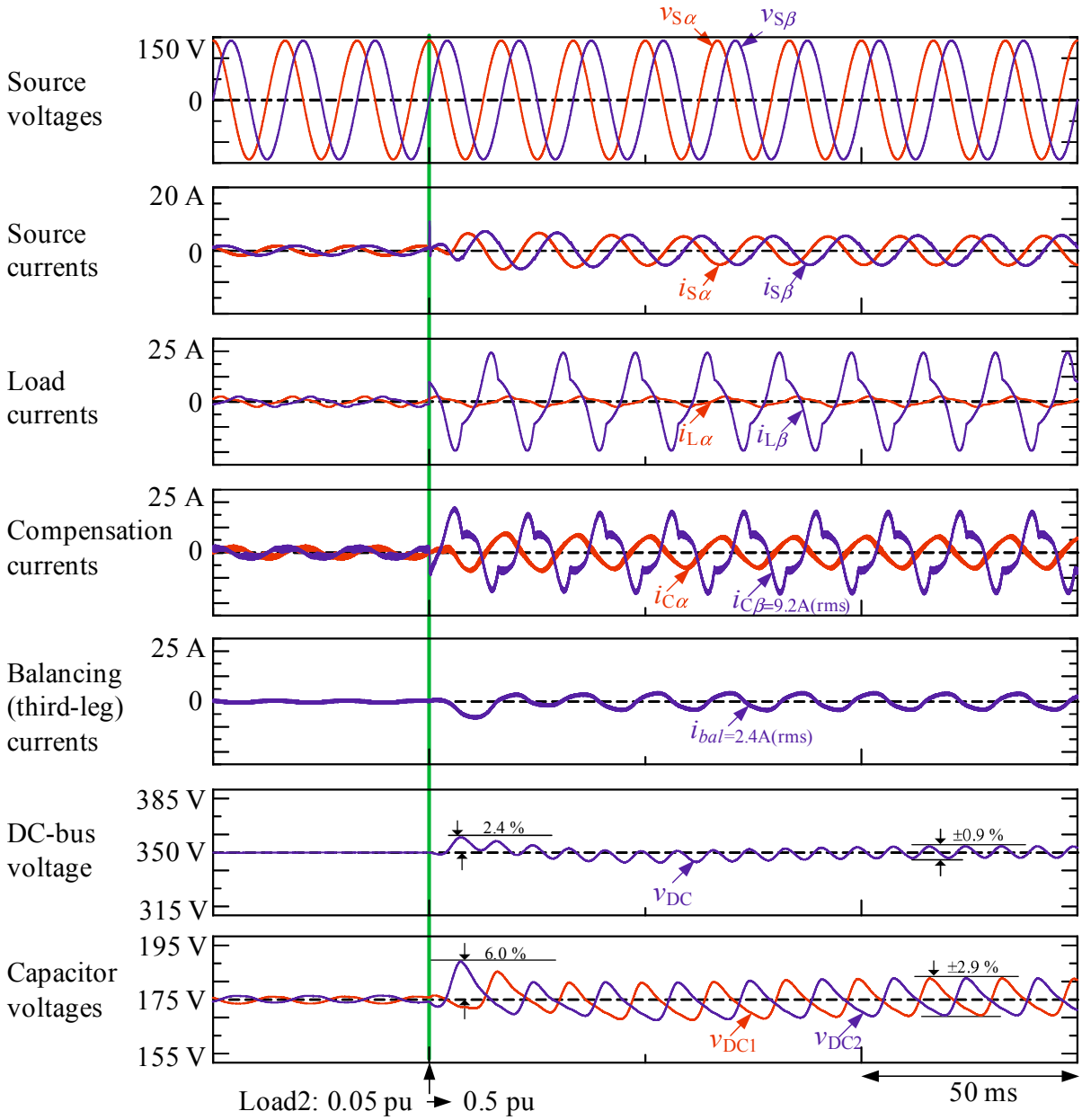

Figure 3.11: Simulation waveforms of proposed APQC with β-phase load variation from 0.05 pu to 0.5 pu for regenerative breaking operation.

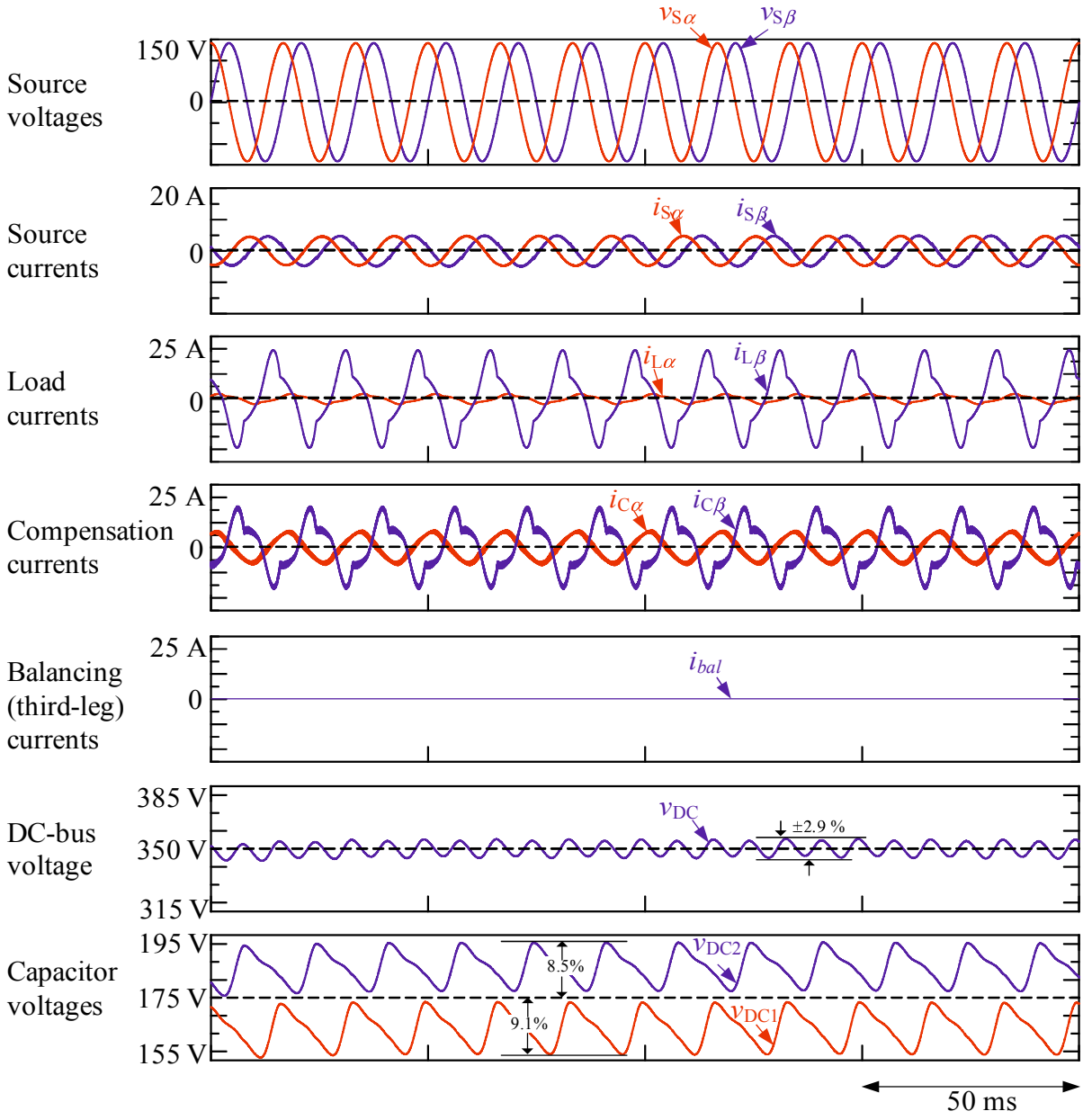

Figure 3.12: Simulation waveforms of proposed APQC without DC voltage balancer control.

Table 3.3 shows the total harmonic distortion (THD%) of the source currents after compensating by the half-bridge inverter based APQC under balanced load conditions and the load currents .

Table 3.3: The total harmonic distortion (THD%) of source currents and load currents in the simulation.

	Source currents (THD%)	Load currents (THD%)
α-phase	1.7%	21%
β-phase	3.0%	24%

From the simulation results, the required current rating in root mean square (rms) value of power switching devices in the proposed half-bridge inverter based APQC are shown in Table 3.4.

Table 3.4: The required current rating of power devices in the proposed half-bridge inverter based APQC in the simulation.

	In normal operation	In regenerative breaking operation
First-leg current (A)	4.3 A	4.2 A
Second-leg current (A)	10.6 A	9.2 A
Third-leg current (A)	3.7 A	2.4 A

Table. 3.5 shows rms value of the current in each leg for the three-leg inverter based APQC [6] and the proposed half-bridge inverter based APQC. Full load condition of Load1 (0.5 pu) and Load2 (0.5 pu) are used in the simulation. An amount of currents flowing into the first- and second-leg are the same in both topologies. But, the third-leg current of three-leg inverter based APQC is about $\sqrt{2}$ times larger than to that of another two legs. But, the third-leg current is lower than another two legs in the half-bridge inverter based APQC. Therefore, third-leg current rating can reduce using proposed half-bridge inverter based APQC. We also constructed the experimental model of the half-bridge inverter based APQC with a DC voltage balancer. Next section will

describe the experimental setup and the experimental results of the half-bridge inverter based APQC.

Table 3.5: The comparison of current rating of power devices in three-leg based APQC and Half-bridge based APQC in the simulation.

	Three-leg based APQC	Half-bridge based APQC
First-leg current (A)	8.9 A	8.9 A
Second-leg current (A)	9.1 A	9.0 A
Third-leg current (A)	12.4 A	8.2 A

3.5 Experimental Setup

Figure 3.13 shows a block diagram of the constructed experimental model. The experimental system is constructed with the Scott-connected transformer, the harmonic generated unbalanced loads, the half-bridge inverter based APQC and the digital signal processor (DSP) control unit. The ratings of the Scott transformer are 3ϕ200 V, 2.5 kVA, 60 Hz on the primary side and 2ϕ100V, 2.5 kVA, 60 Hz in the secondary side, and therefore, winding turns ratio of Scott transformer is $\sqrt{3}:1$ for main winding and 2:1 for teaser winding. The load conditions and the circuit constants of the half-bridge inverter based APQC are the same as in simulation as shown in Tables 3.2 and 3.1.

Control Unit

The control strategy of the experimental model is also the same as in simulation shown in Figure 3.2. A digital signal processor (DSP: TMS320C6713, 225MHz) is used for overall control. Table 3.6 shows Hardware specifications of the digital signal processor and other peripherals. As shown in the constructed experimental model, the line to line voltage v_{bc}, which is synchronized with $v_{S\alpha}$ is detected, and then inputted to the digital signal processor through a 12-bit A/D converter. Using the line to line voltage v_{bc}, the DSP calculates the electrical angle θ by transport delay-

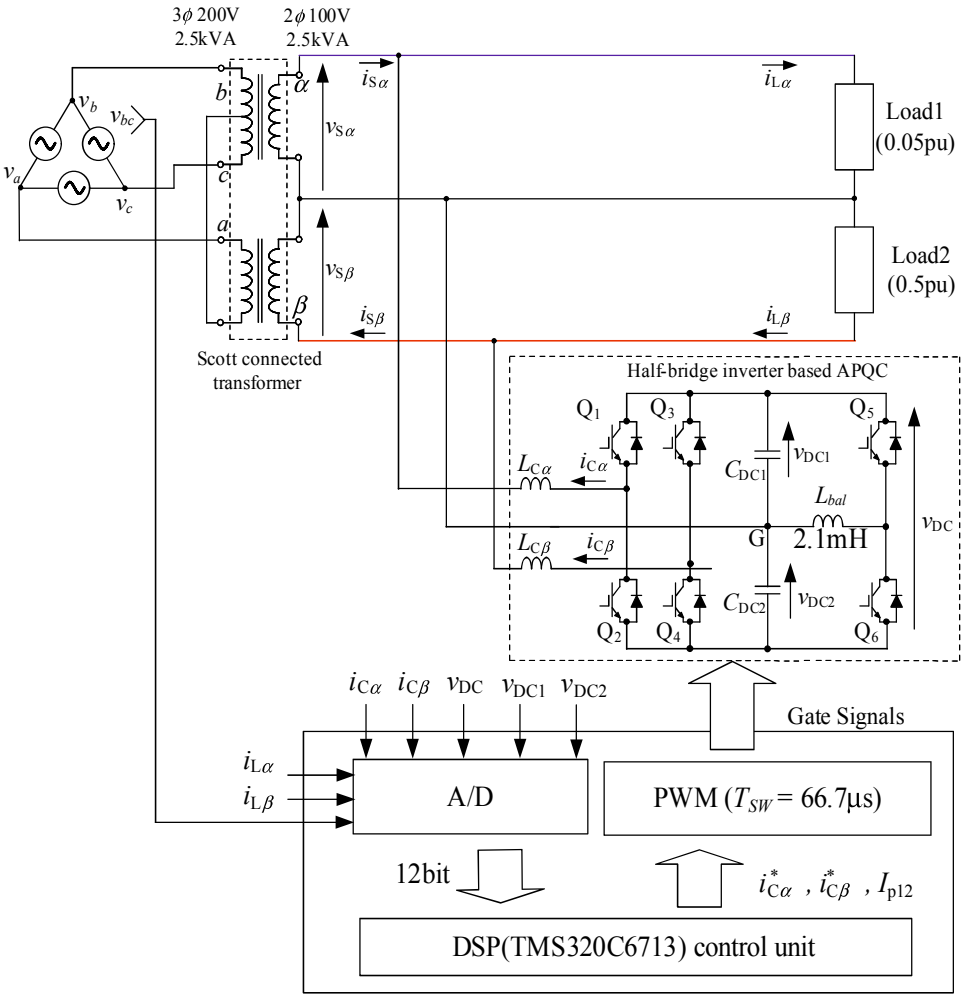

Figure 3.13: Constructed experimental model of the APQC with DC voltage balancer.

based PLL control algorithm. Figure 3.14 shows experimental results of the line to line voltage v_{bc} and the electrical angle θ. Then $\sqrt{2}\cos\omega t$ which is synchronized with the electrical angle of $v_{S\alpha}$, and $\sqrt{2}\sin\omega t$ which is synchronized with electrical angle of $v_{S\beta}$ are calculated using this $\theta(=\omega t)$. The other detected signals for the DSP are the two load currents, the two compensation output currents and the three DC capacitor voltages through the 12-bit A/D converters. Then the effective value of the load currents are calculated using FBD-method based active power detection as in (3.3). Using this effective value, the reference source signal $i^*_{S\alpha}$ and $i^*_{S\beta}$ are calculated as in (3.4). Finally, the reference current values $i^*_{C\alpha}$ and $i^*_{C\beta}$ for the half-bridge inverters are obtained by (3.5). The sine triangle intercept technique is used to control the output currents $i_{C\alpha}$ and $i_{C\beta}$

Table 3.6: Hardware specifications of Digital Signal Processor

DSP Board

CPU	TMS320C6713-225 MHz
Build-in RAM	64 kword(32 bit)
External RAM	2 Mword(32 bit)
Flash ROM	256 kword(16 bit)

PEV Board

PWM	3-phase PWM function	voltage triangular comparison
	Dead time	20 ns ~ 10.22 μs
	Carrier synchronization	Yes
AD Converter	Channel capacity	8 ch
	Simultaneous sampling	4 ch
	Resolution	12 bit
	Conversion time	2 μs
	Input range	±5 V

of the half-bridge inverters. These compensation output currents $i_{C\alpha}$ and $i_{C\beta}$ are also inputted to the DSP for PI current feed-back controllers.

For the DC voltage balancer control, the two DC capacitor voltage are detected by DSP through the 12-bit A/D converter. The error between v_{DC1} and v_{DC2} is amplified with PI controller. Then the switch Q_5 and Q_6 are controlled by the sine triangle intercept technique. The switching frequency of all power switching devices f_{sw} is 15 kHz. Yokogawa SL1000 high-speed data acquisition unit, where sampling rate of 5 μs, is used for the experimental waveforms.

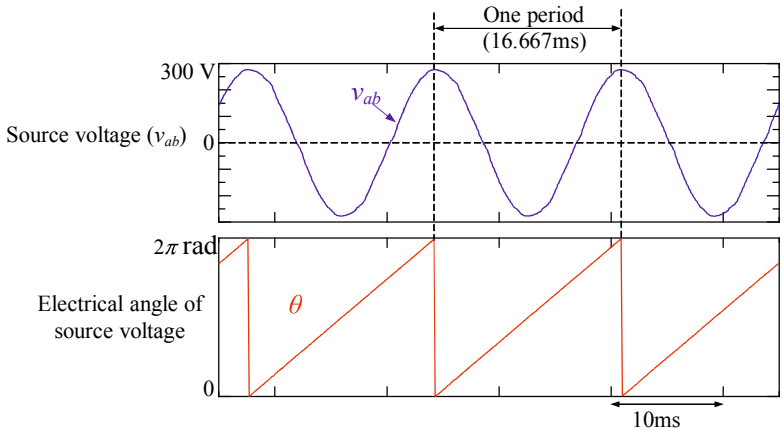

Figure 3.14: Experimental results of transport-delay based PLL in Figure 3.5.

3.6 Experiment Results

3.6.1 Experimental Results for Coasting Operation

Figure 3.15 shows experiment results of proposed APQC, where Load1 0.05 pu was kept constant in α-phase and Load2 was changed from 0.5 pu to 0.05 pu in β-phase. This experimental results demonstrates that the locomotive is just in the coasting on β-phase. The load variation in the experiment is faster than the actual railways operations. Therefore, this experiment results is enough to examine transient response of the proposed APQC system. $v_{S\alpha}$ and $v_{S\beta}$ show the α-phase and β-phase voltages on the secondary side of the Scott transformer. $i_{S\alpha}$ and $i_{S\beta}$ are the source side currents. $i_{L\alpha}$ and $i_{L\beta}$ are load side currents, which are heavily distorted and unbalanced conditions as shown in Table 3.1. $i_{C\alpha}$ and $i_{C\beta}$ are the output currents of the half-bridge based PWM inverter, which performs the active power quality compensator. i_{bal} shows the output current of the third-leg, which performs DC capacitor voltage balancer. v_{DC1}, v_{DC2} show each DC capacitor voltage and v_{DC} is the sum of v_{DC1} and v_{DC2} voltages. The reference dc-link voltage V^*_{DC} in this experiment is 350 V. Before/after the Load2 was changed on β-phase, the source side current $i_{S\alpha}$ and $i_{S\beta}$ are also balanced and sinusoidal. Increasing the ripple amount of capacitor voltage should be avoided when loads were changed from the heavy condition to the light one. In Figure 3.15, the DC capacitor voltage fluctuation is less than 5% in both the transient- and steady-state.

3.6.2 Experimental Results for Accelerating Operation

Figure 3.16 shows experiment results in which Load2 was changed from 0.05 pu to 0.5 pu while Load1 was kept at constant 0.05pu. For standby and service load, 0.05 pu is used. Therefore, we make the experiment with the worst load unbalanced condition of 0.05 pu and 0.5 pu. This experiment demonstrates that the locomotive on the β-phase is just accelerating from coasting. Our load variation is very rapid compare to the actual railways operations. Therefore, this experiment results is enough to examine transient response of the proposed APQC system when light to heavy load variation. Before/after the α-phase load was changed, the source side currents, $i_{S\alpha}$ and $i_{S\beta}$, are balanced and sinusoidal. From the experimental results, the compensation current on β-phase is 10A (rms) and balancing inductor current, i_{bal} is 5.5 A(rms). These values show that third-leg power devices need smaller current rating than another two legs. The THD values of the source currents, $i_{S\alpha}$ and $i_{S\beta}$, are 3.9% and 7.4% after load2 was changed.

3.6.3 Experimental Results for Regenerative Breaking Operation

In regenerative breaking operation, the load current should be opposite direction to that of source voltage like in Figure 3.11. However, this exact load condition is difficult to construct in the experiment model because the load current direction must be opposite before and after load change. The simulation results for accelerating and coasting operation well agree with the experiment results. Therefore we refer to the simulation results for the regenerative breaking operation.

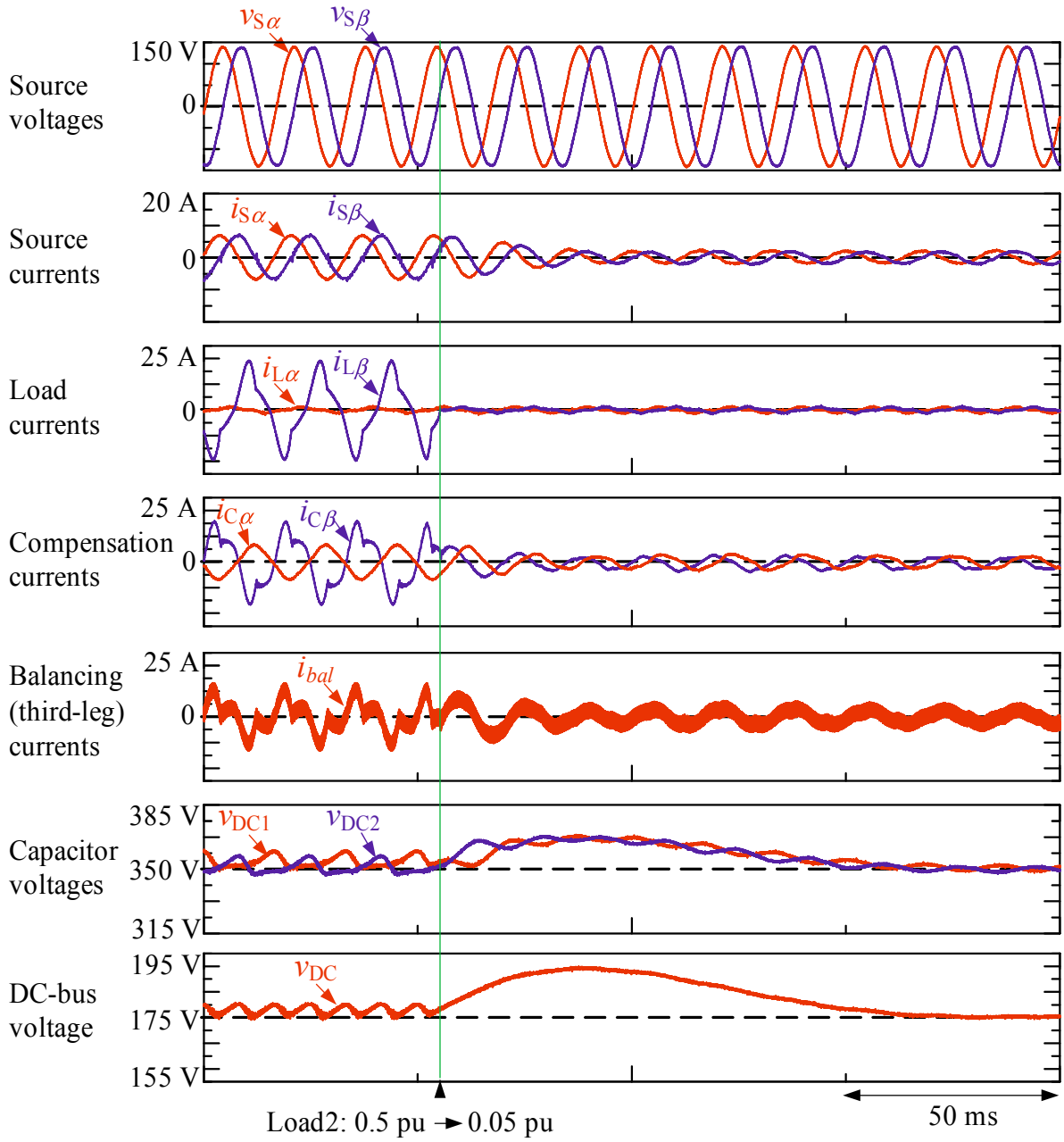

Figure 3.15: Experimental results of proposed APQC with β-phase load variation from 0.5 pu to 0.05 pu for coasting operation.

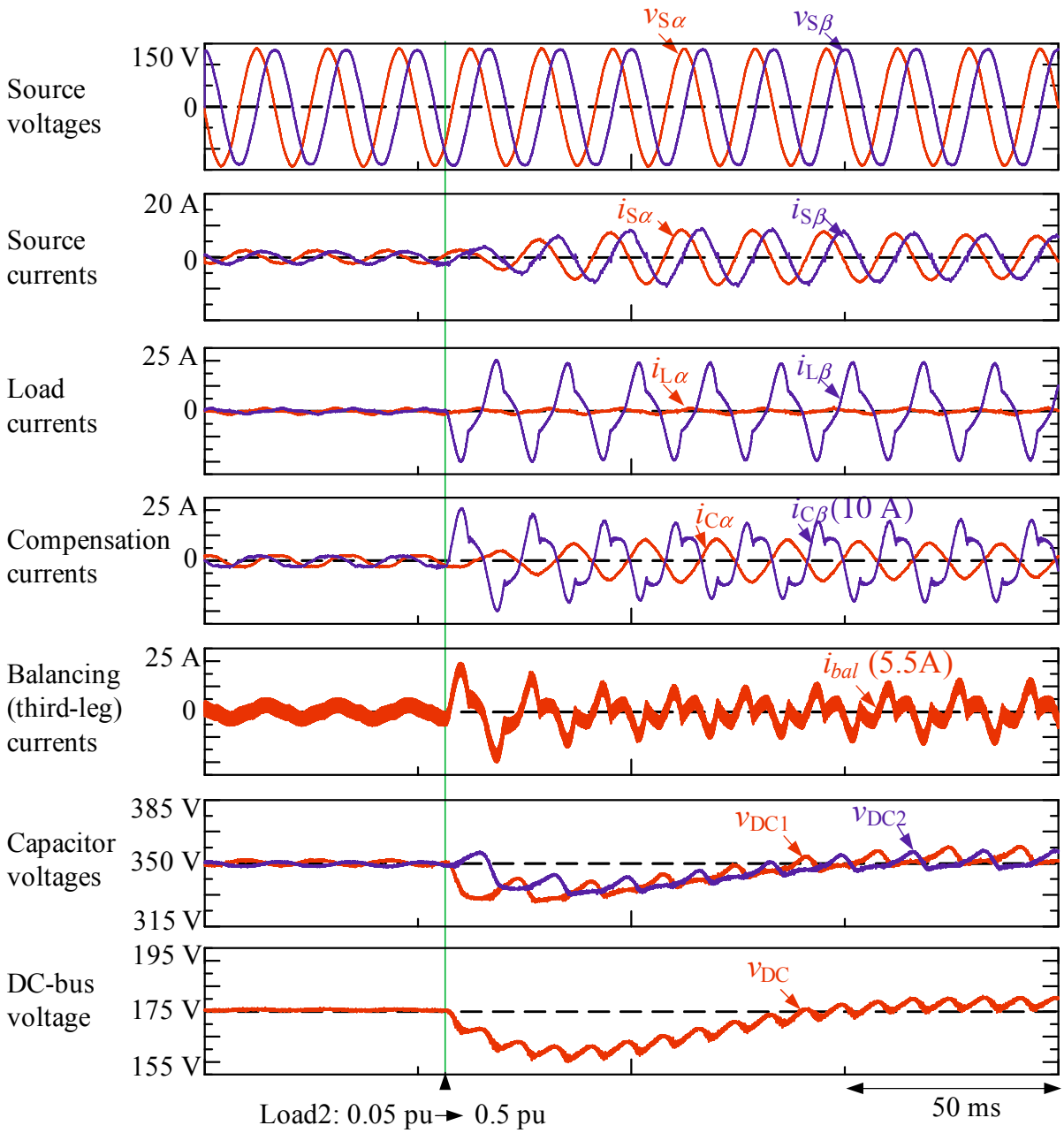

Figure 3.16: Experimental results of proposed APQC with β-phase load variation from 0.05 pu to 0.5 pu for accelerating operation.

Table 3.7 shows the total harmonic distortion (THD%) of the source currents after compensating the harmonic components under balanced load conditions and the load currents .

Table 3.7: The total harmonic distortion (THD%) of source currents and load currents in the experiment.

	Source currents (THD%)	Load currents (THD%)
α-phase	3.9%	21%
β-phase	7.4%	24%

From the experimental results, the required current rating in root mean square (rms) value of power switching devices in the proposed half-bridge inverter based APQC are shown in Table 3.8. The third-leg requires lower current rating than the other two legs.

Table 3.8: The required current rating of power devices in the proposed half-bridge inverter based APQC in the experiment.

	In normal operation
First-leg current (A)	4.5 A
Second-leg current (A)	10.4 A
Third-leg current (A)	5.5 A

3.7 Conclusion

This chapter describes the power supply system of electrified railways, the special purpose Scott connected transformer in traction substation and its power quality problems. Then the previously proposed single-phase based Active Power Quality Compensator are discussed with their advantages and disadvantages. The drawback of the previously proposed three-leg based APQC is that it needs the third-leg power switching devices with $\sqrt{2}$ times larger current rating than other two legs. Therefore, the half-bridge inverter based Active Power Quality Compensator is proposed.

The proposed APQC requires lower third-leg current rating compare to first- and second-leg without changing APQC's performance. The basic principle of the proposed half-bridge inverter based APQC is discussed in details and confirmed both simulation and experiment. The proposed half-bridge inverter based APQC is already published in Journal of the Japan Institute of Power Electronics (2011) with simulation results and in the 2012 IEEE 7^{th} International Power Electronics and Motion Control Conference with the experimental results. In the next chapter, new simple control algorithm with better simulation and experiment results will be shown for half-bridge inverter based Active Power Quality Compensator.

Chapter 4

New Control Strategy with Constant DC Capacitor Voltage Control for Half-bridge Inverter Based Active Power Quality Compensator in Electrified Railways

In chapter3, the basic principle and control algorithm of the half-bridge inverter based Active Power Quality Compensator (APQC) with DC voltage balancer had been discussed in detail. The simulation and the experiment results confirmed that the proposed half-bridge inverter based APQC with DC voltage balancer can reduce third-leg current rating without changing APQC's performance as compared to the previous proposed one [6]. However, the proposed APQC uses the FBD-method to detect the active power of the load currents. This FBD-method requires a significant calculation steps because it is based on the instantaneous power of the load. Therefore we propose a new simpler control strategy for half-bridge inverter based APQC in this chapter to avoid the instantaneous power calculation step in the control strategy.

4.1 Power Circuit Diagram

The power circuit diagram for the half-bridge inverter based APQC with constant DC capacitor voltage control is the same as in chapter 3 and shown again in Figure 4.1. It is composed of three-leg power devices with two common DC capacitors. The first-leg is connected to α-phase and second-leg is connected to β-phase of the Scott transformer through the two single-phase matching transformers. These two legs perform as two half-bridge inverters with common DC-bus. Two half-bridge inverters exchange and balance the active power for α- and β-phase through

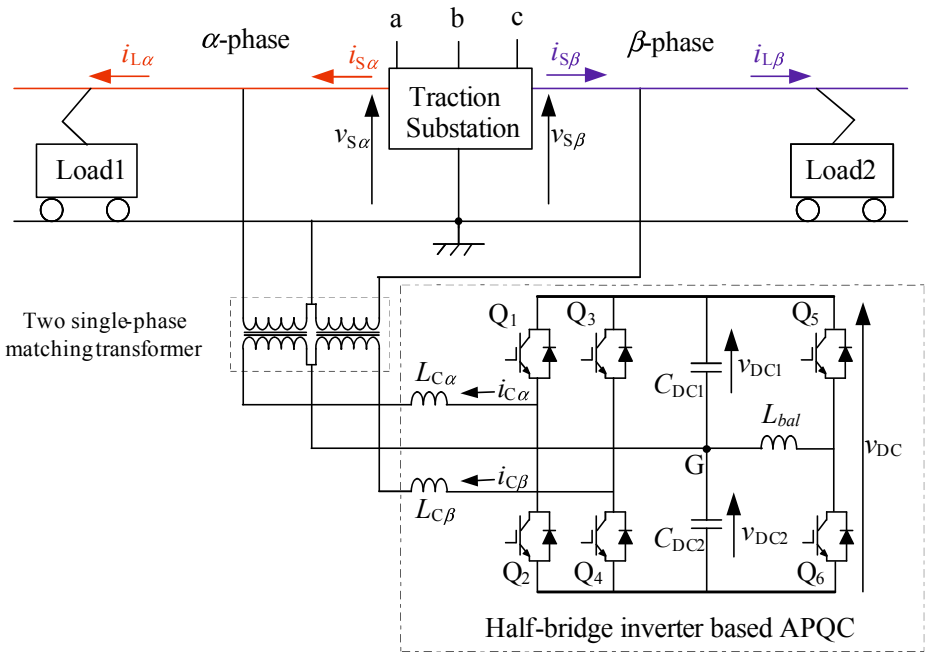

Figure 4.1: Power circuit diagram of half-bridge inverter based APQC with constant DC capacitor voltage control strategy.

two common DC capacitors, compensating reactive and harmonic components of the distorted load currents. The third-leg is used for two DC capacitors voltage control with a small amount of output currents as described in previous chapter.

4.2 Control Strategy

A control strategy of the half-bridge inverter based APQC with constant DC capacitor voltage control has two parts. Figure 4.2(a) shows the two half-bridge inverters control and Figure 4.2(b) shows the two DC capacitors voltage balancing control. The main difference between the Figure 3.2 in the section 3.2 and the Figure 4.2 is the two half-bridge inverters control strategy. In a new control strategy, a constant DC capacitor voltage control strategy is used for active load currents calculation. Therefore, any calculation blocks of the load currents are not necessary for the active load current detection in a new constant DC capacitor voltage control strategy.

The basic principle of a constant DC capacitor voltage control strategy is discussed. Let the

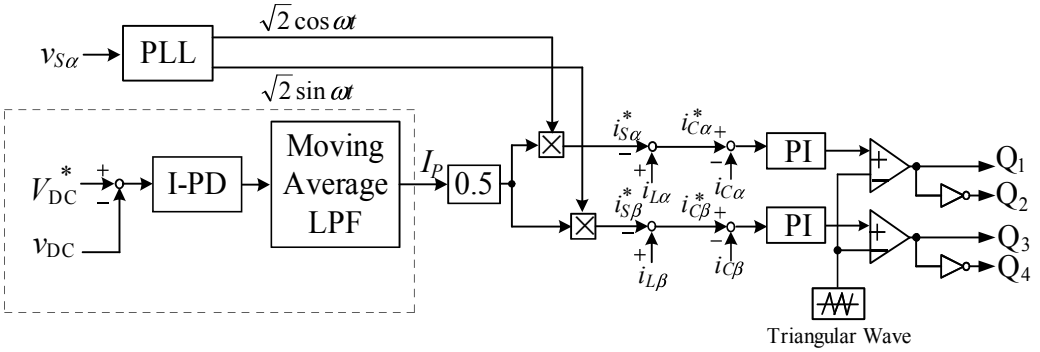

(a) For two half-bridge inverter

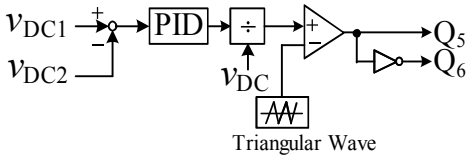

(b) For DC voltage balancer

Figure 4.2: Control strategy of proposed APQC using constant DC capacitor voltage control.

two load currents on α- and β-phase in Figure 4.1 be

$$\begin{aligned} i_{L\alpha} &= \sqrt{2}I_{1\alpha}\cos(\omega t - \phi_{1\alpha}) + \sqrt{2}I_{h\alpha}\cos(h\omega t - \phi_{h\alpha}) \\ &= \sqrt{2}I_{1\alpha}(\cos\phi_{1\alpha}\cos\omega t + \sin\phi_{1\alpha}\sin\omega t) + \sqrt{2}I_{h\alpha}\cos(h\omega t - \phi_{h\alpha}), \\ i_{L\beta} &= \sqrt{2}I_{1\beta}\sin(\omega t - \phi_{1\beta}) + \sqrt{2}I_{h\beta}\sin(h\omega t - \phi_{h\beta}) \\ &= \sqrt{2}I_{1\beta}(\cos\phi_{1\beta}\sin\omega t - \sin\phi_{1\beta}\cos\omega t) + \sqrt{2}I_{h\beta}\sin(h\omega t - \phi_{h\beta}). \end{aligned} \tag{4.1}$$

Let assume that the source currents $i_{S\alpha}$ and $i_{S\beta}$ for the secondary side of the Scott transformer are balanced and sinusoidal after compensating unbalanced active load currents, reactive and harmonic components. At this condition, the source currents can be expressed as

$$\begin{aligned} i_{S\alpha} &= \sqrt{2}I_S\cos\omega t, \\ i_{S\beta} &= \sqrt{2}I_S\sin\omega t, \end{aligned} \tag{4.2}$$

where $I_S = (I_{1\alpha}\cos\phi_{1\alpha} + I_{1\beta}\cos\phi_{1\beta})/2$ is the rms value of the average fundamental active current of the two loads.

From the power circuit diagram of the Figure 4.1, the output currents of APQC are given by

$$\begin{aligned} i_{C\alpha} &= i_{L\alpha} - i_{S\alpha} \\ &= \frac{\sqrt{2}}{2}(I_{1\alpha}\cos\phi_{1\alpha} - I_{1\beta}\cos\phi_{1\beta})\cos\omega t + \sqrt{2}I_{1\alpha}\sin\phi_{1\alpha}\sin\omega t \\ &\quad + \sqrt{2}I_{h\alpha}\cos(h\omega t - \phi_{h\alpha}), \\ i_{C\beta} &= i_{L\beta} - i_{S\beta} \\ &= \frac{\sqrt{2}}{2}(I_{1\beta}\cos\phi_{1\beta} - I_{1\alpha}\cos\phi_{1\alpha})\sin\omega t - \sqrt{2}I_{1\beta}\sin\phi_{1\beta}\cos\omega t \\ &\quad + \sqrt{2}I_{h\beta}\sin(h\omega t - \phi_{h\beta}). \end{aligned} \tag{4.3}$$

The α- and β-phase voltages $v_{S\alpha}$ $v_{S\beta}$ are given as

$$\begin{aligned} v_{S\alpha} &= \sqrt{2}V_S\cos\omega t, \\ v_{S\beta} &= \sqrt{2}V_S\sin\omega t. \end{aligned} \tag{4.4}$$

By Equations (4.3) and (4.4) , the instantaneous power p_C flowing to the APQC are expressed as

$$\begin{aligned} p_C &= v_{S\alpha}\cdot i_{C\alpha} + v_{S\beta}\cdot i_{C\beta} \\ &= V_S(I_{1\alpha}\cos\phi_{1\alpha} - I_{1\beta}\cos\phi_{1\beta})\cos 2\omega t \\ &\quad + V_S I_{h\alpha}\Big[\cos\{(h+1)\omega t - \phi_{h\alpha}\} + \cos\{(h-1)\omega t - \phi_{h\alpha}\}\Big] \\ &\quad + V_S(I_{1\alpha}\sin\phi_{1\alpha} - I_{1\beta}\sin\phi_{1\beta})\sin 2\omega t \\ &\quad - V_S I_{h\beta}\Big[\cos\{(h+1)\omega t - \phi_{h\beta}\} - \cos\{(h-1)\omega t - \phi_{h\beta}\}\Big] \end{aligned} \tag{4.5}$$

The instantaneous power in (4.5) does not include DC components, and therefore the mean value of p_C becomes zero. The balanced source currents $i_{S\alpha}$ and $i_{S\beta}$ with unity power factor in (4.2) are used in instantaneous power calculation. Therefore maintaining the DC capacitor voltage at a constant in a APQC means that the APQC controls the two source currents so the balanced and sinusoidal source currents are achieved. Therefore, constant DC capacitor voltage control strategy can generate effective active load current without any instantaneous power calculation. In the actual operation, the DC capacitor voltage can not be constant because of the unbalanced load currents. Thus, we control the constant mean value of DC capacitor voltage.

To perform a constant DC capacitor voltage control based strategy, the DC capacitor voltage v_{DC} is detected, and then the difference between the reference DC capacitor voltage V_{DC}^* and

the detected DC capacitor voltage v_{DC} is calculated as shown in Figure 4.2. This difference is amplified by the I-PD controller. The amplified value is filtered with moving average low pass filter (LPF) to remove 2ω components, which is caused by the unbalanced load condition. The transfer function of the moving-average LPF is expressed as

$$H(z) = \frac{1}{N} \sum_{n=0}^{N-1} z^{-n}, \tag{4.6}$$

where N is the number of samples. After filtering with the moving-average LPF, the effective value I_P of the source-side active current is obtained by performing constant DC capacitor voltage control. This value is used for two half-bridge inverters control to achieve APQC operation.

In Figure 4.2, $\sqrt{2}\cos\omega t$, which is synchronized with electrical angle of $v_{S\alpha}$ and $\sqrt{2}\sin\omega t$, which is synchronized with electrical angle of $v_{S\beta}$ are generated from the single-phase PLL circuit in dq coordinate [25]. Then the reference source currents $i_{S\alpha}^*$ and $i_{S\beta}^*$ are calculated using the effective value I_P as expressed in below:

$$\begin{aligned} i_{S\alpha}^* &= \sqrt{2} I_P' \cos\omega t, \\ i_{S\beta}^* &= \sqrt{2} I_P' \sin\omega t, \end{aligned} \tag{4.7}$$

where $I_P' = I_P/2$.

The compensation reference signals $i_{C\alpha}^*$ and $i_{C\beta}^*$ of PWM inverters for the two half-bridge inverters are given by

$$\begin{aligned} i_{C\alpha}^* &= i_{L\alpha} - i_{S\alpha}^* \\ i_{C\beta}^* &= i_{L\beta} - i_{S\beta}^* \end{aligned} \tag{4.8}$$

Then, using the PI current feedback control and sine-triangle intercept pulse width modulation technique, the control strategy generates four gate signals for the two half-bridge inverters.

In the DC voltage balancer control, the two DC capacitor voltage, v_{DC1} and v_{DC2}, are detected. Then the difference between v_{DC1} and v_{DC2} is amplified by the PI controller to generate control waveform of the switches Q_5 and Q_6. These switches are controlled by the sine-triangle intercept technique, where the switching frequency is 15kHz.

4.3 Simulation Results

To confirm the proposed half-bridge inverter based APQC with DC voltage balancer, the computer simulation using PSIM software is performed. The circuit parameters of APQC and load conditions are the same as in the section 3.3 of Tables 3.1 and 3.2 except the reference DC capacitor voltage. The reference value of DC-bus voltage v^*_{DC} is 380 V in this simulation. In the electrified railways operations, the load currents are rapidly changed from the rated currents to standby current when the locomotives start coasting operation. On the other hand, the standby currents are rapidly changed to rated currents with different load characteristic when the locomotives start regenerative breaking and accelerating operation from coasting condition. Therefore the proposed APQC is demonstrated with all possible load variations to cope with actual electrified railways operations.

4.3.1 Simulation Results for Coasting Operation

Figure 4.3 shows the simulation results using the proposed new constant DC capacitor voltage control strategy, where the α-phase load current $i_{L\alpha}$ was kept constant in 0.05 pu and β-phase load current $i_{L\beta}$ was changed from 0.5 pu to 0.05 pu. This simulation demonstrates that the coasting operation when the speed of locomotive is reached to coast on β-phase. $v_{S\alpha}$ and $v_{S\beta}$ show the α- and β-phase voltages on the secondary side of the Scott transformer. $i_{S\alpha}$ and $i_{S\beta}$ are the source side currents. $i_{L\alpha}$ and $i_{L\beta}$ are load side currents, which are heavily distorted and unbalanced. Before/after the β-phase load current $i_{L\beta}$ was changed, the source side currents $i_{S\alpha}$ and $i_{S\beta}$ are balanced and sinusoidal. The two DC capacitor voltages, v_{DC1} and v_{DC2}, are balance and ripple amount is 6% in transient-state and ±1.0% in steady-state.

4.3.2 Simulation Results for Accelerating Operation

Figure 4.4 shows simulation results for the accelerating operation. The α-phase load current $i_{L\alpha}$ was kept constant in 0.05 pu and β-phase load current $i_{L\beta}$ was changed from 0.05 pu to 0.5 pu. Before/after β-phase load current $i_{L\beta}$ was changed, the source side currents $i_{S\alpha}$ and $i_{S\beta}$ are balanced and sinusoidal. The THD% of the α-phase source-side currents $i_{S\alpha}$ is 3.2% and β-phase source-side currents $i_{S\beta}$ is 5.5%. The two DC capacitors voltage is balanced and, the ripple

amount is 5.6% in transient-state and ±2.1% in steady-state.

4.3.3 Simulation Results for Regenerative Breaking Operation

Figure 4.5 shows simulation waveforms that demonstrate the regenerative breaking operation of the locomotive, where β-phase load current $i_{L\beta}$ was rapidly changed from 0.05 pu to 0.5 pu in the opposite direction of the normal load current. Before/after the β-phase load current $i_{L\beta}$ was changed, the source side currents, $i_{S\alpha}$ and $i_{S\beta}$, are balanced and sinusoidal. The compensation current $i_{C\beta}$ on β-phase is 9.0A rms and balancing inductor current i_{bal} is 4.2A rms. Therefore the third-leg needs smaller current rating in this mode of operation also. The ripple amount of DC capacitors, v_{DC1} and v_{DC2} are 7.2% in the transient-state and ±2.5% in the steady-state.

Table 4.1 summarizes the total harmonic distortion (THD%) of the source currents after compensating the harmonic components under balanced load conditions and the load currents .

Table 4.1: The total harmonic distortion (THD%) of source currents and load currents in the simulation (with constant DC capacitor voltage control).

	Source currents (THD%)	Load currents (THD%)
α-phase	3.2%	21%
β-phase	5.5%	24%

From the simulation results, the required current rating in root mean square (rms) value of power switching devices in the proposed half-bridge inverter based APQC with constant DC capacitor voltage control strategy are shown in Table 4.2.

Table 4.2: The required current rating of the proposed half-bridge inverter based APQC in the simulation (with constant DC capacitor voltage control).

	In normal operation	In regenerative breaking operation
First-leg current (A)	4.3 A	4.7 A
Second-leg current (A)	10.5 A	8.8 A
Third-leg current (A)	2.5 A	5.5 A

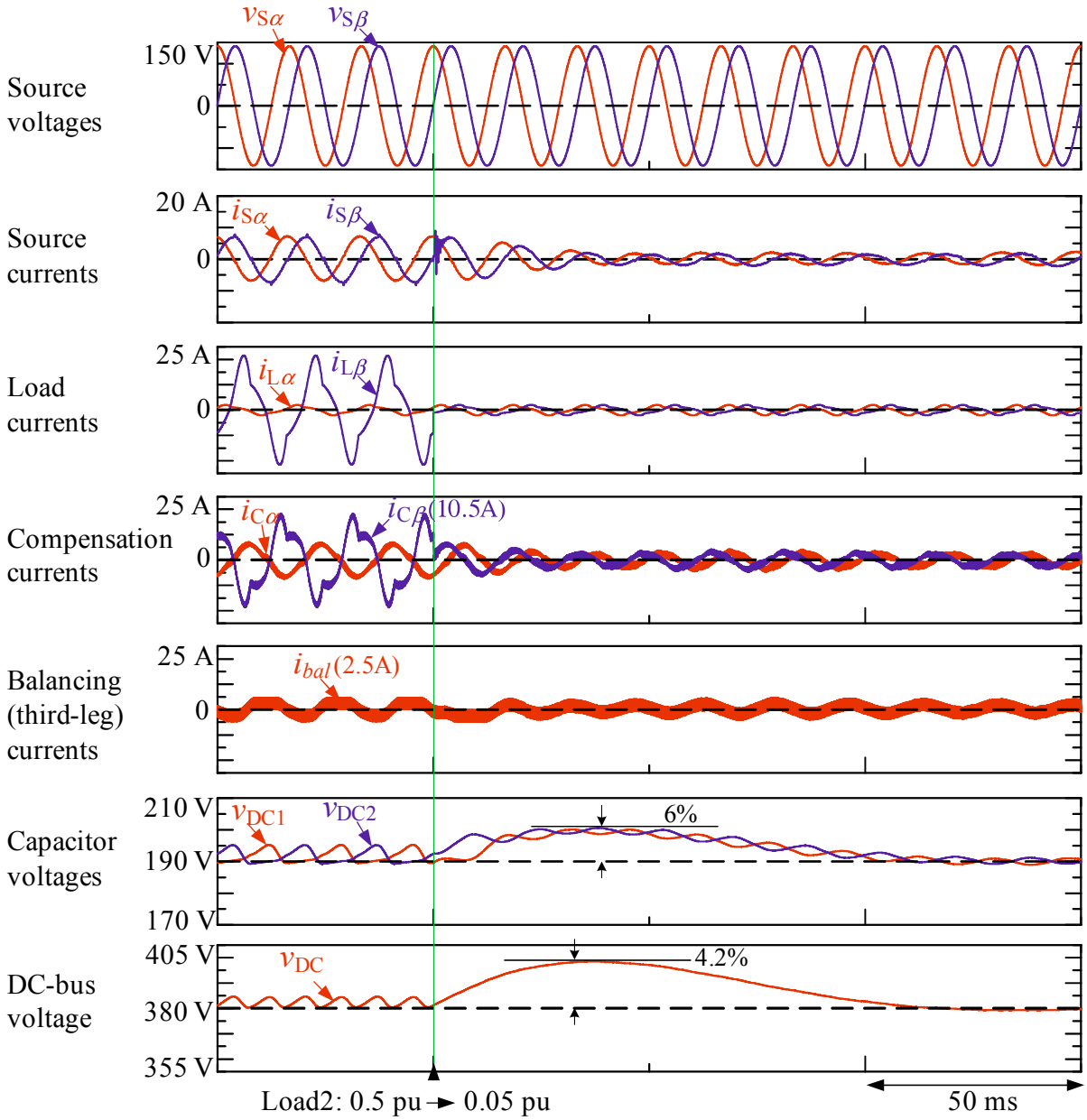

Figure 4.3: Simulation waveforms for coasting operation using constant DC capacitor voltage control (Load2 is changed from 0.5 pu to 0.05 pu).

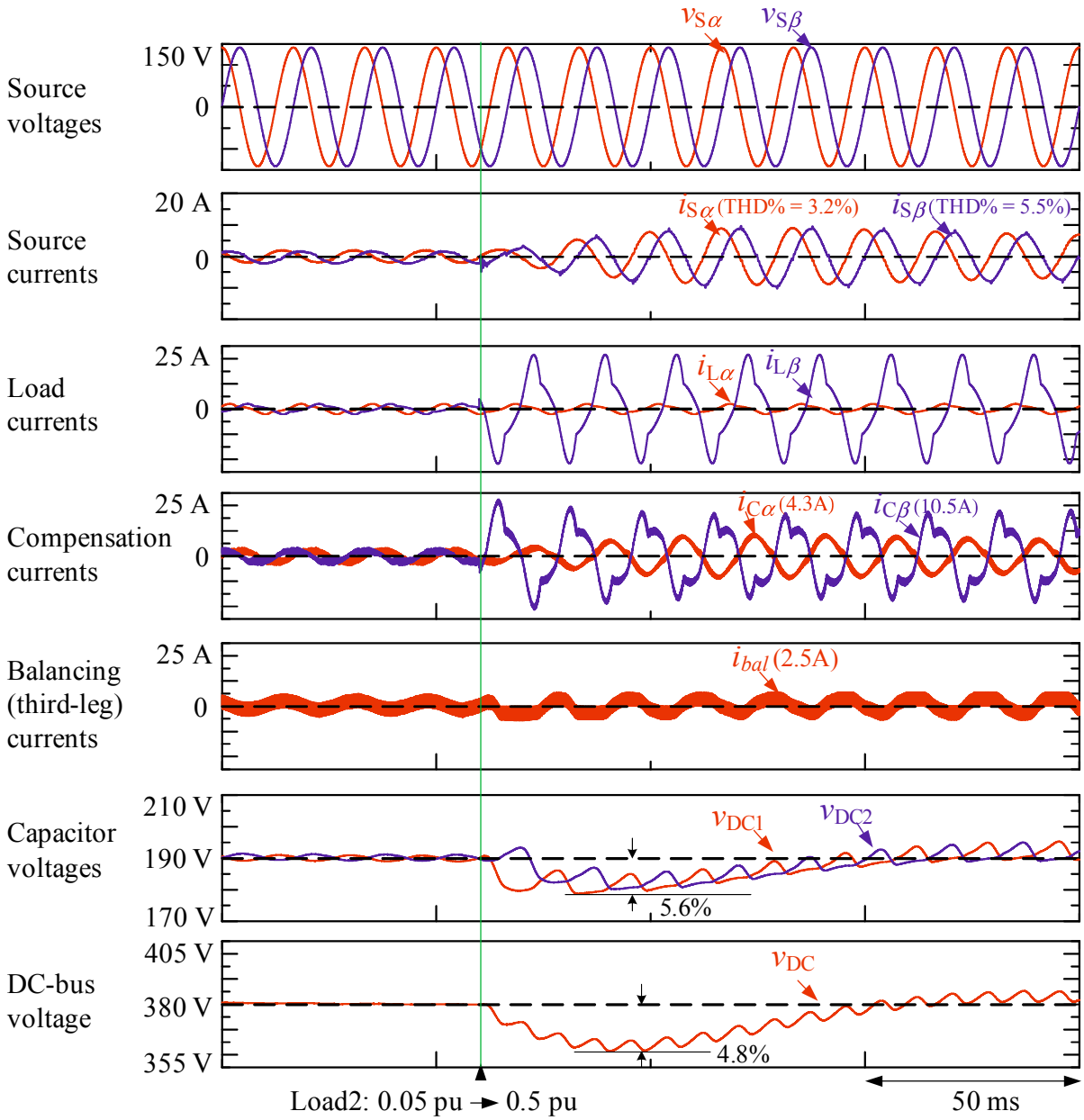

Figure 4.4: Simulation waveforms for accelerating operation using constant DC capacitor voltage control (Load2 is changed from 0.05 pu to 0.5 pu).

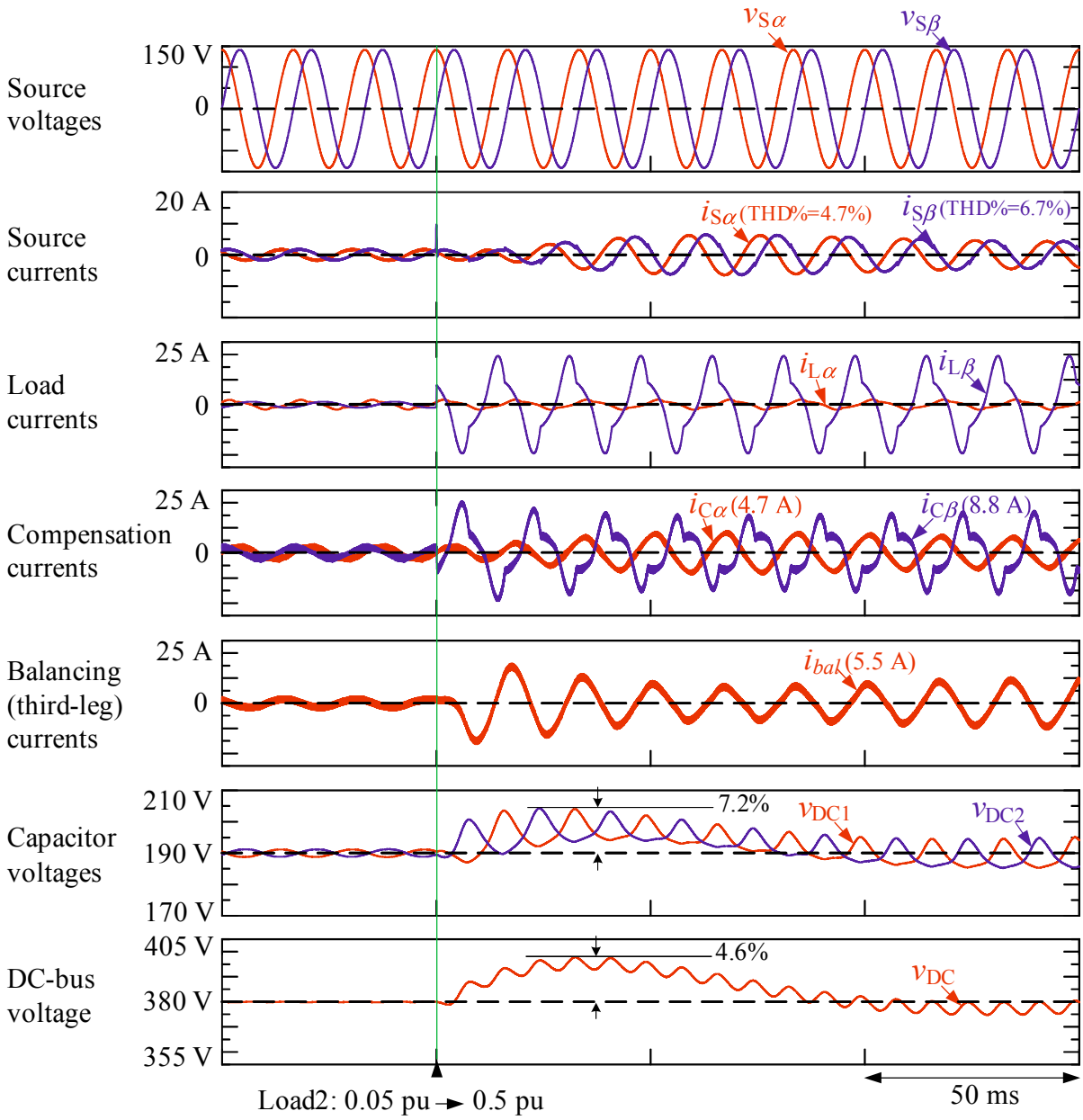

Figure 4.5: Simulation waveforms for regenerative breaking operation using constant DC capacitor voltage control.

4.4 Experimental Setup

Figure 4.6 shows the constructed experimental model for the half-bridge inverter based APQC with constant DC capacitor voltage control.

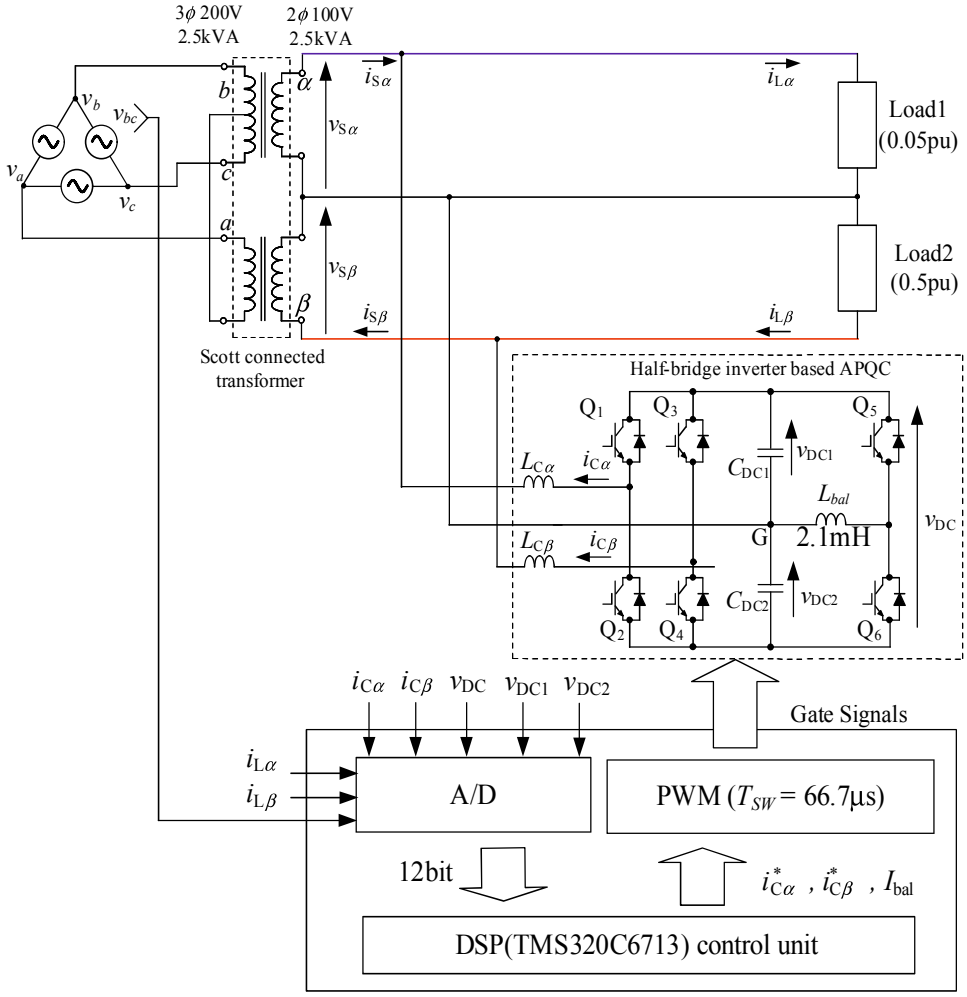

Figure 4.6: Constructed experimental model of the APQC with constant DC capacitor voltage control strategy.

The experimental setup, circuit parameters of the APQC, and load conditions are the same as in the section 3.5 of chapter 3. The same unbalanced load conditions and harmonic contents shown in Table 3.1 are also used in this experiment. The circuit parameter of the APQC are all the same as in Table 3.2 except the reference DC capacitor voltage. In this experiment, the reference DC capacitor voltage V_{DC}^{*} is 380 V. The constant DC capacitor voltage control strategy for the

half-bridge inverter based APQC is used in this experiment, which is different from the previous DC voltage balancer control strategy in chapter3.

4.5 Experiment Results

4.5.1 Experimental Results for Coasting Operation

Figure 4.7 shows experiment results of the half-bridge inverter based APQC with constant DC capacitor voltage control. Load1 with 0.05 pu was kept constant in α-phase and Load2 was changed from 0.5 pu to 0.05 pu in β-phase. This experiment demonstrates that the locomotive is just in the coasting operation from the accelerating on β-phase. The load variation in the experiment is faster than the actual railways operations. Therefore, this experiment results is enough to examine transient response of the proposed APQC system. $v_{S\alpha}$ and $v_{S\beta}$ show the α-phase and β-phase voltages on the secondary side of the Scott transformer. $i_{S\alpha}$ and $i_{S\beta}$ are the source side currents. $i_{L\alpha}$ and $i_{L\beta}$ are load side currents, which are heavily distorted and unbalanced conditions. $i_{C\alpha}$ and $i_{C\beta}$ are the output currents of the half-bridge based PWM inverter, which performs the active power quality compensator. Balancing (third-leg) current i_{bal} balances the two DC capacitor voltages. v_{DC1}, v_{DC2} show each DC capacitor voltage and v_{DC} is the sum of v_{DC1} and v_{DC2} voltages. The reference DC-bus line voltage V_{DC}^{*} in this experiment is 380V. Before/after the Load2 was changed on β-phase, the source side current $i_{S\alpha}$ and $i_{S\beta}$ are also balanced and sinusoidal. Increasing the ripple amount of capacitor voltage should be avoided when loads were changed from the heavy condition to the light one. In Figure 4.7, The two DC capacitor voltages, v_{DC1} and v_{DC2}, are balance and ripple amount is 6% in transient-state and ±1.0% steady-state.

4.5.2 Experimental Results for Accelerating Operation

Figure 4.8 shows experiment results in which load2 was changed from 0.05 pu to 0.5 pu while load1 was kept at constant 0.05 pu. The unbalanced between the 0.05 pu and 0.5 pu is the worst load unbalanced condition. This experiment demonstrates that the locomotive on the β-phase is just accelerating from coasting. The load variation is very rapid compare to the actual railways operations. Therefore, this experiment results is enough to examine transient response of the

proposed APQC system when light to heavy load variation. Before/after the β-phase load current $i_{L\beta}$ was changed, the source side current $i_{S\alpha}$ and $i_{S\beta}$ are also balanced and sinusoidal. The THD% of $i_{S\alpha}$ is 3.9% and $i_{S\beta}$ is 6.8%. The two DC capacitors voltage is balance and the ripple amount are 6% in transient-state and ±2.1% in steady-state. The balancing inductor current i_{bal} is 5.82 A rms although the compensation currents $i_{C\alpha}$, $i_{C\beta}$ are 4.41 A rms and 9.59 A rms, respectively in the steady-state. Therefore, the third-leg current rating can be reduced by the experimental verification.

4.5.3 Experimental Results for Regenerative Breaking Operation

In regenerative breaking operation, the load current should be opposite direction to that of source voltage like in Figure 4.5. However, this exact load condition is difficult to construct in the experiment model because the load current direction must be opposite before and after load change. The simulation results for accelerating and coasting operation well agree with the experiment results. Therefore we refer to the simulation results for the regenerative breaking operation.

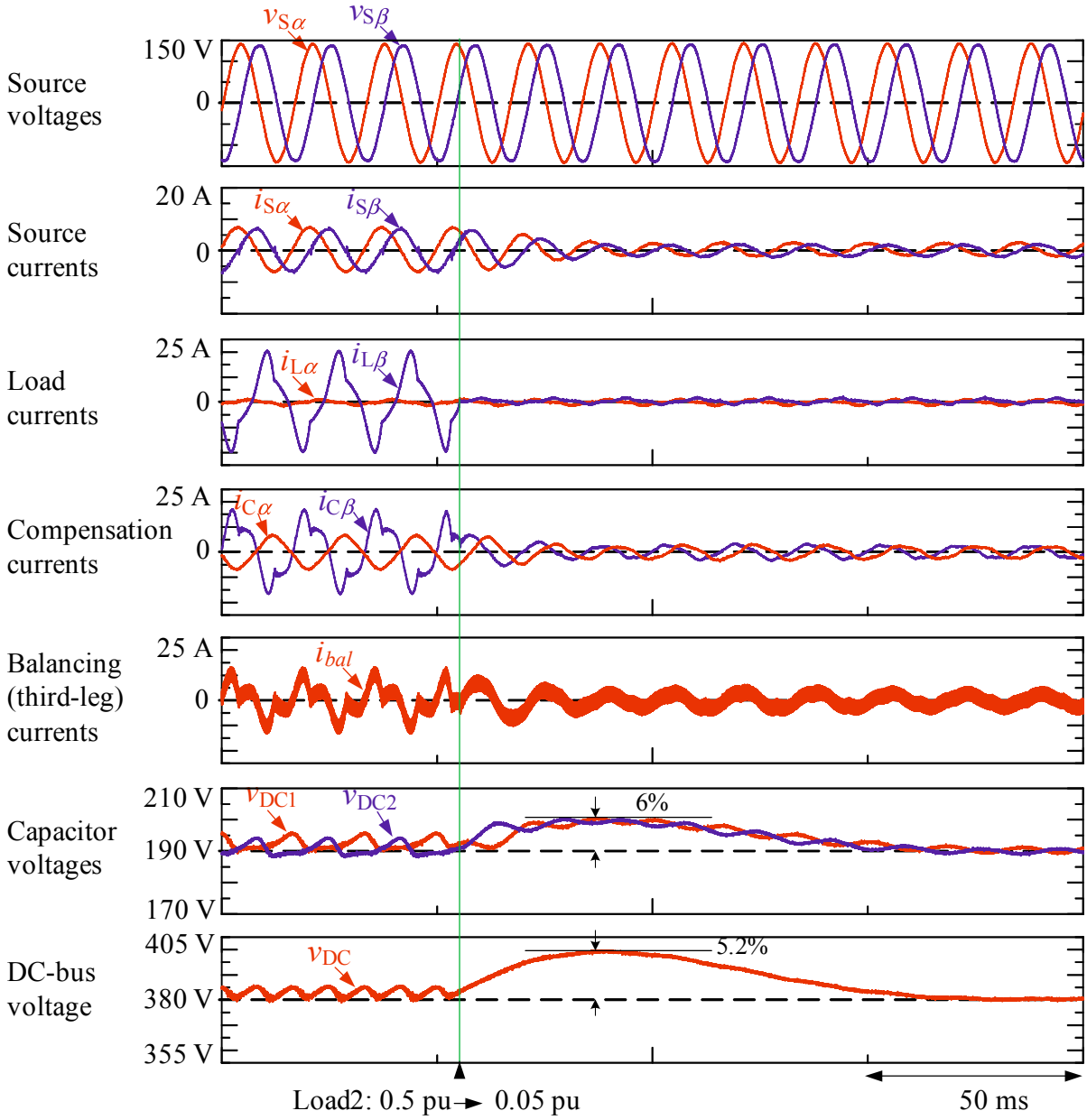

Figure 4.7: Experimental results of coasting operation using constant DC capacitor voltage control (Load2 is changed from 0.5 pu to 0.05 pu).

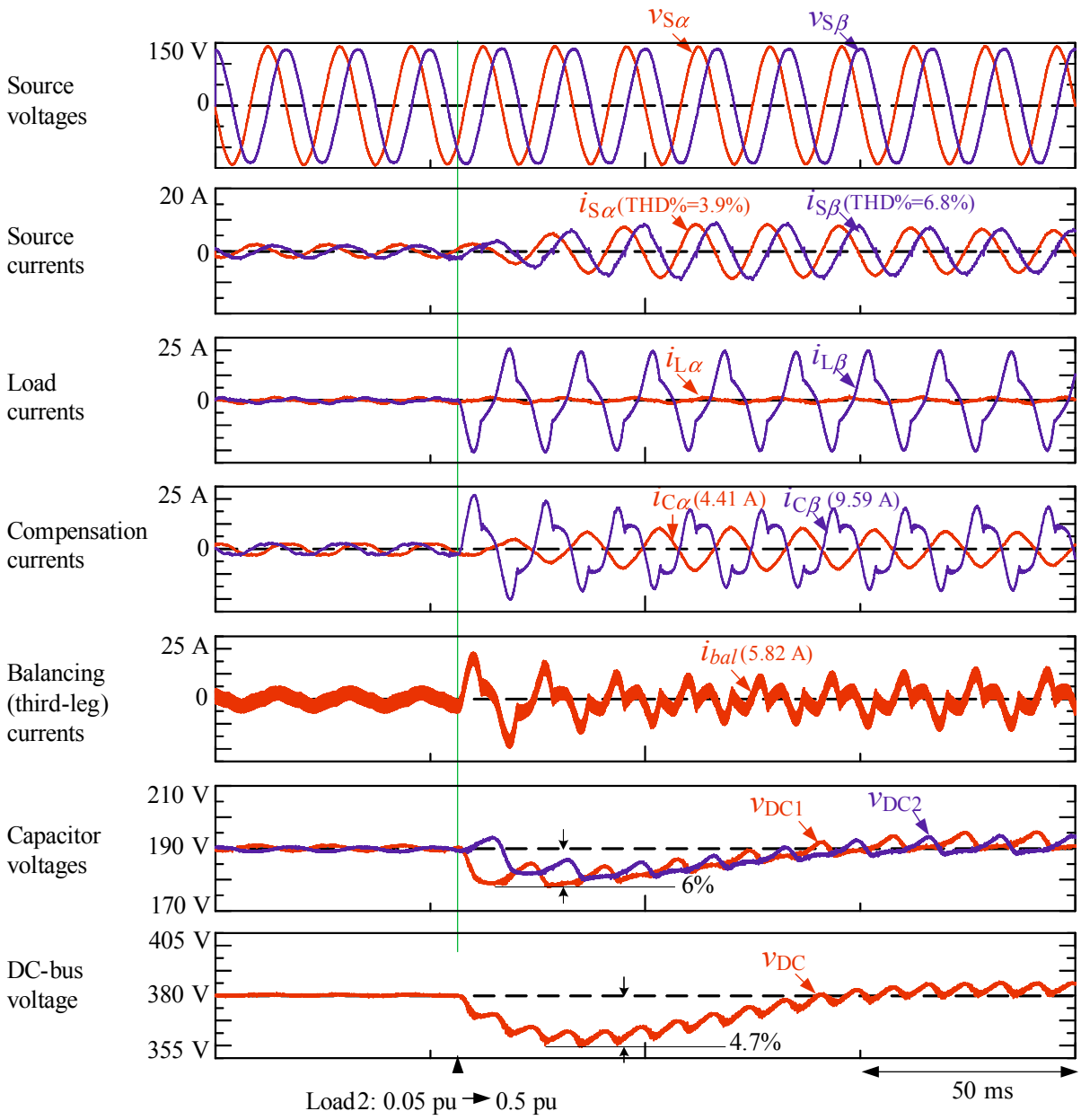

Figure 4.8: Experimental results of accelerating operation using constant DC capacitor voltage control (Load2 is changed from 0.05 pu to 0.5 pu).

Table 4.3 shows the total harmonic distortion (THD%) of the source currents after compensating the harmonic components under balanced load conditions and the load currents.

Table 4.3: The total harmonic distortion (THD%) of source currents and load currents in the experiment.

	Source currents (THD%)	Load currents (THD%)
α-phase	3.9%	21%
β-phase	6.8%	24%

From the experimental results, the required current rating in root mean square (rms) value of power switching devices in the proposed half-bridge inverter based APQC are shown in Table 4.4.

Table 4.4: Comparison of required current rating in the proposed half-bridge inverter based APQC in the experiment.

	In normal operation
First-leg current (A)	4.41 A
Second-leg current (A)	9.59 A
Third-leg current (A)	5.82 A

4.6 Conclusion

In this chapter, the half-bridge inverter based Active Power Quality Compensator with constant DC capacitor voltage control is discussed. The constant DC capacitor voltage control is used not only for DC-link voltage control but also for the effective load currents generation. Therefore, the calculation block of the effective load current detection blocks likes FBD-method [24] is reduced in the control algorithm. The calculation time requirement for the experimental program is discussed. Figure 4.9(a) shows the number of counter of the DSP to run the half-bridge inverter based APQC with DC voltage balancer control program in the section 3.2 and Figure 4.9(b) shows

the number of counter of the DSP to run the half-bridge inverter based APQC with constant DC capacitor voltage control program. T0 is the program begin-time counter recorder and the T1 is

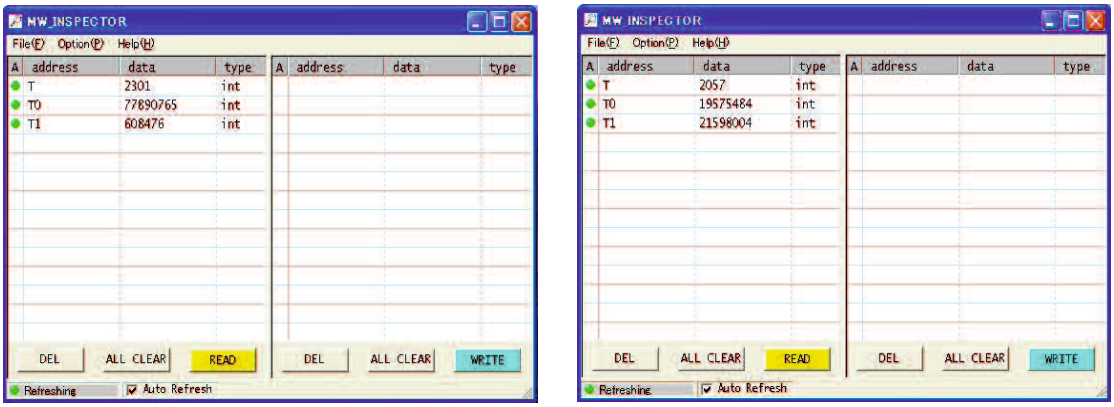

(a) Number of counter for the DC voltage balancer control

(b) Number of counter for the constant DC capacitor voltage control

Figure 4.9: The number of counter of the DSP for DC voltage balancer control strategy and constant DC capacitor voltage control strategy.

the program end-time counter recorder. T is the number of counter for one cycle execution of the program. The DSP clock speed is 225 Mz but the system counter records four cycle per one time. The one counter period of DSP is calculated as

$$T_{counter} = 4/225 \text{ Mz} \tag{4.9}$$

Therefore, the calculation time for the DC voltage balancer control program for one cycle is $2301 * T_{counter} = 40.9\ \mu s$ and the calculation time for constant DC capacitor voltage control program for one cycle is $2057 * T_{counter} = 36.5\ \mu s$. Therefore, the half-bridge inverter based APQC with constant DC capacitor voltage control reduces calculation time by 4.4 μs than the previous control strategy. This simple constant DC capacitor voltage control strategy based APQC has been published in the Institute of Electrical Engineer of Japan (IEEJ) Transactions 2013.

Chapter 5

Constant DC Capacitor Voltage Control Based Strategy for Active Load Balancer in Three-Phase Four-Wire Distribution Systems

5.1 Introduction

In the previous two chapters, the active power quality compensator (APQC) was discussed in the electrified railways systems. These APQC are single-phase power filter systems and their control strategies are specially designed for the single-phase power feeding system. In this chapter, three-phase active power line conditioners and their control strategies in three-phase four-wire distribution systems are discussed.

Electric power distribution is the final state in the delivery of the electric power. In this state, a wide variety of distribution systems are used worldwide for single-phase and three-phase power supply. Figure 5.1 shows the some type of distribution systems for the residential and commercial loads, which are either single-phase or three-phase loads. Among them, three-phase four-wire Y-connected distribution system can supply both single-phase power and three-phase power simultaneously. Therefore, this distribution system are widely used in Europe, and some Asian countries likes Singapore, Korea and Myanmar. However, the drawbacks of the three-phase four-wire distribution system is unbalanced load condition in the distribution transformer as well as in the distribution systems. This unbalanced condition of transformer results in excessive neutral current and higher loss in the distribution transformer. The unbalanced load conditions also cause the unbalanced voltage on the distribution system. The adverse effect of unbalanced

voltages on the consumer appliances, especially on the motor, are described in the section 2.3.3 of Chapter 2. To solve these power quality problem, three-phase active load balancer (ALB), which is a type of three-phase power line conditioner, are proposed in the three-phase four-wire distribution areas. In the next section, the various circuit topologies of the three-phase ALB in three-phase four-wire distribution systems are discussed in detail. Then, the existing three-phase active power line conditioners are analyzed with their control strategies. Finally, the basic principle of the proposed constant DC capacitor voltage control strategy for the active load balancer in three-phase four-wire distribution system is discussed.

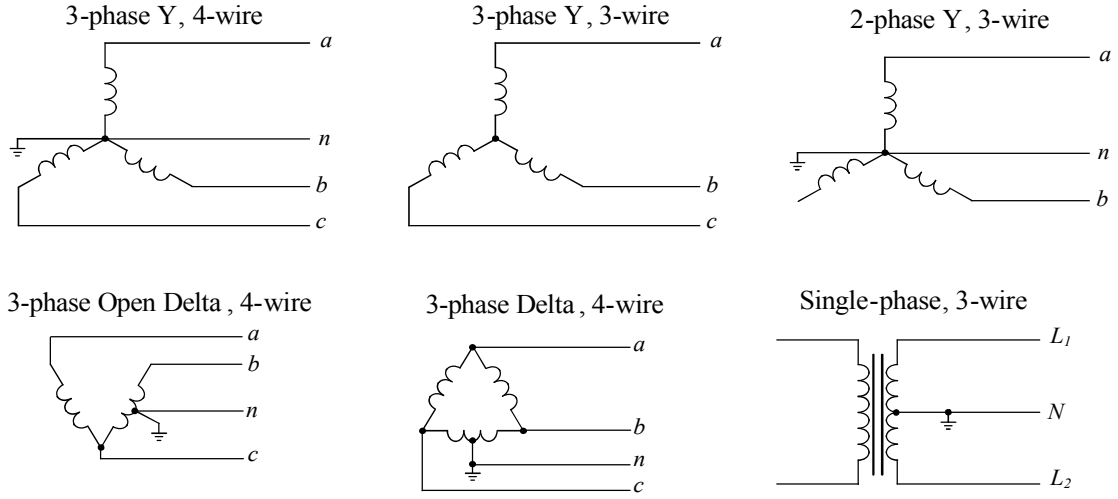

Figure 5.1: Distribution systems for residential and commercial loads.

5.2 Power Circuit Topologies and Existing Control Strategy for Active Load Balancer

The primary function of active load balancer (ALB) is to compensate unbalanced active currents and reactive components to get the balanced currents with high power factor in the distribution systems. In three-phase four-wire distribution systems, zero-sequence current must be included in the compensation currents to get perfect compensation facility. In general, the three-phase active load balancer are designed based on power rating of the system, the distribution system types and required compensation functions. In this section, three-phase active load balancer topologies and existing control strategies in three-phase four-wire distribution systems are discussed.

The inverter topologies in low voltage application areas are basically half-bridge and full-bridge inverter design. In the three-phase four-wire distribution system, the possible inverter topologies for the active load balancer are summarized in below:

- three-leg inverter based ALB with a common DC capacitor;
- three-leg inverter based ALB with two DC capacitors;
- four-leg inverter based ALB with a common DC capacitor.

5.2.1 Three-leg Inverter Based ALB with a Common DC Capacitor

Figure 5.2 shows three-leg inverter based ALB in three-phase four-wire distribution system. The distribution system is composed of three-phase four-wire Y-connected distribution transformer and three single-phase loads. v_{Sa}, v_{Sb} and v_{Sc} are three sources of distribution transformer with neutral grounded. R_a, L_a, R_b, L_b and R_c, L_c are the three single-phase loads. The three legs of the inverter is connected to each phase of the distribution system. Therefore, the load side neutral is directly connected to source side neutral. The three legs generate the compensation currents for each phase.

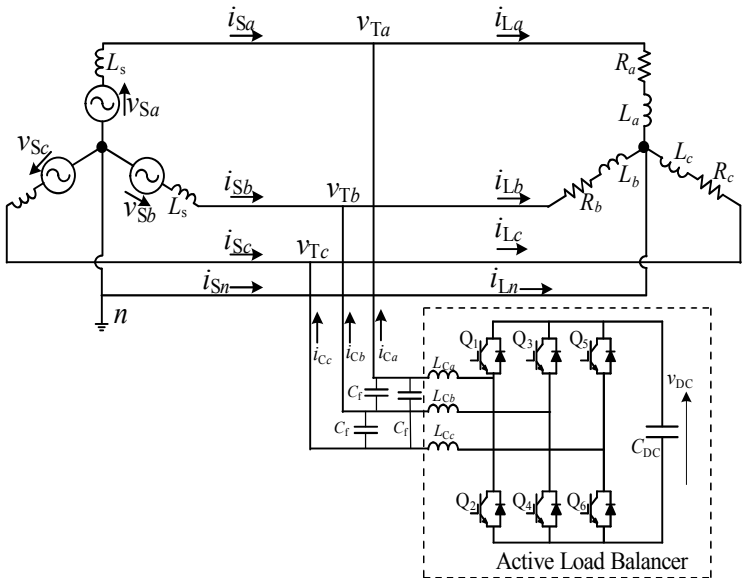

Figure 5.2: Three-leg inverter based ALB with a common DC capacitor.

Figure 5.3 shows the switching patterns of the power devices in three-leg inverter. The switching patterns perform as phase to phase operation due to the lack of fourth leg power devices. From this switching patterns, the equivalent circuit of three-leg inverter based ALB is depicted as Figure 5.4.

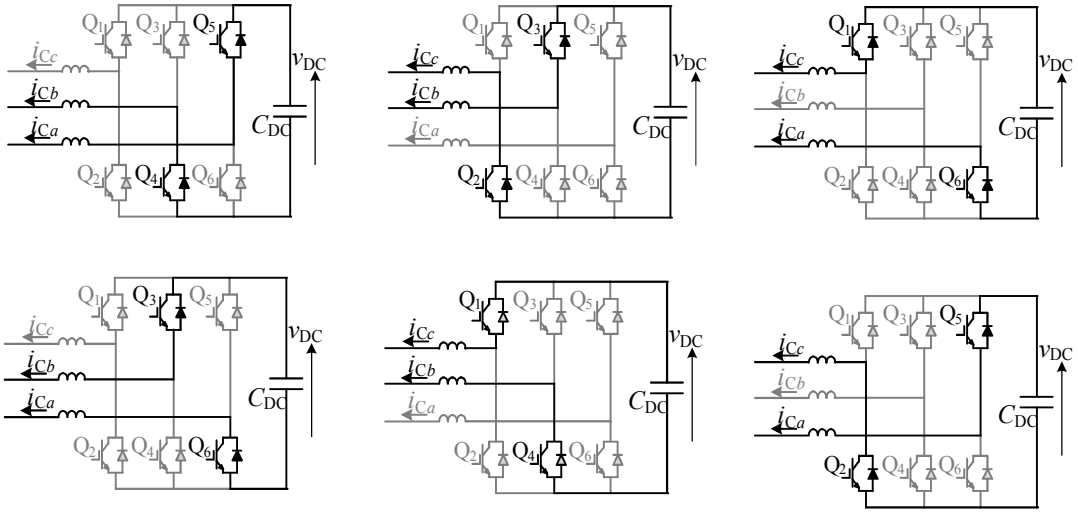

Figure 5.3: Switching patterns in three-leg inverter with a common DC capacitor.

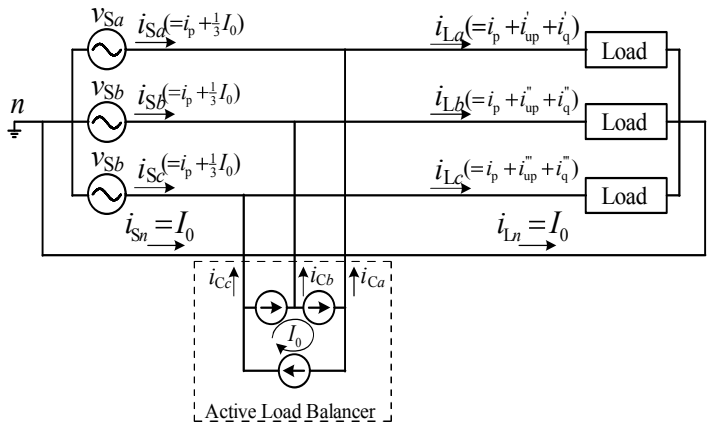

Figure 5.4: Equivalent circuit of three-leg based ALB in three-phase four-wire distribution system.

In this equivalent circuit,

$$
\begin{aligned}
i_{\mathrm{p}} &= \text{average active component of the three load currents,} \\
i_{\mathrm{up}},\ i_{\mathrm{q}} &= \text{unbalanced active component and reactive component of each load currents,} \\
I_0 &= i_{\mathrm{L}a} + i_{\mathrm{L}b} + i_{\mathrm{L}c} = \text{ zero sequence current,} \\
i_{\mathrm{C}a} &= i_{\mathrm{up}}^{'} + i_{\mathrm{q}}^{'} \text{ (without } \frac{1}{3} I_0 \text{ component),} \\
i_{\mathrm{C}b} &= i_{\mathrm{up}}^{''} + i_{\mathrm{q}}^{''} \text{ (without } \frac{1}{3} I_0 \text{ component),} \\
i_{\mathrm{C}c} &= i_{\mathrm{up}}^{'''} + i_{\mathrm{q}}^{'''} \text{ (without } \frac{1}{3} I_0 \text{ component),} \\
\frac{1}{3} I_0 &= \text{zero sequence current component for each phase.}
\end{aligned}
$$

Figure 5.5 shows simulation results of Fig 5.2 with three legs inverter based ALB. $v_{\mathrm{T}a}$, $v_{\mathrm{T}b}$ and $v_{\mathrm{T}c}$ are the a-phase terminal voltage, the b-phase terminal voltage and the c-phase terminal voltage. $i_{\mathrm{S}a}$, $i_{\mathrm{S}b}$ and $i_{\mathrm{S}c}$ are source side currents. $i_{\mathrm{L}a}$, $i_{\mathrm{L}b}$ and $i_{\mathrm{L}c}$ are three single-phase unbalanced load currents and $i_{\mathrm{L}n}$ are neutral line (zero-sequence) current. $i_{\mathrm{C}a}$, $i_{\mathrm{C}b}$ and $i_{\mathrm{C}c}$ are compensation currents generated by ALB. In the simulation results, we can see that the the source side currents $i_{\mathrm{S}a}$, $i_{\mathrm{S}b}$ and $i_{\mathrm{S}c}$ are not balanced. In addition, the simulation results show that the combination of three source currents ($i_{\mathrm{S}a} + i_{\mathrm{S}b} + i_{\mathrm{S}c}$) give the same zero-sequence current ($I_0 = i_{\mathrm{L}a} + i_{\mathrm{L}b} + i_{\mathrm{L}c}$) from the load sides. Therefore, the zero sequence current component cannot be compensated by the ALB. To confirm that, each zero sequence current is removed from each source side currents as ($i_{\mathrm{S}a} - \frac{1}{3} I_0$), ($i_{\mathrm{S}b} - \frac{1}{3} I_0$) and ($i_{\mathrm{S}c} - \frac{1}{3} I_0$). After removing the zero-sequence component from each source current, the balanced source currents can be achieved as shown in lowest waveforms of Figure 5.5. Therefore, the simulation results confirm that the three legs inverter based ALB with a common DC capacitor cannot compensate the zero-sequence current in the three-phase four-wire distribution systems. The DC capacitor voltage v_{DC} is well controlled to its reference value V_{DC}^{*}.

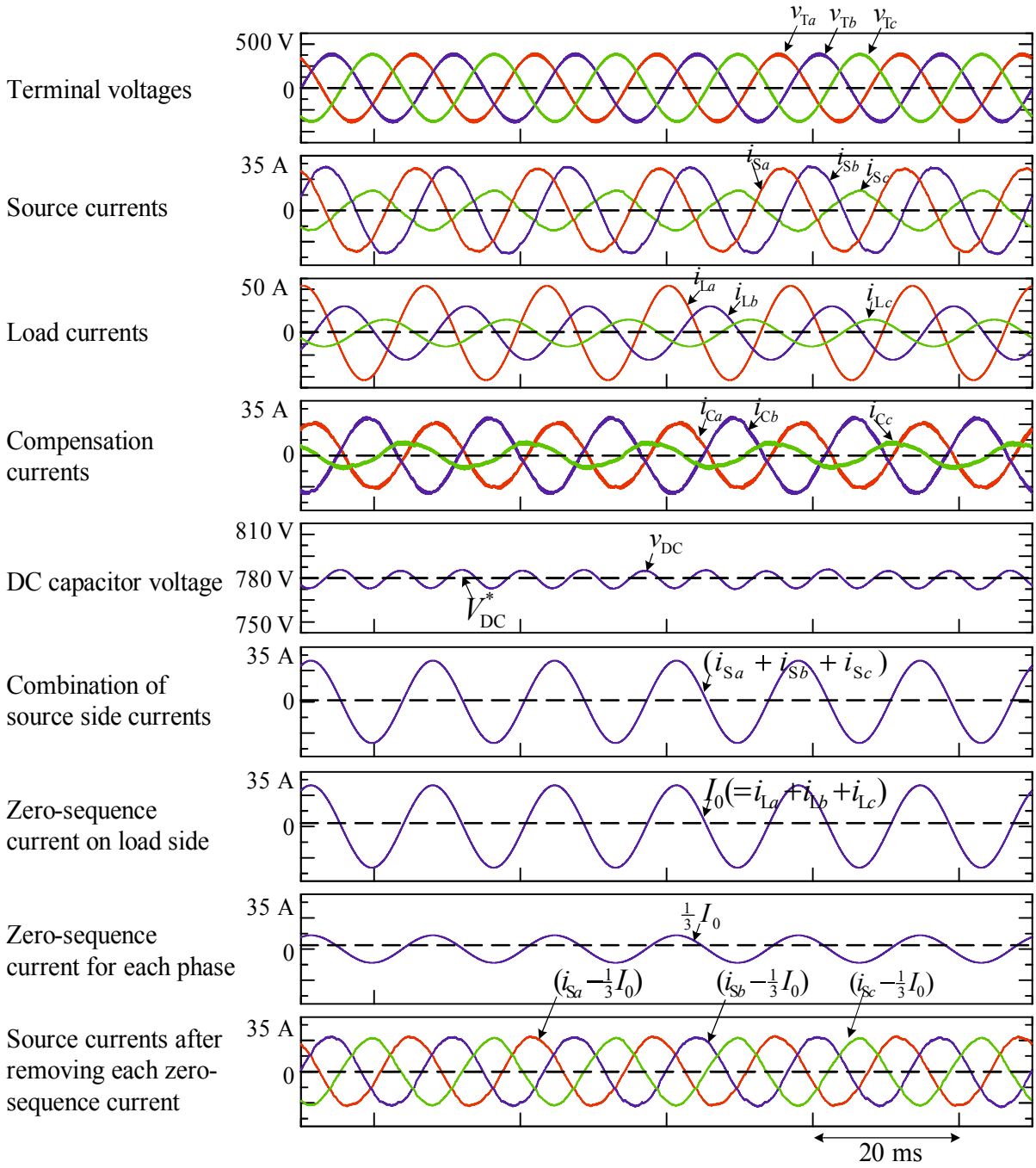

Figure 5.5: Simulation results of three legs inverter based ALB with a common DC capacitor.

5.2.2 Three-leg Inverter Based ALB with Two DC Capacitors

Figure 5.6 shows three-leg inverter with two DC capacitor based ALB in three-phase four-wire distribution systems. The three legs of the inverter is connected to each phase of the distribution system and the mid-point of two DC capacitors is connected to the neutral line of the distribution system. The three-leg generate the compensation currents for each phase including zero-sequence current components.

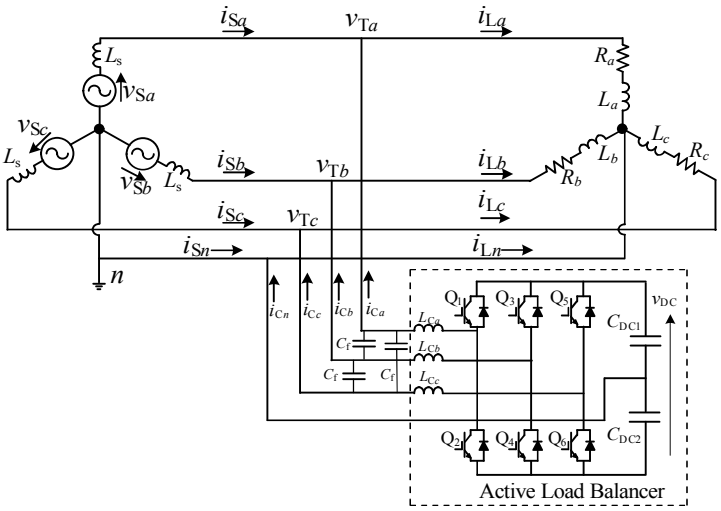

Figure 5.6: Three-leg inverter with two DC capacitors.

Figure 5.7 shows the switching patterns of the three-leg inverter with two DC capacitors. The inverter performs as three half-bridge inverters with a common neutral point at the mid-point of two DC capacitors. From the switching patters, equivalent circuit can be depicted as Figure 5.8. The three legs performs as three current sources with a common neutral point. This common neutral point is connected to the neutral line of the distribution system. In this equivalent circuit,

i_p = average active component of the three load currents,

i_{up}, i_q = unbalanced active component and reactive component of each load currents,

I_0 = $i_{La} + i_{Lb} + i_{Lc}$ = zero sequence current component,

i_{Ca} = $i'_{up} + i'_q$ (including $\frac{1}{3}I_0$ component),

i_{Cb} = $i''_{up} + i''_q$ (including $\frac{1}{3}I_0$ component),

i_{Cc} = $i'''_{up} + i'''_q$ (including $\frac{1}{3}I_0$ component).

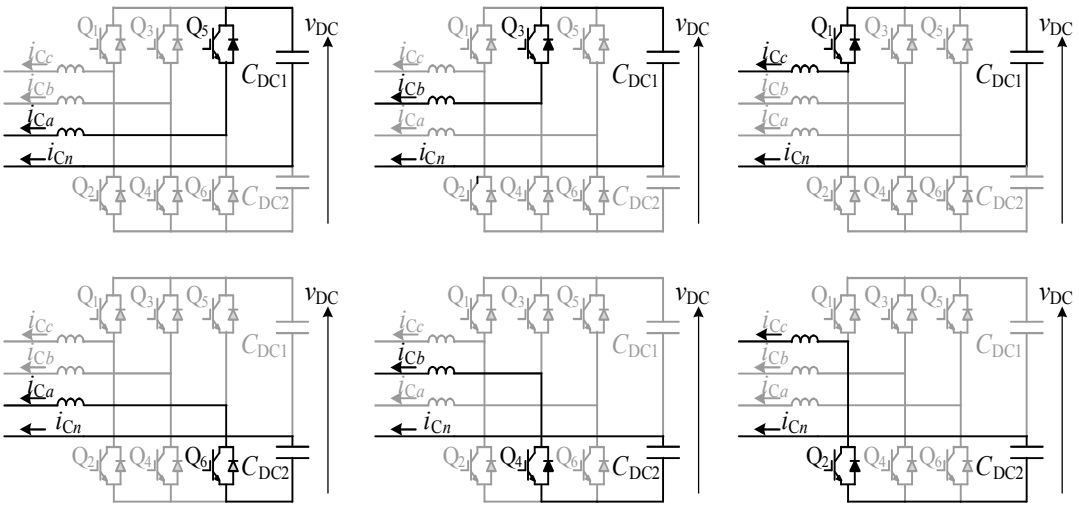

Figure 5.7: Switching patterns in three-leg inverter with two DC capacitors.

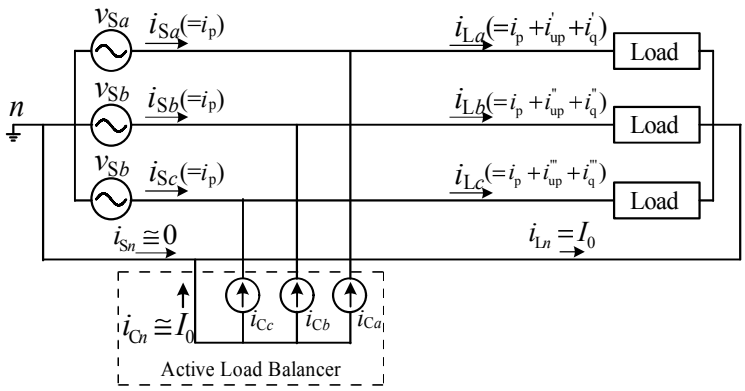

Figure 5.8: Equivalent circuit of three-leg based ALB with two DC capacitors.

Figure 5.9 shows the simulation results of Figure 5.6. v_{Ta}, v_{Tb} and v_{Tc} are the *a*-phase terminal voltage, the *b*-phase terminal voltage and the *c*-phase terminal voltage. i_{Sa}, i_{Sb} and i_{Sc} are source side currents. i_{La}, i_{Lb} and i_{Lc} are three single-phase load currents. The three-leg inverter generate three compensation currents i_{Ca}, i_{Cb} and i_{Cc} including zero-sequence current. The balanced current condition is achieved on the source side i_{Sa}, i_{Sb} and i_{Sc}. The total DC capacitor voltage v_{DC} is well controlled to its reference value V_{DC}^{*}.

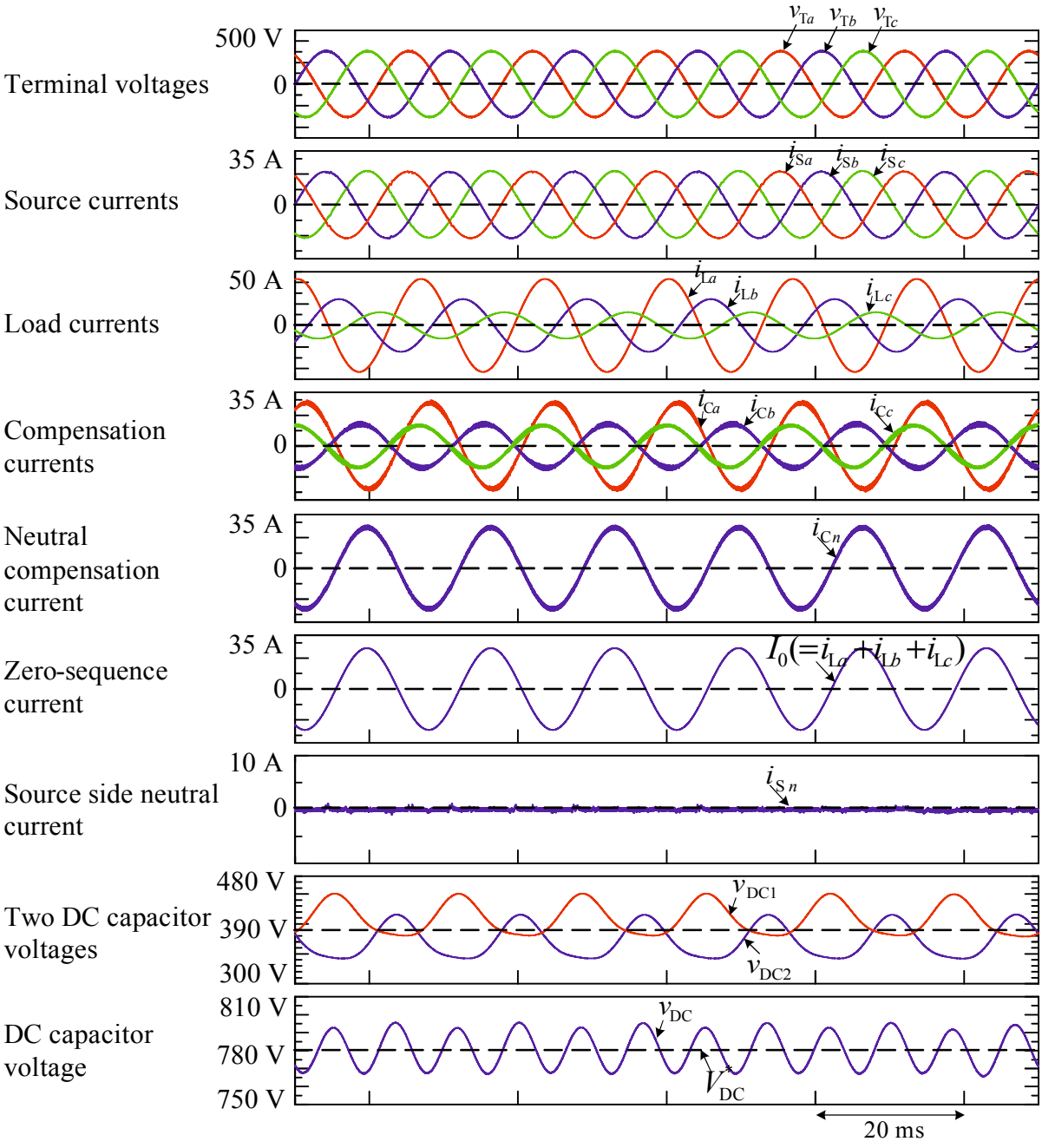

Figure 5.9: Simulation results of three-leg inverter with two DC capacitors.

This three-leg inverter with two DC capacitor based ALB has good compensation characteristic. However, the two DC capacitor voltages v_{DC1} and v_{DC2} tend to be different depending on the unbalanced amount of load currents. Therefore, DC capacitor voltage balancing circuit is necessary and it can results in higher cost and complicated design. This topology, thus, not suitable for the ALB in three-phase four-wire distribution systems.

5.2.3 Four-leg Inverter Based ALB with Common DC Capacitor

Figure 5.10 shows four-leg inverter based ALB in three-phase four-wire distribution systems. Three-leg of the inverter is connected to each phase of the distribution system and the fourth leg is connected to the neutral.

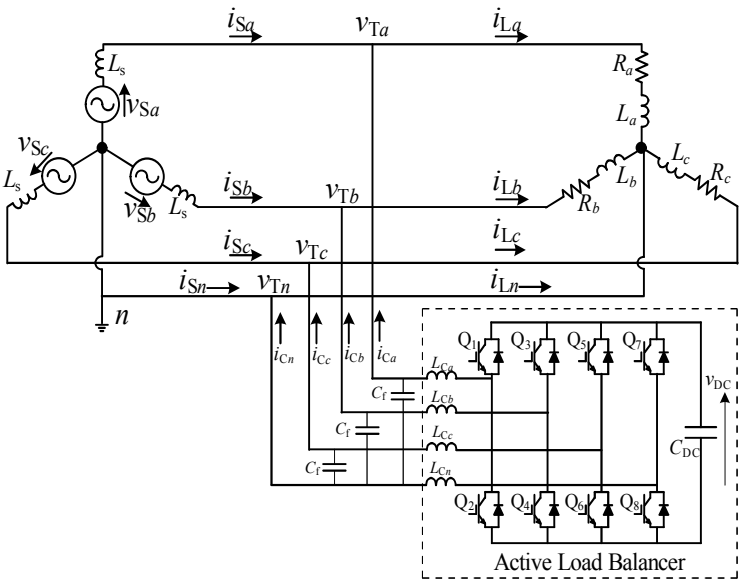

Figure 5.10: Four-leg inverter based ALB with a common DC capacitor.

Figure 5.11 shows the switching patterns of the power devices in four-leg inverter based ALB. The fourth leg performs as common leg of the other three legs. Therefore, the three-leg generate the compensation currents for each phase while the fourth leg generates the zero-sequence current, simultaneously. Based on the switching patterns as shown in Figure 5.11, the equivalent circuit of four-leg inverter based ALB is depicted as Figure 5.12 in three-phase four

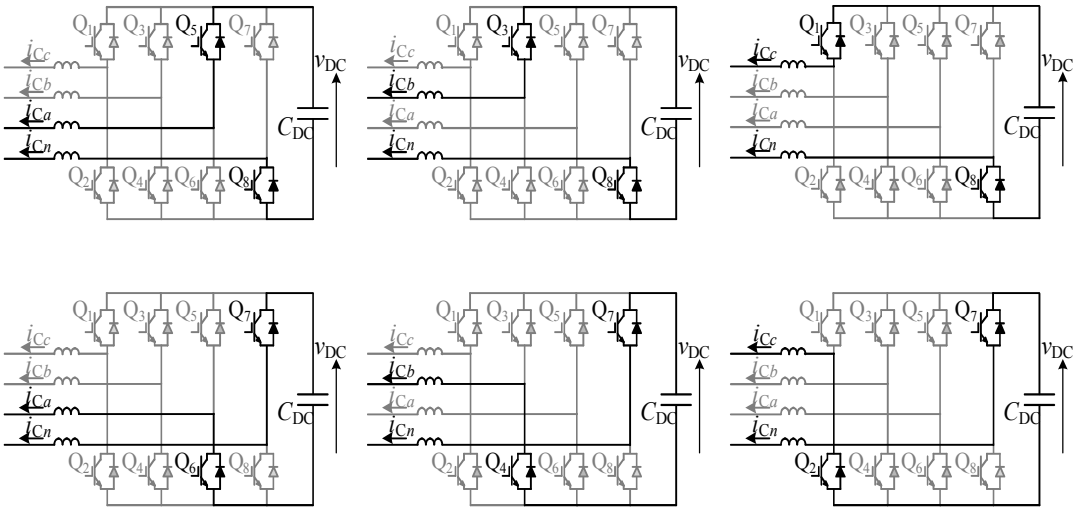

Figure 5.11: Switching patterns in the four-leg inverter.

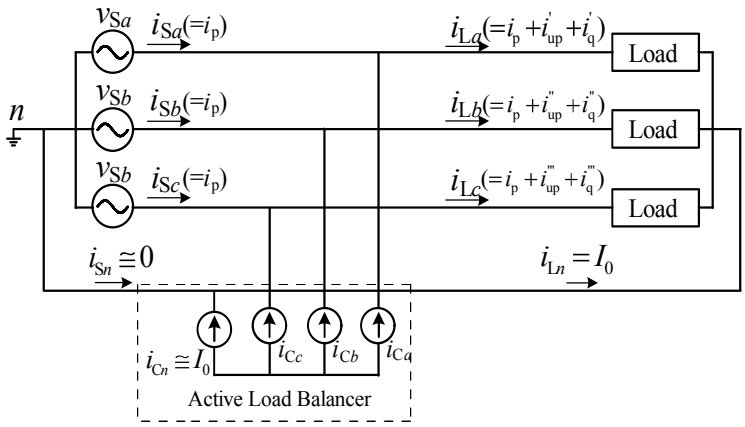

Figure 5.12: Equivalent circuit of the four-leg based ALB in three-phase four-wire distribution systems.

wire distribution systems. In this equivalent circuit,

i_{p} = average active component of three load currents,

i_{up}, i_{q} = unbalanced active component and reactive component of each load currents,

I_0 = $i_{\mathrm{L}a} + i_{\mathrm{L}b} + i_{\mathrm{L}c}$ = zero sequence current,

$i_{\mathrm{C}a}$ = $(i_{\mathrm{up}}' + i_{\mathrm{q}}')$ including $\frac{1}{3}I_0$ component,

$i_{\mathrm{C}b}$ = $(i_{\mathrm{up}}'' + i_{\mathrm{q}}'')$ including $\frac{1}{3}I_0$ component,

$i_{\mathrm{C}c}$ = $(i_{\mathrm{up}}''' + i_{\mathrm{q}}''')$ including $\frac{1}{3}I_0$ component.

Figure 5.13 shows simulation results of Fig 5.10 with four legs inverter based ALB. v_{Ta}, v_{Tb} and v_{Tc} are the a-phase terminal voltage, the b-phase terminal voltage and the c-phase terminal voltage. i_{Sa}, i_{Sb} and i_{Sc} are source side currents, and i_{Sn} are neutral line current in the source side. i_{La}, i_{Lb} and i_{Lc} are three single-phase load currents and i_{Ln} are neutral line (zero-sequence) current on the load side. i_{Ca}, i_{Cb}, i_{Cc} and i_{Cn} are compensation currents generated by ALB. The three source currents i_{Sa}, i_{Sb} and i_{Sc} are balanced and sinusoidal with good power factor. The zero-sequence load current i_{Ln} is compensated by the fourth leg compensation current i_{Cn} generated by ALB. Therefore, zero-sequence current on source side is nearly zero providing perfect compensation of ALB. The DC capacitor voltage v_{DC} is well controlled to its reference value V^*_{DC}.

Table 5.1 shows the utilization comparison of the ALB topologies. The three-leg based ALB with a common DC capacitor is not good for zero-sequence current compensation. Therefore, this topology is suitable for the three-phase three-wire system. The three-leg based ALB with two DC capacitors has good compensation characteristic, but it needs an extra circuit to control two DC capacitor voltages. The four-leg based ALB with a common DC capacitor has good compensation characteristic and DC voltage utilization, but it needs more power devices. Adding the one more leg is better than adding the extra circuit for controlling the two DC capacitor voltage from the design simplicity and economic point of view. Therefore, four-leg based ALB topology is used in our proposed system.

Table 5.1: The utilization comparison of the ALB with their topologies.

	Compensation facility	DC voltage control
Three-leg based ALB with a common DC capacitor	not good for zero-sequence current compensation	good
Three-leg based ALB with two DC capacitors	good	needs an extra circuit to control two DC capacitor voltages
Four-leg based ALB with a common DC capacitor	good	good

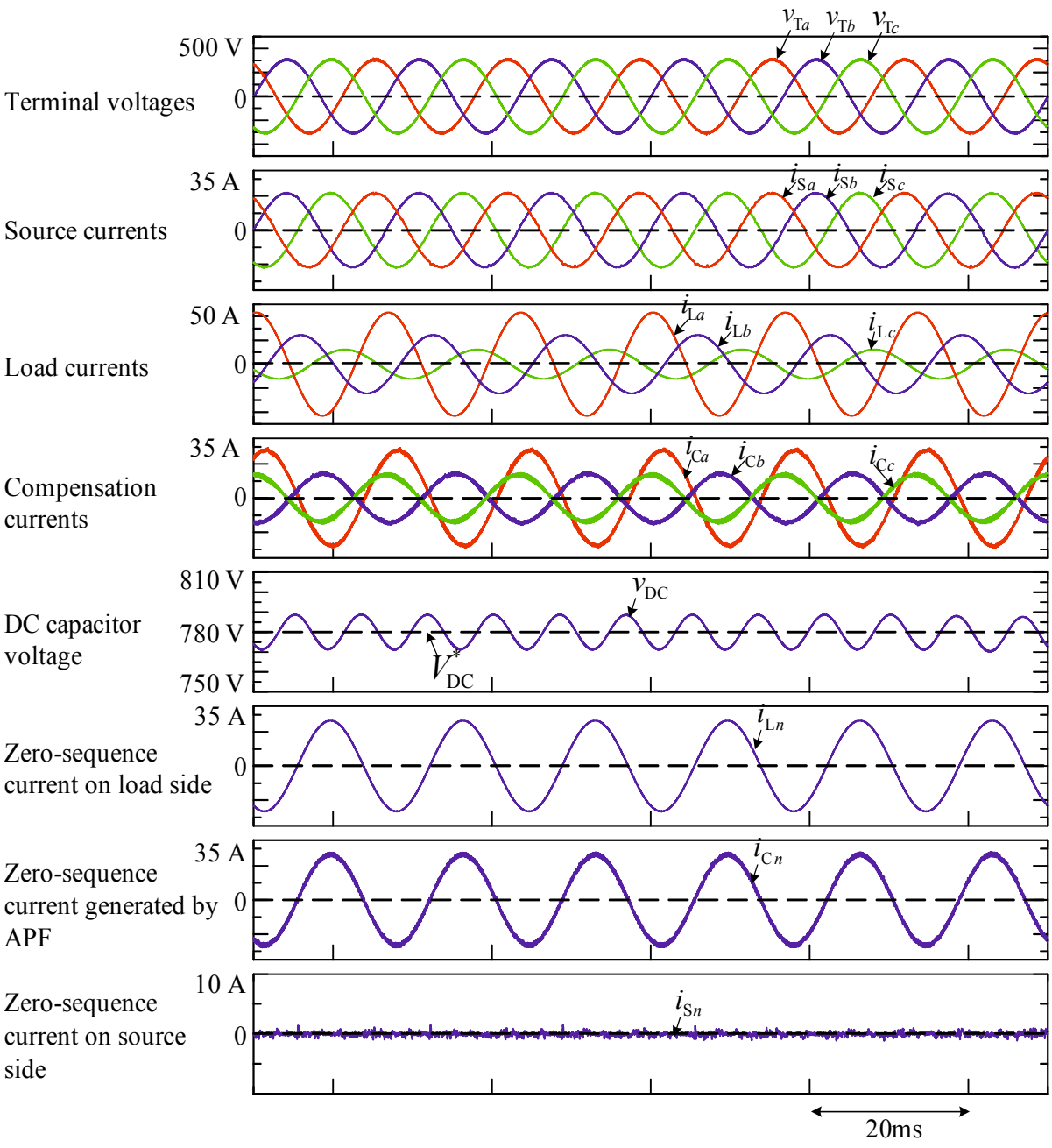

Figure 5.13: Simulation results of the four legs inverter based ALB.

5.2.4 Existing Control Strategy for the Active Load Balancer

Power theory under the unbalanced load and/or non-sinusoidal condition has been motivated in power converter utilizations. Accurate tracking of the active power, reactive power in the distribution system is necessary to operate the active load balancer efficiently. The control strategies of the ALB are different based on the theory of active and reactive power detection method in three-phase systems. This section will describe the various ALB control strategies with their core power detection method in three-phase four-wire distribution systems.

In 1984, Prof. H. Akagi developed the instantaneous reactive power theory for the active and reactive power detection method in three-phase systems [7]. Figure 5.14 shows the basic concept of instantaneous reactive power theory. In this method, three source voltages and the three source currents are transformed from abc to $\alpha\beta$ coordinates. Then the instantaneous real power, p and

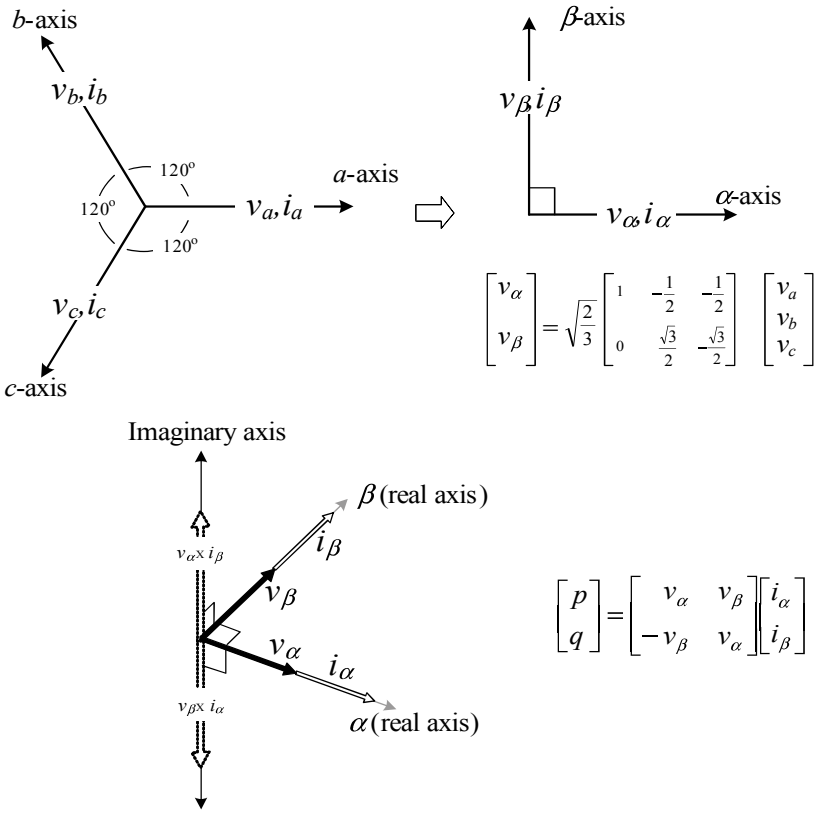

Figure 5.14: The instantaneous active-reactive power theory.

the instantaneous imaginary power, q are calculated as

$$\begin{bmatrix} p \\ q \end{bmatrix} = \begin{bmatrix} v_\alpha & v_\beta \\ -v_\beta & v_\alpha \end{bmatrix} \begin{bmatrix} i_{L\alpha} \\ i_{L\beta} \end{bmatrix}. \tag{5.1}$$

Using this theory, the three load currents can be decomposed as follow:

$$\begin{aligned} i_{L\alpha} &= \frac{v_\alpha}{v_\alpha^2 + v_\beta^2}\bar{p} + \frac{v_\alpha}{v_\alpha^2 + v_\beta^2}\tilde{p} + \frac{-v_\beta}{v_\alpha^2 + v_\beta^2}\bar{q} + \frac{-v_\beta}{v_\alpha^2 + v_\beta^2}\tilde{q}, \\ i_{L\beta} &= \frac{v_\beta}{v_\alpha^2 + v_\beta^2}\bar{p} + \frac{v_\beta}{v_\alpha^2 + v_\beta^2}\tilde{p} + \frac{v_\alpha}{v_\alpha^2 + v_\beta^2}\bar{q} + \frac{v_\alpha}{v_\alpha^2 + v_\beta^2}\tilde{q}, \end{aligned} \tag{5.2}$$

on the $\alpha\beta$ axes. Where $\bar{p}$ and $\tilde{p}$ are dc and ac component of the instantaneous real power and $\bar{q}$ and $\tilde{q}$ are dc and ac component of the instantaneous imaginary power. The first terms of the right-hand side of (5.2) are the instantaneous value of the fundamental active currents on α and β phases. The third terms are the instantaneous value of fundamental reactive currents. The second and the fourth terms are the instantaneous value of the harmonic currents from real power and imaginary power.

A. Nava et. al has proposed the control strategy for the four-leg based ALB, which is based on the instantaneous reactive power theory [9]. Figure 5.15 shows the instantaneous reactive power theory based control block diagram of the ALB in three-phase four-wire distribution systems. In their method, the three source voltages and three source currents are transformed from the abc to $\alpha\beta$ coordinates. Then, the instantaneous reactive currents, the right hand side of the third term of (5.2), and the instantaneous harmonic current components, the right hand side of the second and fourth terms of (5.2), are calculated using a significant number of calculation steps. The combination of these three terms gives reference compensation currents, i_{C0}^* $i_{C\alpha}^*$ $i_{C\beta}^*$, on the $\alpha\beta$ co-ordinate. Constant DC capacitor voltage control block is commonly added in the control strategy for DC capacitor voltage control. These reference compensation currents are retransformed into abc coordinate for the ALB operation. Other control strategies in [8–10] are also based on the instantaneous reactive power theory, and thus they also require the similar calculation steps for the ALB control strategies.

These control strategies give precise reference compensation currents for the ALB, but a significant number of calculation steps are necessary making it complicated design and slower response. Therefore, this dissertation proposes the simple control strategies for four-leg based ALB in three-phase four-wire distribution system.

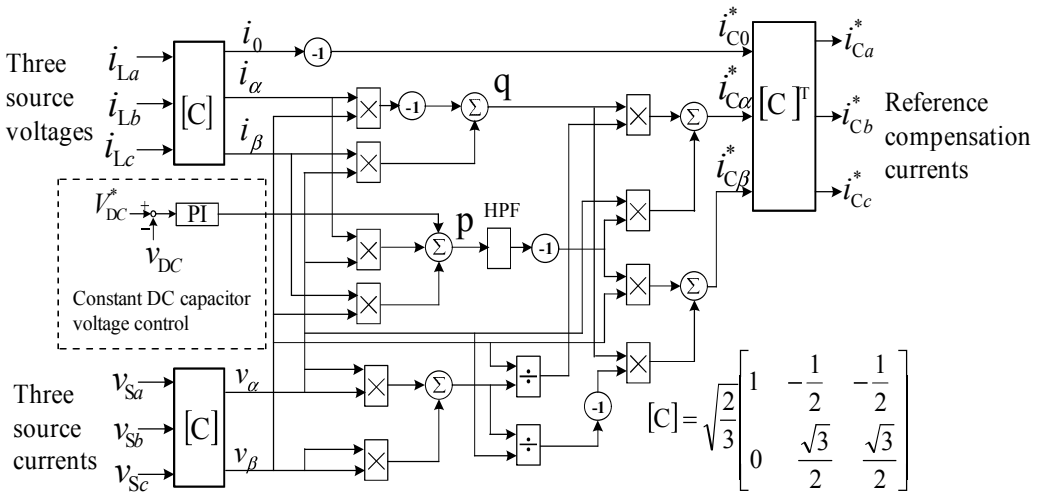

Figure 5.15: Control block diagram of the ALB by A. Nava et al..

5.3 Constant DC Capacitor Voltage Control Strategy Based Active Load Balancer

A new constant DC capacitor voltage control strategy for active load balancer (ALB) is proposed in this section to avoid complicated calculation steps in the reference compensation currents calculation. The basic principle of the constant DC capacitor voltage control strategy is discussed in detail. Then, the proposed control strategy is confirmed by both simulation and experiment.

5.3.1 Power Circuit Diagram

Figure 5.16 shows the power circuit of the ALB in three-phase four-wire distribution systems. The distribution system is composed of three-phase four-wire Y-connected distribution transformer (secondary-side) and three single-phase loads. v_{Sa}, v_{Sb} and v_{Sc} are three sources of distribution transformer with neutral grounded. The three single-phase unbalanced loads are composed of R_a, L_a, R_b, L_b and R_c, L_c. The ALB is constructed with four legs power switching devices with a common DC capacitor. The three legs of the ALB is connected to the *a*-phase, *b*-phase and *c*-phase of the distribution system, and the fourth leg is connected to the neutral. The unbalanced active and reactive currents drawn by the three single-phase load are compensated by the ALB.

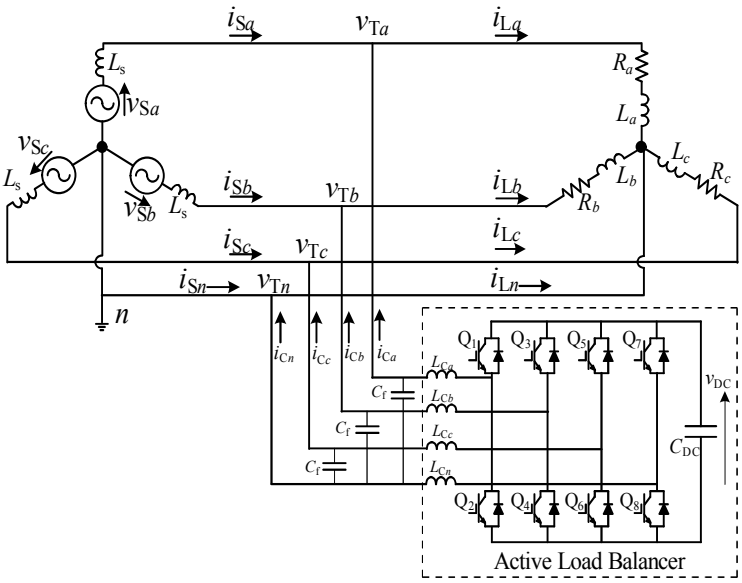

Figure 5.16: Power circuit diagram of the ALB.

5.3.2 Constant DC Capacitor Voltage Control Strategy

Figure 5.17 shows the proposed constant DC capacitor voltage control strategy for the ALB. The control strategy includes the reference source currents calculation by constant DC capacitor voltage control, the reference compensation currents calculation and the current feedback control. The principle of the reference source current calculation in the ALB using constant DC capacitor voltage control is discussed. The three-phase terminal voltages v_{Ta}, v_{Tb} and v_{Tc} in Figure 5.17 are expressed as

$$\begin{aligned} v_{Ta} &= \sqrt{2}V_{\mathrm{T}}\cos(\omega t), \\ v_{Tb} &= \sqrt{2}V_{\mathrm{T}}\cos(\omega t - \frac{2\pi}{3}), \\ v_{Tc} &= \sqrt{2}V_{\mathrm{T}}\cos(\omega t - \frac{4\pi}{3}). \end{aligned} \tag{5.3}$$

The load currents i_{La}, i_{Lb} and i_{Lc} drawn by each single-phase load are also shown by

$$\begin{aligned} i_{La} &= \sqrt{2}I_a\cos(\omega t - \phi_a), \\ i_{Lb} &= \sqrt{2}I_b\cos(\omega t - \frac{2\pi}{3} - \phi_b), \\ i_{Lc} &= \sqrt{2}I_c\cos(\omega t - \frac{4\pi}{3} - \phi_c). \end{aligned} \tag{5.4}$$

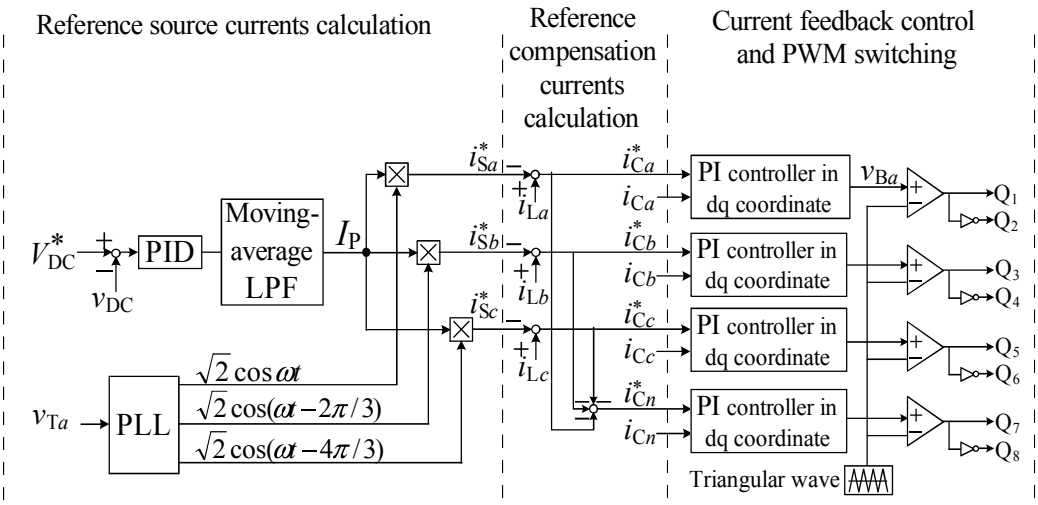

Figure 5.17: Constant DC capacitor voltage control strategy.

Let us assume that the three-phase source currents i_{Sa}, i_{Sb} and i_{Sc} are balanced with a unity power factor after compensating the unbalanced active and reactive load currents. The three-phase source currents, therefore, can be expressed as

$$\begin{aligned} i_{Sa} &= \sqrt{2}I_S\cos(\omega t), \\ i_{Sb} &= \sqrt{2}I_S\cos(\omega t - \frac{2\pi}{3}), \\ i_{Sc} &= \sqrt{2}I_S\cos(\omega t - \frac{4\pi}{3}), \end{aligned} \tag{5.5}$$

where $I_S = (I_a\cos\phi_a + I_b\cos\phi_b + I_c\cos\phi_c)/3$. This I_S is the theoretical rms value of the balanced active current for each phase in the three-phase power-feeding system under all unbalanced load conditions.

From (5.4) and (5.5), the compensation currents of the ALB are calculated as

$$\begin{aligned} i_{Ca} &= i_{La} - i_{Sa}, \\ &= \sqrt{2}I_a\sin\omega t\,\sin\phi_a + \frac{\sqrt{2}}{3}\left(2I_a\cos\phi_a - I_b\cos\phi_b - I_c\cos\phi_c\right)\cos\omega t, \\ i_{Cb} &= i_{Lb} - i_{Sb}, \\ &= \sqrt{2}I_b\sin(\omega t - \frac{2\pi}{3})\,\sin\phi_b + \frac{\sqrt{2}}{3}\left(2I_b\cos\phi_b - I_a\cos\phi_a - I_c\cos\phi_c\right)\cos(\omega t - \frac{2\pi}{3}), \\ i_{Cc} &= i_{Lc} - i_{Sc}, \\ &= \sqrt{2}I_c\sin(\omega t - \frac{4\pi}{3})\,\sin\phi_c + \frac{\sqrt{2}}{3}\left(2I_c\cos\phi_c - I_a\cos\phi_a - I_b\cos\phi_b\right)\cos(\omega t - \frac{4\pi}{3}). \end{aligned} \tag{5.6}$$

Equation (5.6) gives the theoretical compensation currents of the ALB so that the balanced source current is achieved in the distribution transformer. The instantaneous power p_{C} flowing into the ALB can be calculated as

$$\begin{aligned} p_{\mathrm{C}} &= v_{\mathrm{T}a} \cdot i_{\mathrm{C}a} + v_{\mathrm{T}b} \cdot i_{\mathrm{C}b} + v_{\mathrm{T}c} \cdot i_{\mathrm{C}c} \\ &= \Big(2I_a\cos\phi_a - I_b\cos\phi_b - I_c\cos\phi_c + \sqrt{3}I_b\sin\phi_b - \sqrt{3}I_c\sin\phi_c\Big)\frac{1}{2}V_{\mathrm{T}}\cos(2\omega t) + \\ &\quad \Big(2I_a\sin\phi_a - I_b\sin\phi_b - I_c\sin\phi_c - \sqrt{3}I_b\cos\phi_b + \sqrt{3}I_c\cos\phi_c\Big)\frac{1}{2}V_{\mathrm{T}}\sin(2\omega t). \end{aligned} \tag{5.7}$$

Equation (5.7) does not contain the DC component, and therefore, the mean value of the instantaneous power p_{C} becomes zero. This suggest that the DC capacitor voltage is constant if the source currents are balanced as can be seen from (5.5). Therefore, maintaining a constant DC capacitor voltage in the ALB in Figure 5.16 means that the ALB controls the three source currents so that they can satisfy a balanced condition with a unity power factor. Thus, the constant DC capacitor voltage control can detect the reference source currents of the ALB for a three-phase four-wire distribution system.

To perform the constant DC capacitor voltage control, the DC capacitor voltage v_{DC} is detected in Figure 5.16. Then the difference between the detected DC capacitor voltage v_{DC} and the reference DC capacitor voltage V^*_{DC} is amplified by the PID controller. The output value of the PID controller is input into a moving-average low-pass filter (LPF). The moving-average LPF is designed to remove 2ω frequency components. The transfer function of the moving-average LPF is expressed as

$$H(z) = \frac{1}{N}\sum_{n=0}^{N-1} z^{-n}, \tag{5.8}$$

where N is the number of samples and can be expressed as

$$N = \frac{1}{f_C T_s}, \tag{5.9}$$

where T_s is the sampling time interval and f_C is the cutoff frequency. T_s is set to 83.3μs for the 12 kHz switching frequency and f_C is set to 120Hz in LPF. Therefore moving-average LPF remove 2ω frequency components. After filtering with the moving-average LPF, the effective value I_{P} of the source-side active current is obtained by performing constant DC capacitor voltage control. To calculate the reference source currents for the ALB, the a-phase terminal voltage $v_{\mathrm{T}a}$

is detected and then the electrical angle ($\theta_{\mathrm{T}} = \omega t$) is calculated using a single-phase phased-lock loop (PLL) [25]. Then, $\sqrt{2}\cos(\omega \mathrm{t})$, which is synchronized with the a phase, $\sqrt{2}\cos(\omega \mathrm{t} - \frac{2\pi}{3})$, which is synchronized with the b phase, and $\sqrt{2}\cos(\omega \mathrm{t} - \frac{4\pi}{3})$, which is synchronized with c phase, are calculated using θ_{T}. Using these calculated values and the effective value I_{P}, the reference source currents for each phase are calculated as

$$\begin{aligned} i^*_{\mathrm{S}a} &= \sqrt{2} I_{\mathrm{P}} \cos(\omega t), \\ i^*_{\mathrm{S}b} &= \sqrt{2} I_{\mathrm{P}} \cos(\omega t - \frac{2\pi}{3}), \\ i^*_{\mathrm{S}c} &= \sqrt{2} I_{\mathrm{P}} \cos(\omega t - \frac{4\pi}{3}). \end{aligned} \tag{5.10}$$

By comparing the reference source currents with the detected load currents, the reference compensation currents are given as:

$$\begin{aligned} i^*_{\mathrm{C}a} &= i_{\mathrm{L}a} - i^*_{\mathrm{S}a}, \\ i^*_{\mathrm{C}b} &= i_{\mathrm{L}b} - i^*_{\mathrm{S}b}, \\ i^*_{\mathrm{C}c} &= i_{\mathrm{L}c} - i^*_{\mathrm{S}c}, \\ i^*_{\mathrm{C}n} &= -\left(i^*_{\mathrm{C}a} + i^*_{\mathrm{C}b} + i^*_{\mathrm{C}c}\right). \end{aligned} \tag{5.11}$$

The above calculation steps are the reference compensation current of the ALB, which gives the same compensation currents as Fig. 5.15.

In the current feedback control, PI controllers in dq coordinates are used to avoid the steady-state error of the feedback control in the ALB [27]. The operation principle is identical among the phases and neutral as shown in Figure 5.17. Figure 5.18 shows the block diagram of PI controller in dq coordinate, where $i^*_{\mathrm{C}a}$ is the reference signal, $i_{\mathrm{C}a}$ is the detected signal and $v_{\mathrm{B}a}$ is the feedback control output. As shown in Figure 5.18, the a-phase reference compensation current $i^*_{\mathrm{C}a}$ is delayed by $T_{\mathrm{S}}/4$, where T_{S} is the cycle of the a-phase source voltage. $i^*_{\mathrm{C}a}$ corresponds to the α-component, and the delayed current through the $T_{\mathrm{S}}/4$ delay block corresponds to the β-component. Using θ_{T}, i.e., the electrical angle of the a-phase terminal voltage generated by the PLL, the α- and β-components are transformed into $i^*_{\mathrm{d}a}$ and $i^*_{\mathrm{q}a}$, respectively. The compensation output current $i_{\mathrm{C}a}$ is also transformed into $i_{\mathrm{d}a}$ and $i_{\mathrm{q}a}$ in the same way. The differences between the reference currents $i^*_{\mathrm{d}a}$, $i^*_{\mathrm{q}a}$ and the detected currents $i_{\mathrm{d}a}$, $i_{\mathrm{q}a}$ are amplified by the PI controller in dq coordinates. The amplified values are retransformed into the a-phase components. Then,

using the pulse width modulation (PWM) technique, the gate signals for the power switching devices of the ALB are generated.

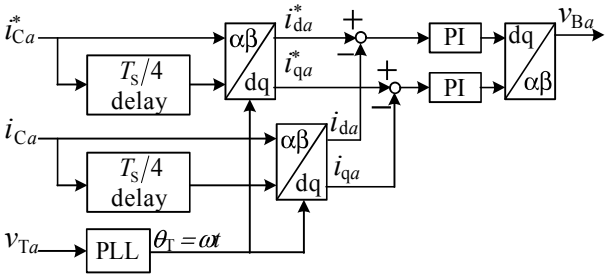

Figure 5.18: PI controller in dq coordinate.

5.4 Simulation Results

To confirm the validity and high practicability of the proposed constant DC capacitor voltage control based strategy for the ALB, digital computer simulation is implemented using PSIM software. The circuit parameters for the distribution transformer in Figure 5.16 are shown in Table 5.2. The rating of the distribution transformer is 3-phase 380V, 21.5kVA and 60Hz. The line-to-line voltage of 380V used in the simulation is similar to that for a practical three-phase four-wire distribution system. The base value is 7.1kVA for each single phase system. The three single-phase loads are shown in Table 5.3. The load conditions for *a*-phase include two different loads, while the *b*-phase and *c*-phase loads are kept constant. The unbalanced load percentage is calculated as the ratio of the negative-sequence to positive-sequence values in accordance with the International Electrotechnical Commission (IEC) standard. Table 5.4 shows the circuit constants for the four-leg based ALB in Fig. 5.16. The reference value of the DC capacitor voltage V^*_{DC} is set to 780V.

Figure 5.19 shows the simulation results for the ALB in Figure 5.16 with the proposed constant DC capacitor voltage control based strategy. v_{Ta}, v_{Tb} and v_{Tc} are the *a*-phase terminal voltage, *b*-phase terminal voltage and *c*-phase terminal voltage, respectively. The *a*-phase load current i_{La} is varied from 0.9 pu to 0.2 pu while the *b*-phase and *c*-phase load currents, i_{Lb} and i_{Lc}, are kept constant. The unbalanced load percentage is 31% before load variation and 30% after

Table 5.2: Parameters of the distribution transformer in the simulation.

Item	Symbol	Value
Rated power of transformer		21.5 kVA
Rated power for each phase		7.1 kVA
Rated line-to-line rms voltage	v_o	380 V
Rated line to neutral rms voltage	v_{Sa}, v_{Sb}, v_{Sc}	220 V
Rated frequency	f	60 Hz

Table 5.3: Load conditions of three-phase four-wire distribution system.

Item	Symbol	Value
a-phase load (large load condition)	R_a	6.1 Ω
(0.9 pu, power factor 0.8)	L_a	12 mH
a-phase load (small load condition)	R_a	25 Ω
(0.2 pu, power factor 0.8)	L_a	50 mH
b-phase load	R_b	10 Ω
(0.5 pu, power factor 0.8)	L_b	20 mH
c-phase load	R_c	20 Ω
(0.25 pu, power factor 0.8)	L_c	40 mH
unbalanced load percent (with a-phase large load)		31%
unbalanced load percent (with a-phase small load)		30%

load variation. Before/after load current variation, the three source currents i_{Sa}, i_{Sb} and i_{Sc} are balanced with a unity power factor as shown in Figure 5.19. The source currents i_{Sa}, i_{Sb} and i_{Sc} settled to their steady state within two periods. In the literature [12], it takes five periods to settle the currents to their steady state. Therefore, we can confirm that the proposed constant DC capacitor voltage control based strategy enables a good dynamic response of the ALB. Because

Table 5.4: Circuit constants of active load balancer in the simulation.

Item	Symbol	Value
Reference DC capacitor voltage	V^*_{DC}	780 V
Capacity of capacitor	C_{DC}	2200 μF
Compensation inductance	L_{Ca}, L_{Cb}, L_{Cc}, L_{Cn}	2.5 mH
Switching frequency	f_{sw}	12 kHz

of the unbalanced load condition in both heavy and light load conditions, zero-sequence current is flowed in the load-side. The ALB generates the zero-sequence currents which was very closed with the zero-sequence current of the loads. Thus, the transformer neutral current $i_{\mathrm{S}n}$ is nearly zero as shown in Figure 5.19. The DC capacitor voltage v_{DC} is well controlled to its reference value V^*_{DC} in both the transient and steady states. The amount of ripple of the DC capacitor voltage is within the acceptable range of under 3% in both the transient and steady states.

Figure 5.20 shows the simulation results upon varying the *a*-phase load current $i_{\mathrm{L}a}$ from 0.2 pu to 0.9 pu while the *b*-phase and *c*-phase load currents $i_{\mathrm{L}b}$ and $i_{\mathrm{L}c}$ are kept constant. The unbalanced load percentage is 30% before load variation and 31% after load variation. Before/after load current variation, the source currents $i_{\mathrm{S}a}$, $i_{\mathrm{S}b}$ and $i_{\mathrm{S}c}$ are balanced with a unity power factor. The DC capacitor voltage v_{DC} is also well controlled to its reference value in this load variation. The amount of ripple of the DC capacitor voltage in the transient state is 2.8%.

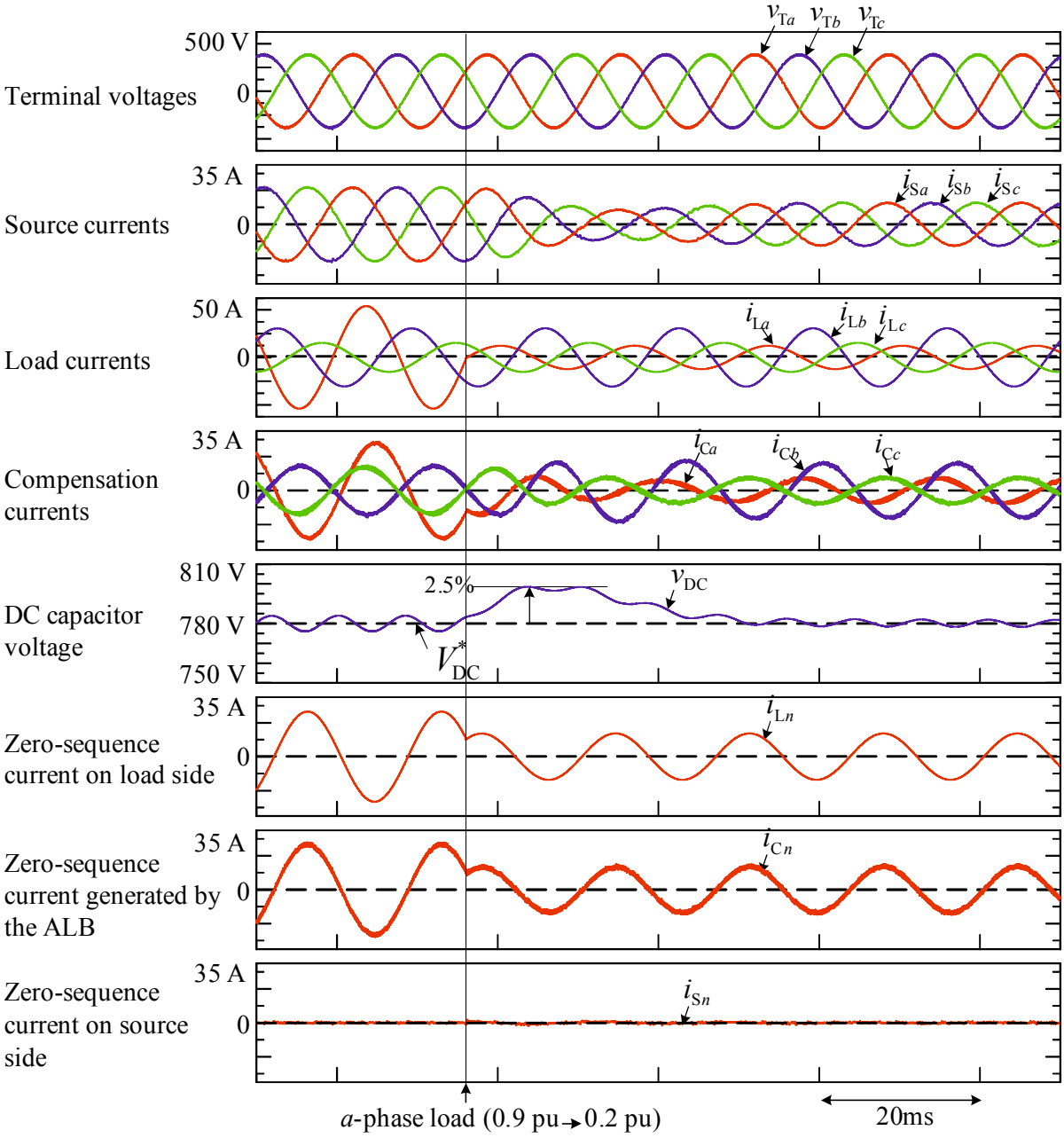

Figure 5.19: Simulation results of the proposed ALB with constant DC capacitor voltage control strategy (from heavy to light load variation).

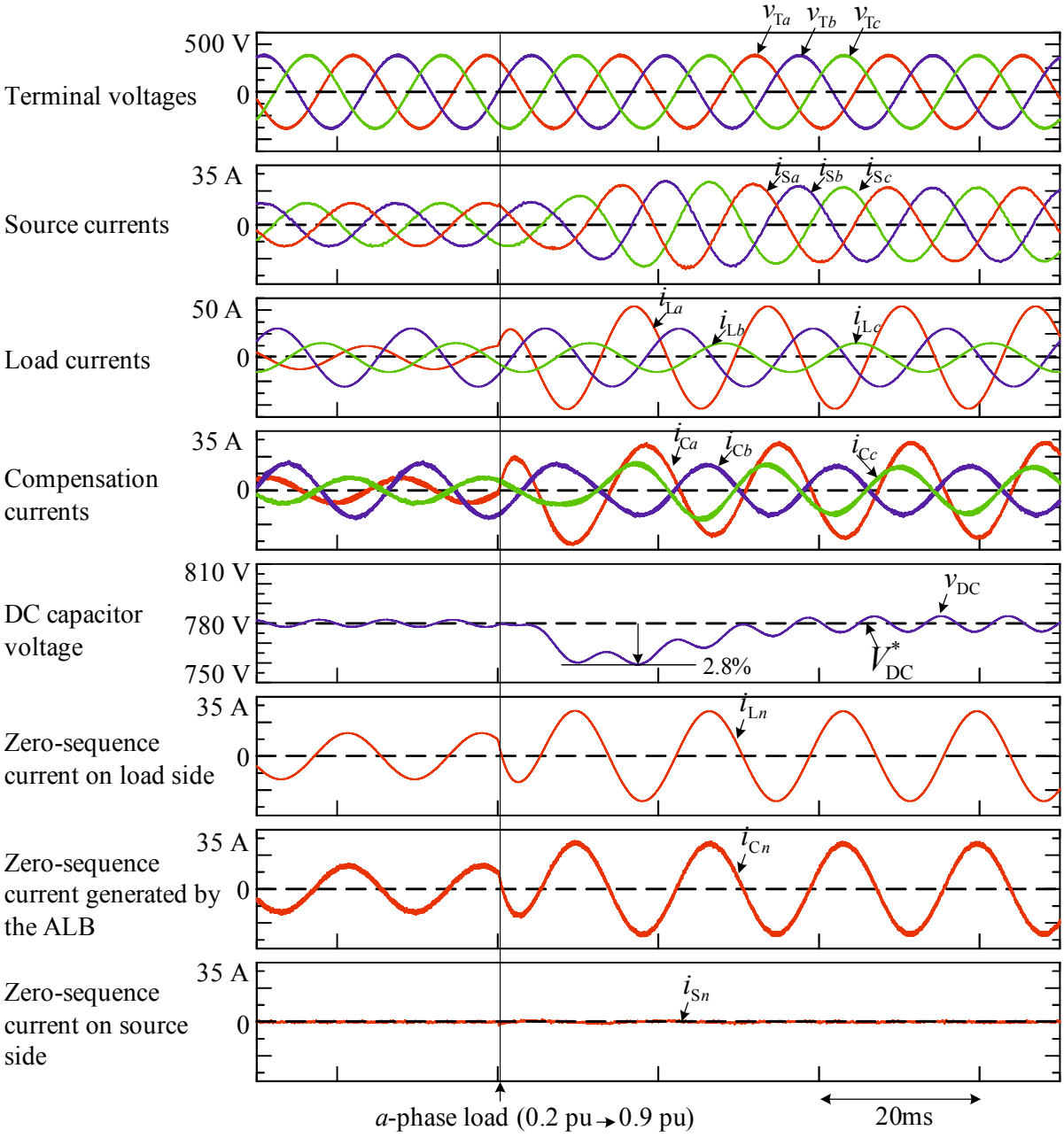

Figure 5.20: Simulation results of the proposed ALB with constant DC capacitor voltage control strategy (from light to heavy load variation).

5.5 Experimental Results

A reduced-scale experimental model of the proposed ALB is constructed and tested to demonstrate the validity and high practicability of the proposed constant DC capacitor voltage control based strategy. Figure 5.21 shows a block diagram of the constructed experimental model. A Δ-Y connected distribution transformer is used in the experiment. The utility three-phase system distributes 200V in Japan. Therefore, a line-to-line voltage of 200V is used in the experiment instead of 380V. The rating of the transformer is 3-phase, 200 V, 6 kVA and 60 Hz on both the primary and secondary sides as shown in Table 5.5. The load conditions of the distribution system are the same as those in Table 5.3. The circuit constants of the ALB in the experiment are shown in Table 5.6. A digital signal processor (DSP: TMS320C6713, 225MHz) is used in the experimental setup.

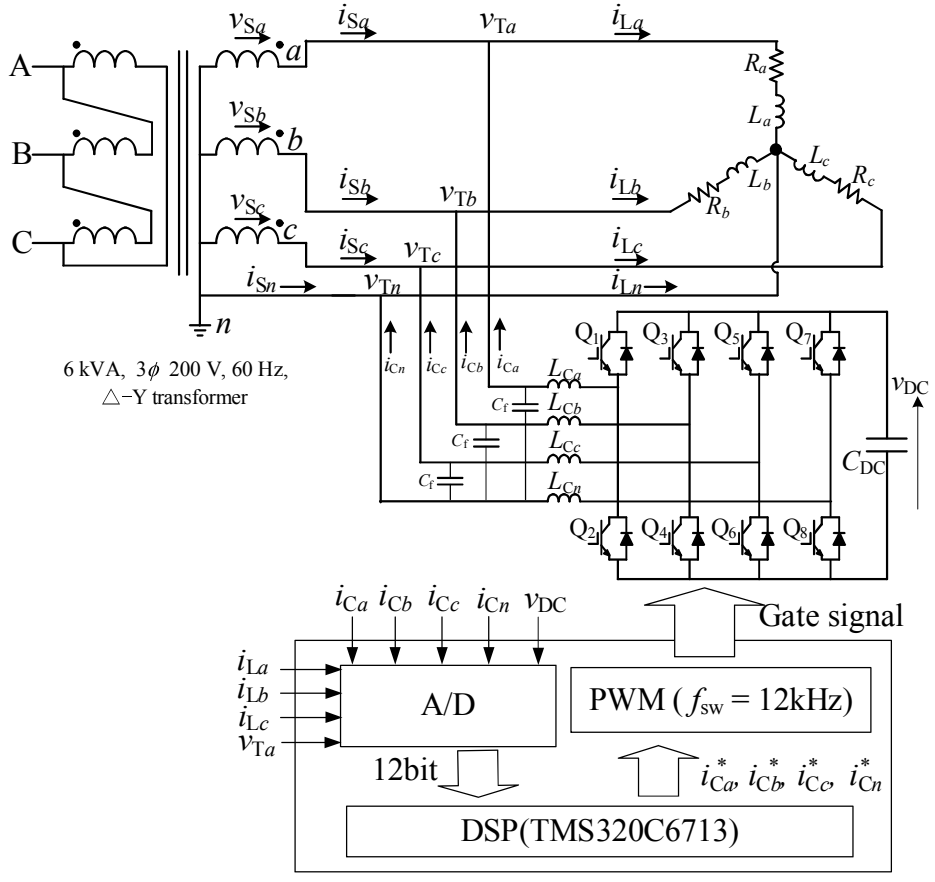

Figure 5.21: Constructed experimental model of the ALB.

Table 5.5: Parameters of distribution transformer in the experiment.

Item	Symbol	Value
Rated power of transformer		6 kVA
Rated power on each phase		2 kVA
Rated line to line rms voltage in both primary and secondary side		200 V
Rated line to neutral rms voltage in secondary side	v_{Sa}, v_{Sb}, v_{Sc}	115 V
Rated frequency	f	60 Hz

Table 5.6: Circuit constants of active load balancer in the experiment.

Item	Symbol	Value
Reference DC capacitor voltage	V^*_{DC}	385 V
Capacity of capacitor	C_{DC}	2200 μF
Compensation inductance	$L_{Ca}, L_{Cb}, L_{Cc}, L_{Cn}$	1.5 mH
Switching frequency	f_{sw}	12 kHz

As shown in the block diagram, the line-to-neutral voltage v_{Ta} is detected and then inputted to the DSP through a 12-bit A/D converter. The other signals detected for the DSP are the three load currents, the three compensation output currents and the DC capacitor voltage through the 12-bit A/D converters. In the DSP, the effective value I_p of the source-side active current is detected using the constant DC capacitor voltage control strategy. Then, $\sqrt{2}\cos(\omega t)$, which is synchronized with the a-phase, $\sqrt{2}\cos(\omega t - \frac{2\pi}{3})$, which is synchronized with the b-phase, and $\sqrt{2}\cos(\omega t - \frac{4\pi}{3})$, which is synchronized with the c-phase, are calculated using θ_T. Finally, the compensation reference values i^*_{Ca}, i^*_{Cb} and i^*_{Cc} for the ALB are obtained by (5.11). The sine triangle intercept technique is used to control the output currents i_{Ca}, i_{Cb} and i_{Cc}. These compensation output currents are also inputted to the DSP for current feed back control, where the PI controller in dq coordinates are also constructed. A Yokogawa SL1000 high-speed data acquisition unit with a

sampling rate of 5μs is used.

First, the effective value I_p of the source-side active current which is generated by the constant DC capacitor voltage control in the DSP is analyzed. Figure 5.22 shows the experimental waveforms of the three terminal voltages v_{Ta} v_{Tb} v_{Tc}, the three load currents i_{La} i_{Lb} i_{Lc}, the calculated active current from the detected terminal voltages and load currents, and the detected effective active current I_p, which is generated by the constant DC capacitor voltage control. The detected effective active current I_p generated by the constant DC capacitor voltage control is closely the same as calculated values using the terminal voltages and load currents. Therefore, the calculation steps of the active load current can be reduced in the constant DC capacitor voltage control based strategy.

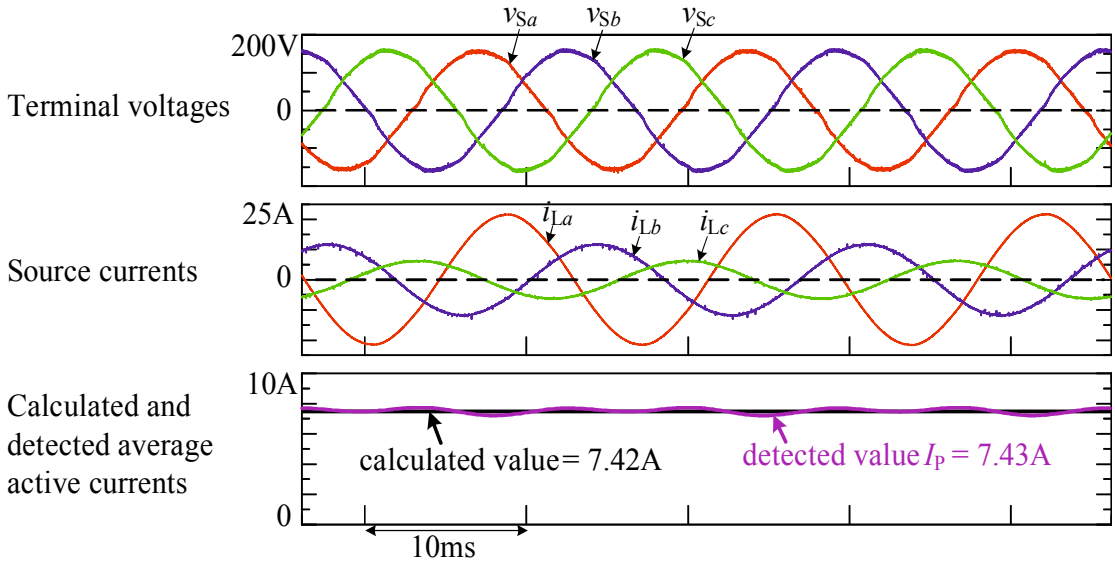

Figure 5.22: Comparison of detected load current by constant DC capacitor voltage control and the calculated value.

Figure 5.23 shows the experiment results for the ALB in Figure 5.21 with the proposed constant DC capacitor voltage control based strategy. The *a*-phase load current i_{La} is changed from 0.9 pu to 0.2 pu while the *b*-phase load i_{Lb} and *c*-phase load i_{Lc} are kept constant. Before and after load current variation, the source currents i_{Sa}, i_{Sb} and i_{Sc} are balanced. The fourth leg of the ALB generates the same zero-sequence current of the load-side providing very small amount of current flow in the source-side neutral current i_{Sn}. The DC capacitor voltage v_{DC} closely follows its

reference value V^*_{DC} in the transient and steady states. The amount of ripple of the DC capacitor voltage is less than 2.3% in both the transient and steady states.

Figure 5.24 shows the experiment results for the ALB in Figure 5.21 upon varying the *a*-phase load current from 0.2 pu to 0.9 pu. The source currents i_{Sa}, i_{Sb} and i_{Sc} are balanced with a unity power factor. The DC capacitor voltage v_{DC} is well controlled to its reference value V^*_{DC} in the transient and steady states. The amount of ripple of the DC capacitor voltage is less than 2.5% in both transient and steady states.

The reduction of distribution transformer loss is the one of primary reason for installing the ALB in three-phase four-wire distribution systems. Therefore, loss analysis was performed using experimental model of Figure 5.21. The primary-side (input) and secondary-sides (output) power of the distribution transformer are detected with and without ALB under the same condition. The results are shown in Table 5.7.

Table 5.7: Loss analysis of distribution transformer.

Item	Primary-side (input power)	Secondary-side (output power)	Loss
Without ALB	2506.5 W	2423.0 W	83.5 W
With ALB	2573.9 W	2523.7 W	50.2 W

The results confirm that the ALB can reduce the loss of the distribution transformer. But, some amount of power is used for the ALB operation. By comparing the results, the ALB can reduce loss about 33 W but it use about 100 W for its operation. However, the distribution line loss caused by reactive power and the efficiency improvement of the consumer loads should be taken into account in actual operation of the ALB.

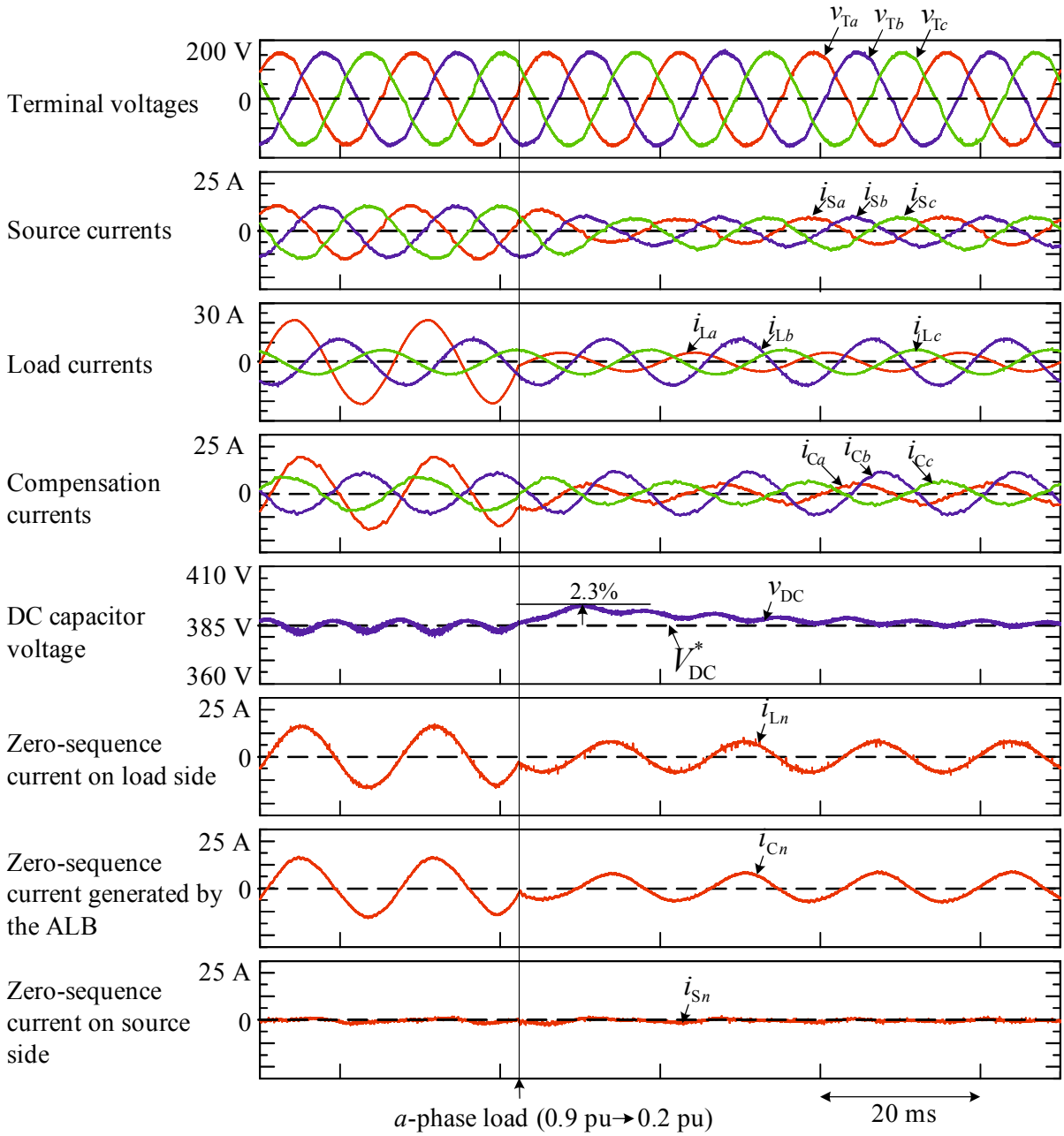

Figure 5.23: Experimental results of the proposed ALB with constant DC capacitor voltage control strategy (from heavy to light load variation).

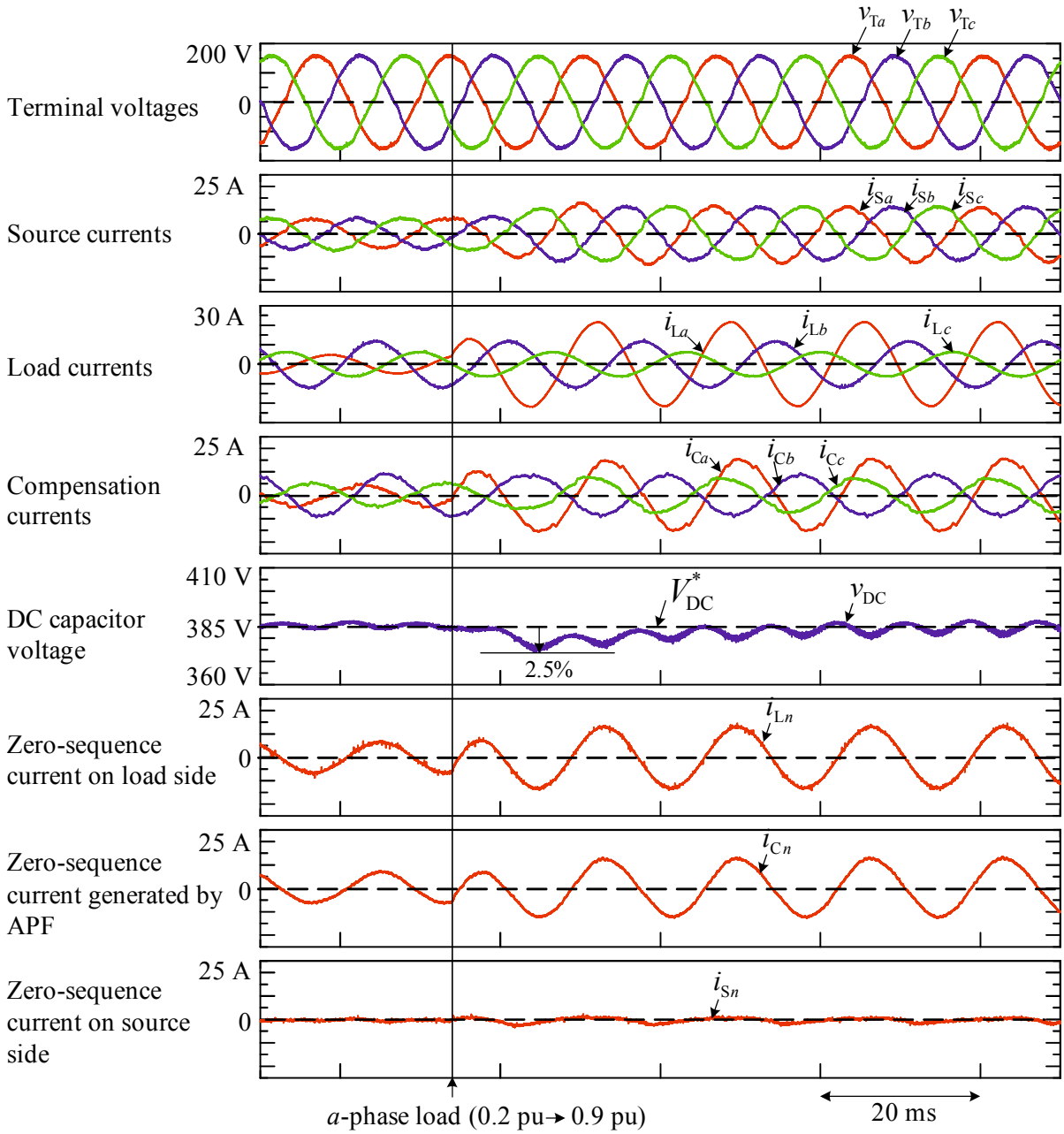

Figure 5.24: Experimental results of the proposed ALB with constant DC capacitor voltage control strategy (from light to heavy load variation).

5.6 Conclusion

In this chapter, the active load balancer with constant DC capacitor voltage control based strategy was discussed in three-phase four-wire distribution systems. Three-phase four-wire distribution systems can generate zero sequence current of the loads. Thus, the four-leg inverter based ALB is selected in the proposed circuit topology of the ALB to compensate the zero-sequence current of the loads. The basic principle of the constant DC capacitor voltage control strategy was discussed in three-phase four-wire distribution systems. The instantaneous power flow of the ALB gives important suggestion that maintaining the DC capacitor voltage at constant can generate the effective active current of the load for any unbalanced load conditions. Therefore, the calculation block of active and reactive load currents can be reduced in the proposed constant DC capacitor voltage control strategy. Figure 5.25 shows the required calculation steps for compensation currents in existing control strategy in Figure 5.25(a) [9] and the proposed constant DC capacitor voltage control strategy in Figure 5.25(b).

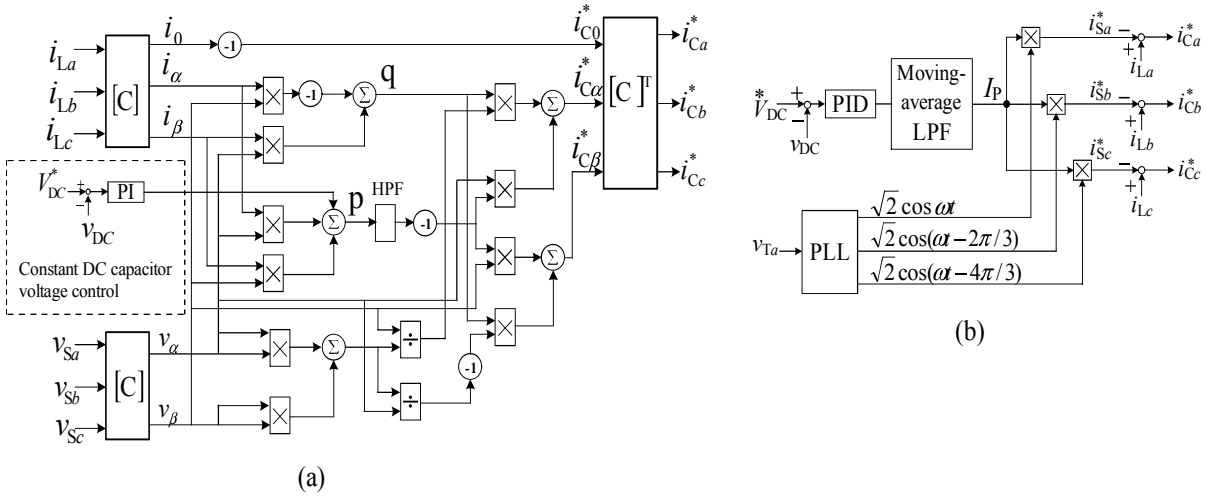

Figure 5.25: Required calculation steps of compensation currents in existing control strategy (a) and the constant DC capacitor voltage control strategy (b).

The proposed constant DC capacitor voltage control based strategy for the ALB in three-phase four-wire distribution system has been published the Institute of Electrical Engineer of Japan (IEEJ) Journal of Industry Applications with the simulation results and Journal of International Conference on Electrical Machines and Systems with the experimental results.

Chapter 6

Reactive Power Control Strategy Based on DC Capacitor Voltage Control for Active Load Balancer in Three-Phase Four-Wire Distribution Systems

6.1 Introduction

In the previous chapter, the constant DC capacitor voltage control based strategy for the active load balancer (ALB) was discussed and confirmed by both simulation and experiment in the three-phase four-wire distribution systems. The distribution transformer loss is also analysis with/without the ALB using experimental data. Using the ALB can reduce power loss of the distribution transformer, which are caused by unbalanced and reactive component of load currents. In the ALB design, the relative power rating of the active load balancer (ALB) with the distribution system is also important. Minimum power rating the ALB power rating is necessary in practical application. In this chapter, a new reactive power control strategy based on DC capacitor voltage control is proposed to reduce the power rating of the ALB. The basic principle of a new reactive power control strategy is discussed in detail using instantaneous power flow of the ALB and then confirmed by digital computer simulation using PSIM software. The experimental verification is also performed to validate the feasibility of the proposed control strategy. Then, the relationships between the power rating of the ALB and reactive power of source side currents are discussed using theoretical calculation, simulation and experimental results.

6.2 Power Circuit Diagram

The power circuit diagram of the active load balancer (ALB) for the reactive power control based strategy is the same as in the chapter 5 and it is shown again in 6.1. The three-phase four-wire distribution system is composed of three-phase four-wire Y-connected distribution transformer (secondary-side) and three unbalanced single-phase loads. v_{Sa}, v_{Sb} and v_{Sc} are three sources of distribution transformer with neutral grounded. The three single-phase unbalanced loads are composed of R_a, L_a, R_b, L_b and R_c, L_c. The ALB is constructed with four legs power switching devices with a common DC capacitor. The three legs of the ALB is connected to the *a*-phase, *b*-phase and *c*-phase of the distribution system, and the fourth leg is connected to the neutral. The unbalanced active and reactive currents drawn by the unbalanced single-phase load is compensated by the ALB.

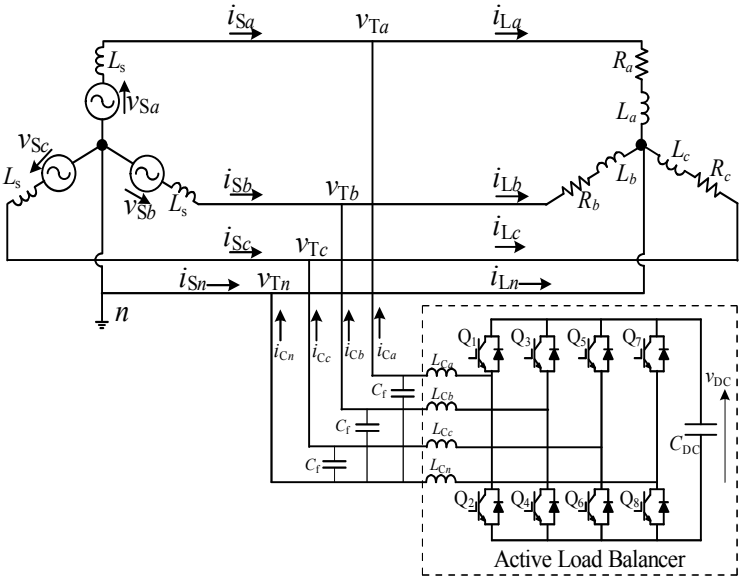

Figure 6.1: Power circuit diagram of the ALB.

6.3 Reactive Power Control Strategy

Figure 6.2 shows the complete reactive power control strategy based on DC capacitor voltage control for the ALB in the three-phase four-wire distribution systems. The control strategy in-

cludes the reference source currents calculation using constant DC capacitor voltage control, the reference compensation currents calculation and the current feedback control.

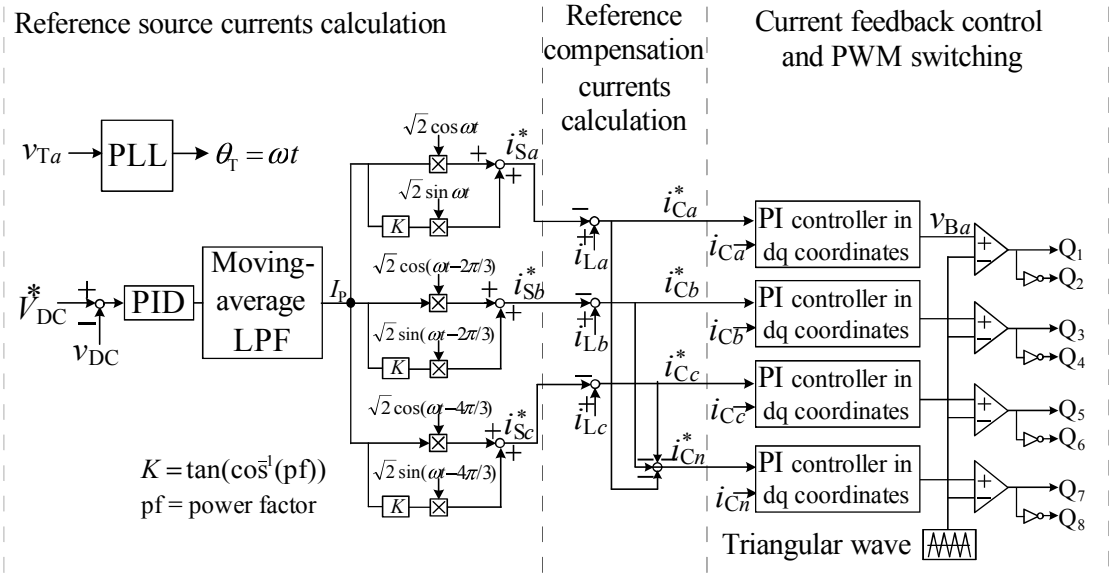

Figure 6.2: Reactive power control strategy based on DC voltage control.

The principle of the reference source current calculation for the ALB with the reactive power control strategy is discussed. The three-phase terminal voltages v_{Ta}, v_{Tb} and v_{Tc} in Figure 6.1 are

$$\begin{aligned} v_{Ta} &= \sqrt{2}V_{T}\cos(\omega t), \\ v_{Tb} &= \sqrt{2}V_{T}\cos(\omega t - \frac{2\pi}{3}), \\ v_{Tc} &= \sqrt{2}V_{T}\cos(\omega t - \frac{4\pi}{3}). \end{aligned} \tag{6.1}$$

The load currents i_{La}, i_{Lb}, and i_{Lc} drawn by each single-phase load are also expressed as

$$\begin{aligned} i_{La} &= \sqrt{2}I_{a}\cos(\omega t - \phi_{a}), \\ i_{Lb} &= \sqrt{2}I_{b}\cos(\omega t - \frac{2\pi}{3} - \phi_{b}), \\ i_{Lc} &= \sqrt{2}I_{c}\cos(\omega t - \frac{4\pi}{3} - \phi_{c}). \end{aligned} \tag{6.2}$$

Let us assume that the three-phase source currents i_{Sa}, i_{Sb}, and i_{Sc} are balanced with a power factor of $\cos\theta$ after compensating the unbalanced active components with reactive power control.

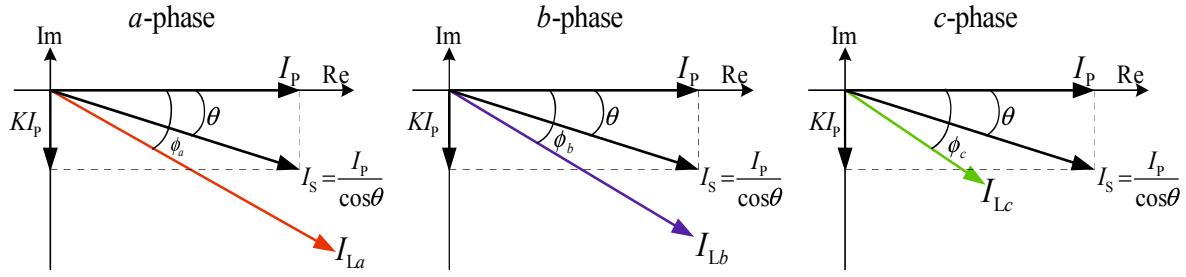

$$I_P = (I_a\cos\phi_a + I_b\cos\phi_b + I_c\cos\phi_c)/3, \quad K = \tan(\cos^{-1}(\text{pf})), \quad \text{pf=source-side power factor}$$

Figure 6.3: Phasor representation of reactive power control strategy.

The three-phase source currents, therefore, can be expressed as

$$\begin{aligned} i_{Sa} &= \sqrt{2}I_S\cos(\omega t - \theta), \\ i_{Sb} &= \sqrt{2}I_S\cos(\omega t - \frac{2\pi}{3} - \theta), \\ i_{Sc} &= \sqrt{2}I_S\cos(\omega t - \frac{4\pi}{3} - \theta), \end{aligned} \tag{6.3}$$

where $I_S = (I_a\cos\phi_a + I_b\cos\phi_b + I_c\cos\phi_c)/(3\cos\theta)$ as shown in Figure 6.3. I_S is the theoretical rms value of the balanced source current with a power factor of $\cos\theta$ for each phase and I_P is the theoretical average rms value of the active current for any unbalanced load condition. From (6.2) and (6.3), the compensation currents of the ALB are calculated as

$$\begin{aligned} i_{Ca} &= i_{La} - i_{Sa} \\ &= (I_a\cos\phi_a - I_S\cos\theta)\sqrt{2}\cos(\omega t) + (I_a\sin\phi_a - I_S\sin\theta)\sqrt{2}\sin(\omega t), \\ i_{Cb} &= i_{Lb} - i_{Sb} \\ &= (I_b\cos\phi_b - I_S\cos\theta)\sqrt{2}\cos(\omega t - \frac{2\pi}{3}) + (I_b\sin\phi_b - I_S\sin\theta)\sqrt{2}\sin(\omega t - \frac{2\pi}{3}), \\ i_{Cc} &= i_{Lc} - i_{Sc} \\ &= (I_c\cos\phi_c - I_S\cos\theta)\sqrt{2}\cos(\omega t - \frac{4\pi}{3}) + (I_c\sin\phi_c - I_S\sin\theta)\sqrt{2}\sin(\omega t - \frac{4\pi}{3}). \end{aligned} \tag{6.4}$$

The instantaneous power p_{C} flowing to the ALB can be calculated as

$$\begin{aligned} p_{\mathrm{C}} &= v_{\mathrm{T}a} \cdot i_{\mathrm{C}a} + v_{\mathrm{T}b} \cdot i_{\mathrm{C}b} + v_{\mathrm{T}c} \cdot i_{\mathrm{C}c} \\ &= \left(2I_a\cos\phi_a - I_b\cos\phi_b - I_c\cos\phi_c + \sqrt{3}I_b\sin\phi_b - \sqrt{3}I_c\sin\phi_c\right)\frac{1}{2}V_{\mathrm{T}}\cos(2\omega t) + \\ &\quad \left(2I_a\sin\phi_a - I_b\sin\phi_b - I_c\sin\phi_c - \sqrt{3}I_b\cos\phi_b + \sqrt{3}I_c\cos\phi_c\right)\frac{1}{2}V_{\mathrm{T}}\sin(2\omega t). \end{aligned} \tag{6.5}$$

The mean value of the instantaneous power p_{C} in (6.5) is zero, while the source currents in (6.3) are balanced with the same phase angle θ. Thus, maintaining a constant DC capacitor voltage in the ALB will result in a balanced condition with a predefined power factor $\cos\theta$ on the source side. Therefore, the constant DC capacitor voltage control can ideally be used for the reactive power control strategy of the ALB in three-phase four-wire distribution systems. In practical applications, the instantaneous DC capacitor voltage is not constant owing to the 2ω components caused by the unbalanced load conditions. Thus, the constant mean value of the DC capacitor voltage is controlled in the proposed method.

To perform constant DC capacitor voltage control, the DC capacitor voltage v_{DC} is detected in Figure 6.1. Then the difference between the detected DC capacitor voltage v_{DC} and the reference DC capacitor voltage V^*_{DC} is amplified by the PID controller as shown in Figure 6.2. The output value of the PID controller is input to a moving-average low-pass filter (LPF). The moving-average LPF is designed to remove the 2ω components, where ω is the angular frequency of the terminal voltage. The transfer function of the moving-average LPF is expressed as

$$H(z) = \frac{1}{N}\sum_{n=0}^{N-1} z^{-n}, \tag{6.6}$$

where N is the number of samples. After filtering with the moving-average LPF, the effective active value I_{P} of the source-side active current is obtained by performing constant DC capacitor voltage control.

To calculate the reference source currents for the ALB, the a-phase terminal voltage $v_{\mathrm{T}a}$ is detected, and then the electrical angle ($\theta_{\mathrm{T}} = \omega t$) is generated using a single-phase phased-lock loop (PLL) [25]. Next, $\sqrt{2}\cos(\omega t)$, $\sqrt{2}\cos(\omega t - \frac{2\pi}{3})$, $\sqrt{2}\cos(\omega t - \frac{4\pi}{3})$, $\sqrt{2}\sin(\omega t)$, $\sqrt{2}\sin(\omega t - \frac{2\pi}{3})$, and $\sqrt{2}\sin(\omega t - \frac{4\pi}{3})$ are calculated using θ_{T}. Using these calculated values and the effective value

I_P, the reference source currents for each phase are calculated as

$$\begin{aligned} i^*_{Sa} &= \sqrt{2}I_P\cos(\omega t) + K\sqrt{2}I_P\sin(\omega t), \\ i^*_{Sb} &= \sqrt{2}I_P\cos(\omega t - \frac{2\pi}{3}) + K\sqrt{2}I_P\sin(\omega t - \frac{2\pi}{3}), \\ i^*_{Sc} &= \sqrt{2}I_P\cos(\omega t - \frac{4\pi}{3}) + K\sqrt{2}I_P\sin(\omega t - \frac{4\pi}{3}), \end{aligned} \tag{6.7}$$

where $K = \tan(\cos^{-1}(\text{pf}))$ as shown in Figure 6.3. Therefore, the source side power factor can be adjusted by changing the value of K.

For the reference compensation current calculation, the calculated reference source currents i^*_{Sa} i^*_{Sb} i^*_{Sc} are compared with the detected load currents i_{La} i_{La} and i_{Lc}. Finally, the reference compensation signals for the ALB are expressed as

$$\begin{aligned} i^*_{Ca} &= i_{La} - i^*_{Sa}, \\ i^*_{Cb} &= i_{Lb} - i^*_{Sb}, \\ i^*_{Cc} &= i_{Lc} - i^*_{Sc}, \\ i^*_{Cn} &= -\left(i^*_{Ca} + i^*_{Cb} + i^*_{Cc}\right). \end{aligned} \tag{6.8}$$

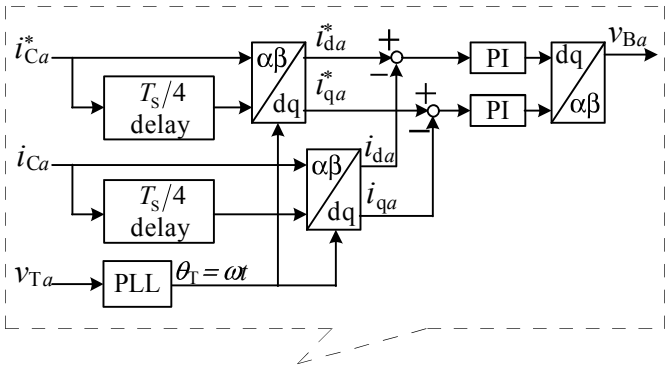

Figure 6.4: PI controller in dq coordinate.

In the current feedback control, PI controllers in dq coordinates are used to avoid the steady-state error of the feedback control in the ALB [27]. Figure 5.18 shows the block diagram of PI controller in dq coordinate, where i^*_{Ca} is the reference signal, i_{Ca} is the detected signal and v_{Ba} is the feedback control output. The operation principle is identical among the phases and neutral as shown in Figure 5.17. As shown in Figure 5.18, the *a*-phase reference compensation current

i^*_{Ca} is delayed by $T_S/4$, where T_S is the cycle of the a-phase source voltage. i^*_{Ca} corresponds to the α-component, and the delayed current through the $T_S/4$ delay block corresponds to the β-component. Using θ_T, i.e., the electrical angle of the a-phase terminal voltage generated by the PLL, the α- and β-components are transformed into i^*_{da} and i^*_{qa}, respectively. The compensation output current i_{Ca} is also transformed into i_{da} and i_{qa} in the same way. The differences between the reference currents i^*_{da}, i^*_{qa} and the detected currents i_{da}, i_{qa} are amplified by the PI controller in dq coordinates. The amplified values are retransformed into the a-phase components. Then, using the pulse width modulation (PWM) technique, the gate signals for the power switching devices of the ALB are generated.

6.4 Simulation Results

To confirm the validity and high practicability of the proposed reactive power control strategy for the ALB, digital computer simulation is implemented using PSIM software. The circuit parameters for the distribution transformer, the load conditions and the four-leg based ALB are the exactly the same as in chapter 5. The parameters of distribution transformer in Figure 6.1 are shown again in Table 6.1. The rating of the distribution transformer is 3-phase 380V, 21.5kVA and 60Hz. The line-to-line voltage of 380V used in the simulation is similar to that for a practical three-phase four-wire distribution system. The base value is 7.1kVA for each single phase system. The three single-phase loads are shown in Table 6.2. The load conditions for a-phase include two different loads, while the b-phase and c-phase loads are kept constant. The unbalanced load percentage is calculated as the ratio of the negative-sequence to positive-sequence values in accordance with the International Electrotechnical Commission (IEC) standard. Table 6.3 shows the circuit constants for the four-leg based ALB in Fig. 6.1. The reference value of the DC capacitor voltage V^*_{DC} is set to 780V.

Figure 6.5 shows the simulation waveforms for the ALB in Figure 6.1 with the proposed reactive power control strategy. v_{Ta}, v_{Tb}, and v_{Tc} are the a-phase, b-phase, and c-phase terminal voltages, respectively. The a-phase load current i_{La} is varied from 0.9 pu to 0.2 pu, while the b-phase and c-phase load currents, i_{Lb} and i_{Lc}, are kept constant. The unbalanced load percentage is 31% before the load variation and 30% after the load variation. The power factor is set to 0.9

Table 6.1: Parameters of the distribution transformer in the simulation.

Item	Symbol	Value
Rated power of transformer		21.5 kVA
Rated power for each phase		7.1 kVA
Rated line-to-line rms voltage	v_o	380 V
Rated line to neutral rms voltage	v_{Sa}, v_{Sb}, v_{Sc}	220 V
Rated frequency	f	60 Hz

Table 6.2: Load conditions of three-phase four-wire distribution system.

Item	Symbol	Value
a-phase load (large load condition)	R_a	6.1 Ω
(0.9 pu, power factor 0.8)	L_a	12 mH
a-phase load (small load condition)	R_a	25 Ω
(0.2 pu, power factor 0.8)	L_a	50 mH
b-phase load	R_b	10 Ω
(0.5 pu, power factor 0.8)	L_b	20 mH
c-phase load	R_c	20 Ω
(0.25 pu, power factor 0.8)	L_c	40 mH
unbalanced load percent (with a-phase large load)		31%
unbalanced load percent (with a-phase small load)		30%

in the control strategy in accordance with the Japanese guidelines [28]. Before and after the load current variation, the three source currents i_{Sa}, i_{Sb}, and i_{Sc} are balanced as shown in Fig. 6.5. The power factor, cosθ, is 0.9 under the heavy-load condition and 0.91 under the light-load condition. A slight difference in the power factor was occured because of the filter capacitor effect of the ALB. Because of the unbalanced load condition in both heavy and light load conditions, zero-

Table 6.3: Circuit constants of active load balancer.

Item	Symbol	Value
Reference DC capacitor voltage	V^*_{DC}	780 V
Capacity of capacitor	C_{DC}	2200 μF
Compensation inductance	L_{Ca}, L_{Cb}, L_{Cc}, L_{Cn}	2.5 mH
Switching frequency	f_{sw}	12 kHz

sequence current $i_{\mathrm{L}n}$ is flowed in the load-side. The ALB generates the zero-sequence currents which was nearly the same with the zero-sequence current of the loads. Thus, the transformer neutral current $i_{\mathrm{S}n}$ is nearly zero as shown in Figure 6.5. The DC capacitor voltage v_{DC} is well controlled with respect to its reference value V^*_{DC} in both the transient and steady states. The ripple in the DC capacitor voltage is 2.8% in the transient state and less than $\pm$1% in the steady state.

Figure 6.6 shows the simulation results upon varying the a-phase load current $i_{\mathrm{L}a}$ from 0.2 pu to 0.9 pu while the b-phase and c-phase load currents $i_{\mathrm{L}b}$ and $i_{\mathrm{L}c}$ are kept constant. The unbalanced load percentage is 30% before load variation and 31% after load variation. Before/after load current variation, the source currents $i_{\mathrm{S}a}$, $i_{\mathrm{S}b}$ and $i_{\mathrm{S}c}$ are balanced with with a predefined power factor. The DC capacitor voltage v_{DC} is also well controlled to its reference value in this load variation. The amount of ripple of the DC capacitor voltage in the transient state is 2.8%.

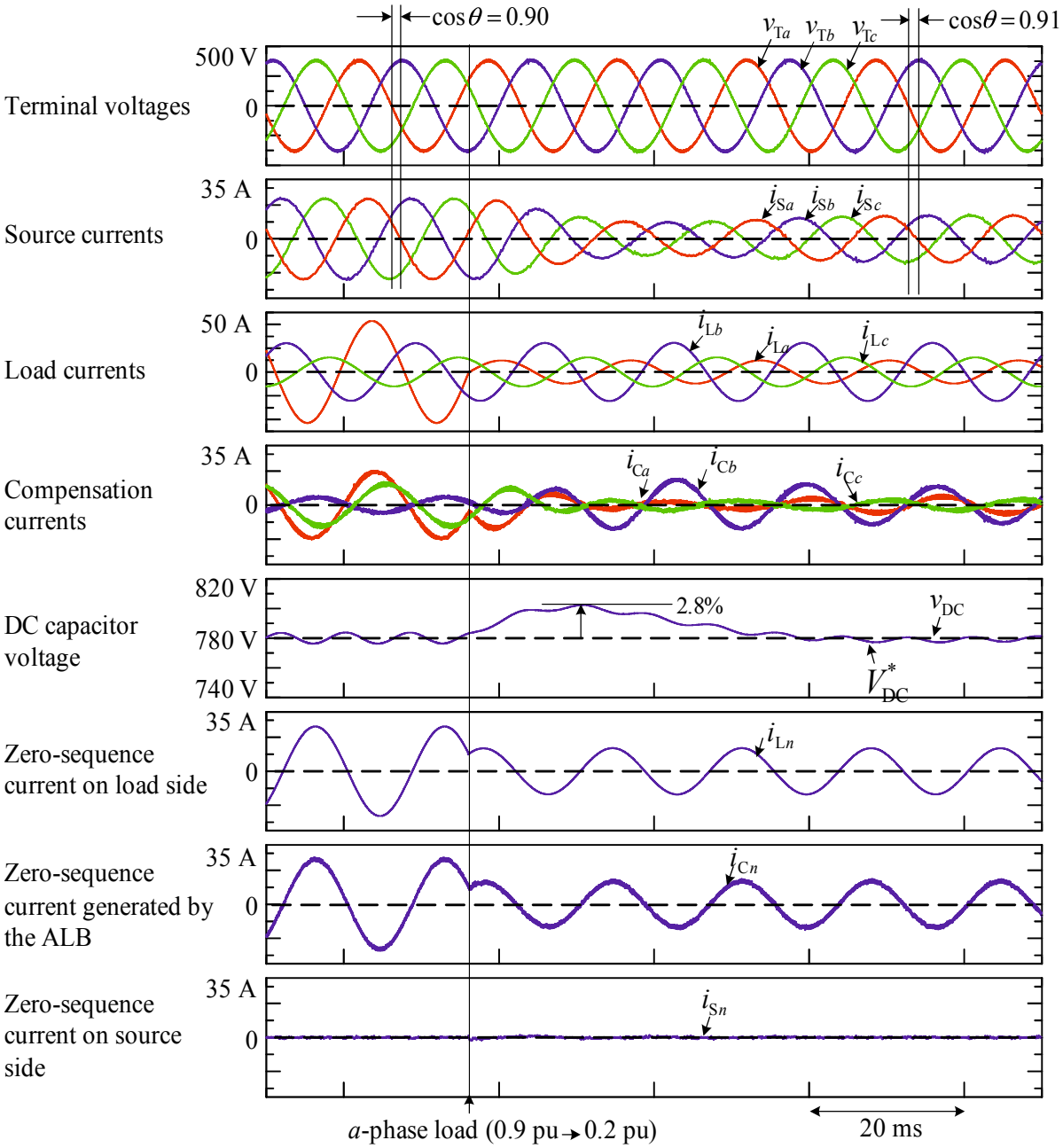

Figure 6.5: Simulation results of the proposed ALB with reactive power control strategy (from heavy to light load variation).

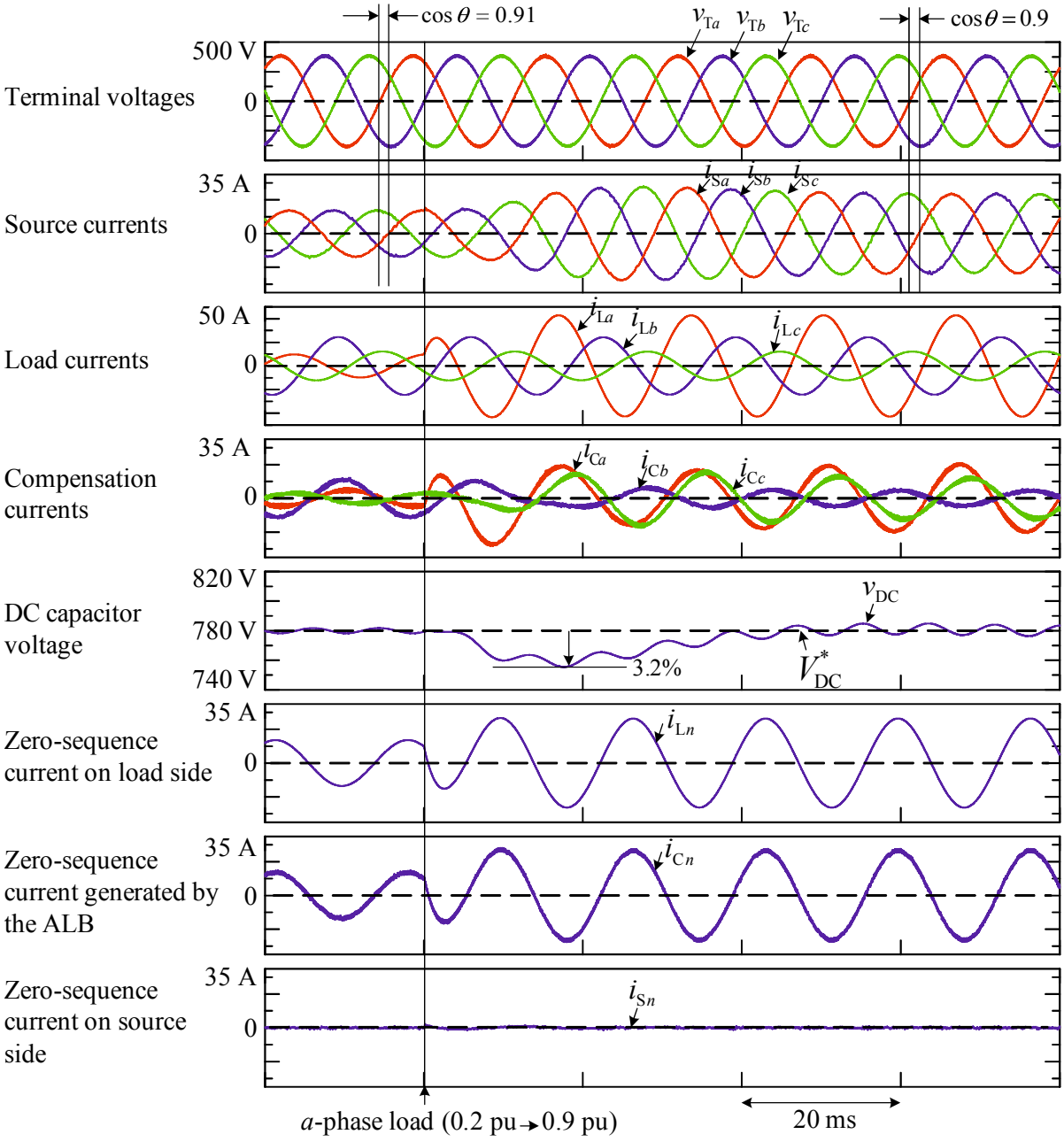

Figure 6.6: Simulation results of the proposed ALB with reactive power control strategy (from light to heavy load variation).

6.5 Experimental Results

A reduced-scale experimental model of the ALB with the proposed reactive power control strategy is constructed and tested to demonstrate the validity and high practicability of the proposed systems. The constructed experimental model is exactly the same as in chapter 5 and shown again in Figure 6.7. A Δ-Y connected distribution transformer is used in the experiment. The utility three-phase system distributes 200V in Japan. Therefore, a line-to-line voltage of 200V is used in the experiment instead of 380V. The rating of the transformer is 3-phase, 200 V, 6 kVA and 60 Hz on both the primary and secondary sides as shown in Table 6.1. The load conditions of the distribution system are the same as those in Table 6.2. The circuit constants of the ALB in the experiment are shown in Table 5.6. A digital signal processor (DSP: TMS320C6713, 225MHz) is used in the experimental setup.

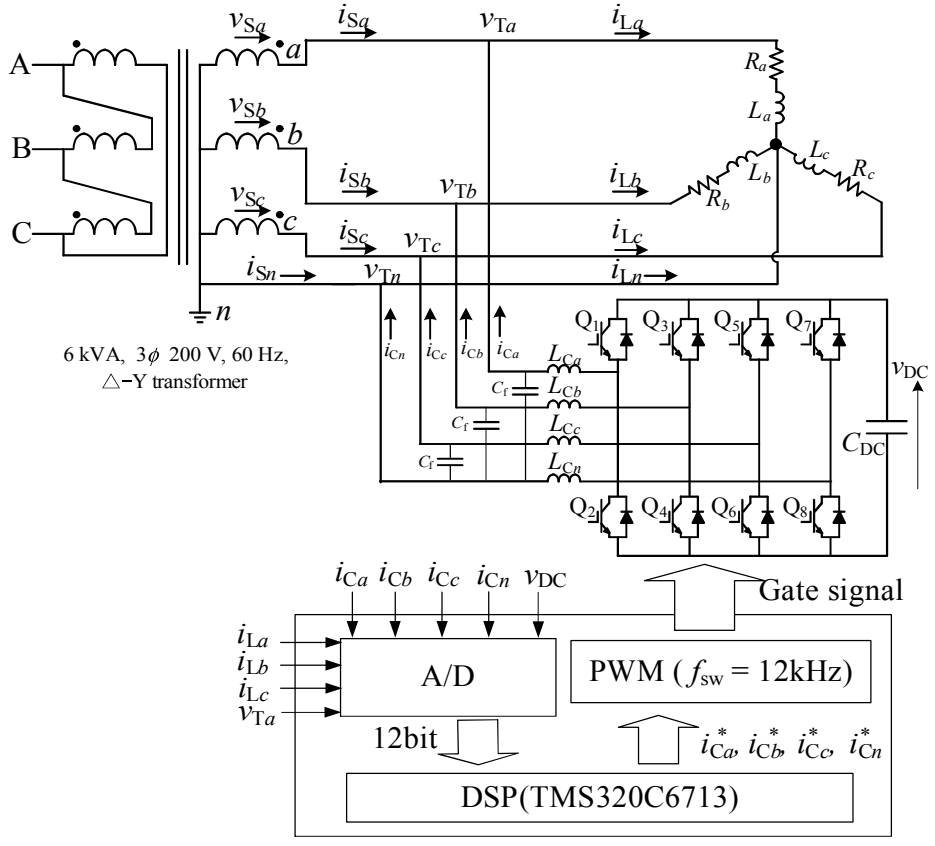

Figure 6.7: Constructed experimental model of the ALB with the reactive power control strategy.

As shown in the experimental diagram, the line-to-neutral voltage v_{Ta} is detected and then inputted to the DSP through a 12-bit A/D converter. The other signals detected for the DSP are the three load currents, the three compensation output currents and the DC capacitor voltage through the 12-bit A/D converters. In the DSP, the effective value I_p of the source-side active current is detected using the constant DC capacitor voltage control strategy. Then, $\sqrt{2}\cos(\omega t)$, $\sqrt{2}\cos(\omega t - \frac{2\pi}{3})$, $\sqrt{2}\cos(\omega t - \frac{4\pi}{3})$, $\sqrt{2}\sin(\omega t)$, $\sqrt{2}\sin(\omega t - \frac{2\pi}{3})$, and $\sqrt{2}\sin(\omega t - \frac{4\pi}{3})$ are calculated using θ_{T}. Finally, the compensation reference values i^*_{Ca}, i^*_{Cb} and i^*_{Cc} for the ALB are calculated as shown in the phasor diagram in 6.3 in the DSP. The sine triangle intercept technique is used to control the output currents i_{Ca}, i_{Cb}, i_{Cc} and i_{Cn}. These compensation output currents are also inputted to the DSP for current feed back control, where the PI controller in dq coordinates are also constructed. A Yokogawa SL1000 high-speed data acquisition unit with a sampling rate of 5μs is used.

Figure 6.8 shows the experiment results for the ALB in Figure 6.7 with the proposed reactive power control strategy. The *a*-phase load current i_{La} is changed from 0.9 pu to 0.2 pu while the *b*-phase load i_{Lb} and *c*-phase load i_{Lc} are kept constant. Before and after load current variation, the source currents i_{Sa}, i_{Sb} and i_{Sc} are balanced. The power factor, cosθ, is 0.9 under the heavy-load condition and 0.91 under the light-load condition. A slight difference in the power factor was occurred because of the filter capacitor effect of the ALB. The fourth leg of the ALB generates the same zero-sequence current of the load-side providing very small amount of current flow in the source-side neutral current i_{Sn}. The DC capacitor voltage v_{DC} closely follows its reference value V^*_{DC} in the transient and steady states. The amount of ripple of the DC capacitor voltage is less than 2.5% in both the transient and steady states.

Figure 6.9 shows the experimental results upon varying the *a*-phase load current i_{La} from 0.2 pu to 0.9 pu while the *b*-phase and *c*-phase load currents i_{Lb} and i_{Lc} are kept constant. The unbalanced load percentage is 30% before load variation and 31% after load variation. Before/after load current variation, the source currents i_{Sa}, i_{Sb} and i_{Sc} are balanced with with a predefined power factor. The DC capacitor voltage v_{DC} is also well controlled to its reference value in this load variation. The amount of ripple of the DC capacitor voltage in the transient state is 2.8%.

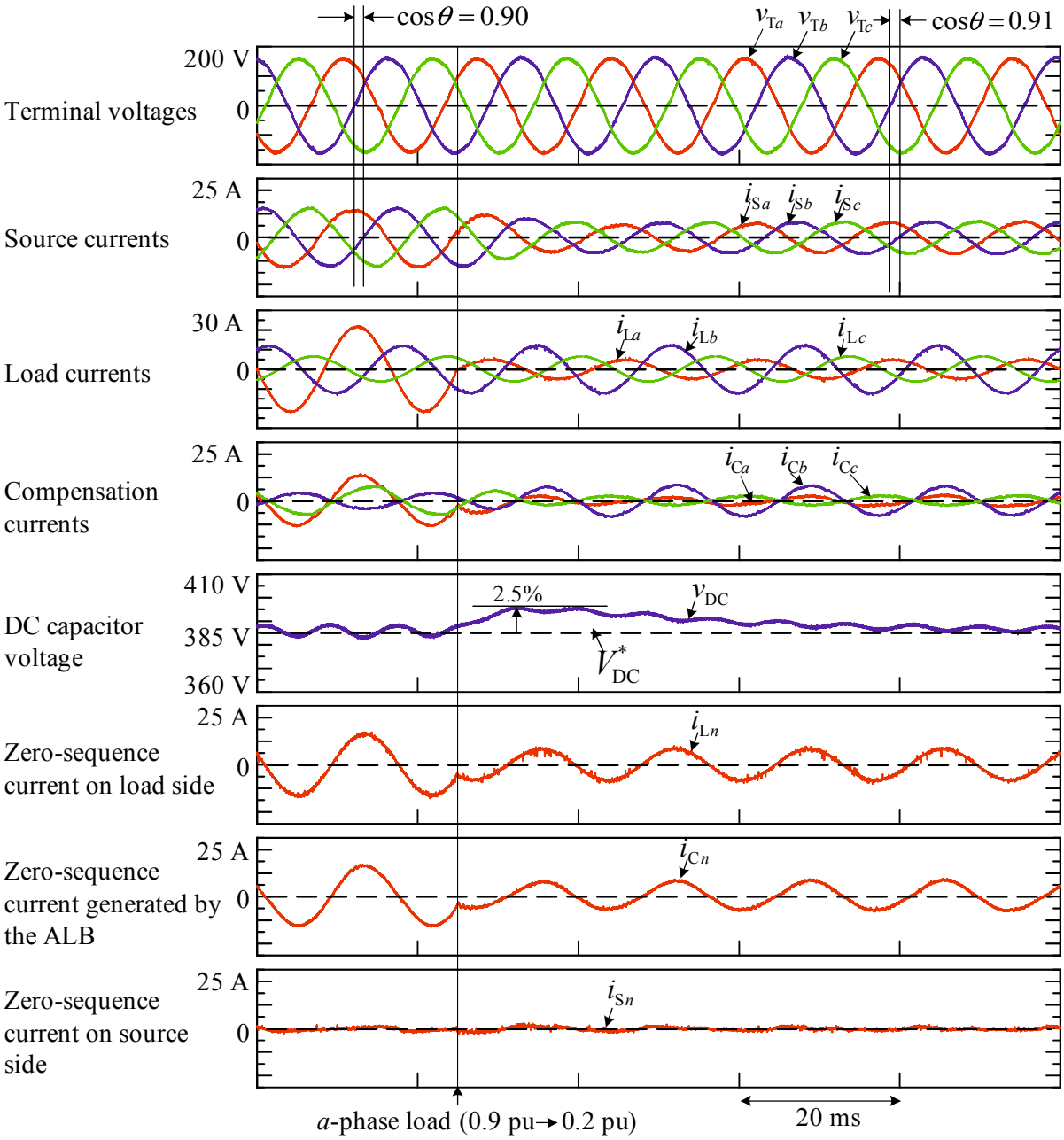

Figure 6.8: Experimental results of the proposed ALB with reactive power control strategy (from heavy to light load variation).

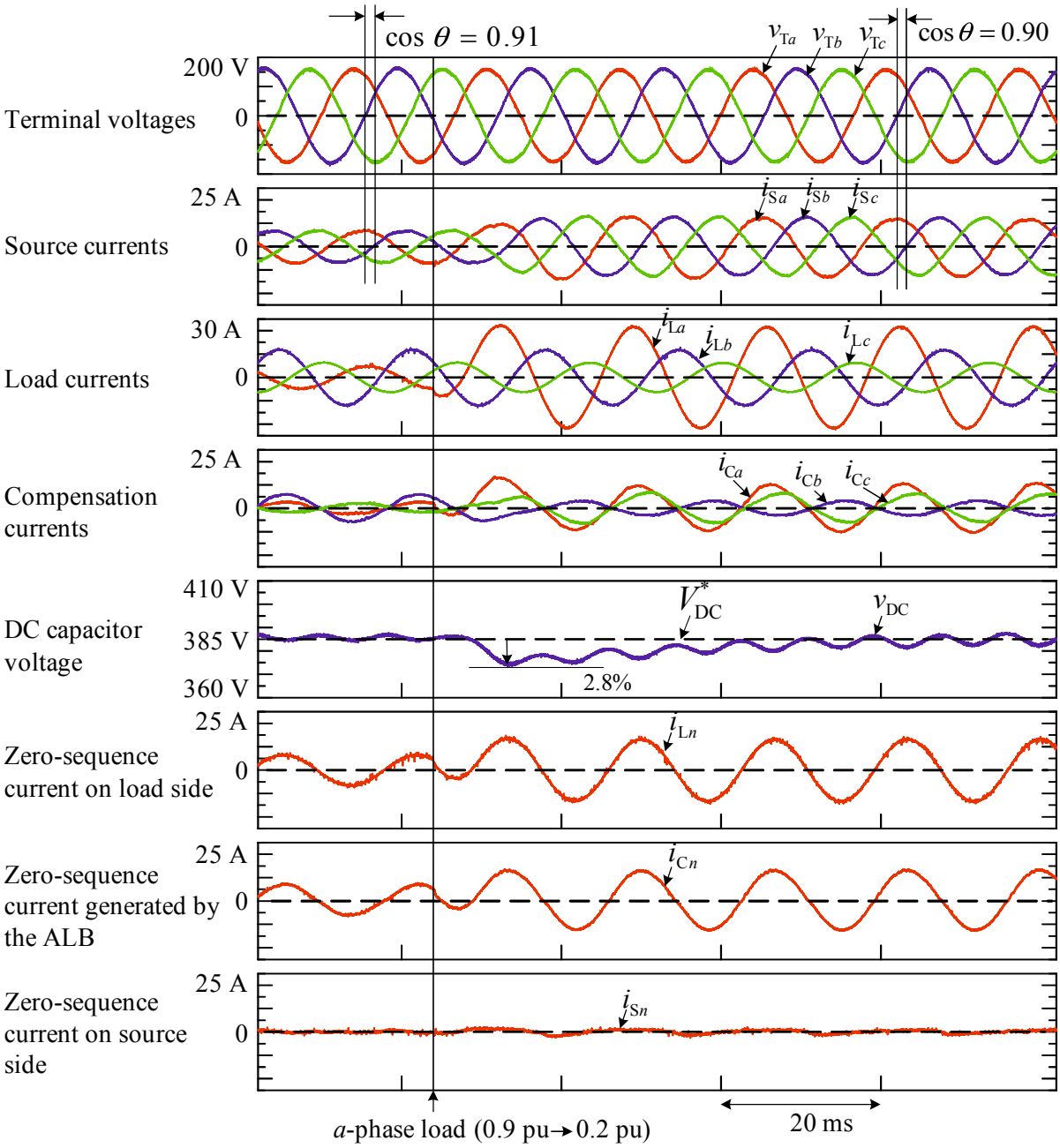

Figure 6.9: Experimental results of the proposed ALB with reactive power control strategy (from heavy to light load variation).

The required power rating S_C of the ALB with four-leg switching devices is discussed. Fig. 6.10 shows the equivalent circuit of the ALB in three-phase four-wire distribution systems.

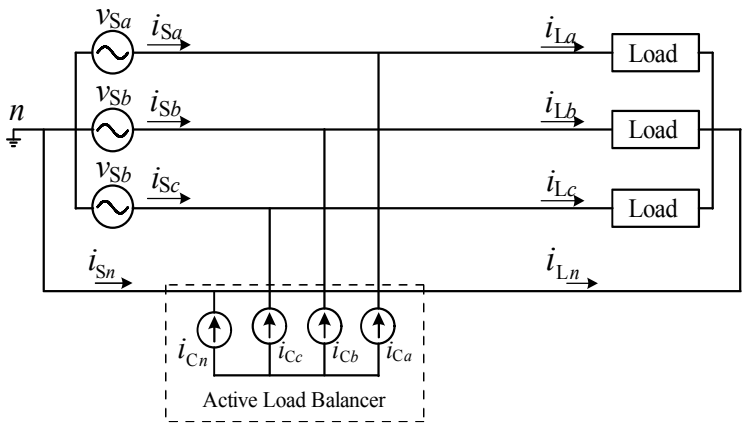

Figure 6.10: Equivalent circuit of the ALB in three-phase four-wire distribution systems.

Each leg of the ALB is represented by a current source. From the equivalent circuit, it is seen that the neutral-leg current should be included in the required power rating calculation of the ALB. The power rating of ALB S_C is given by

$$S_C = V_T(I_{Ca} + I_{Cb} + I_{Cc} + I_{Cn}). \tag{6.9}$$

where V_T is the rms line-to-neutral voltage and I_{Ca}, I_{Cb}, I_{Cc} and I_{Cn} are the rms compensation currents of the ALB. From (6.4) and (6.8), the rms compensation currents are given by

$$\begin{aligned}
I_{Ca} &= \left((I_a\cos\phi_a - I_P)^2 + (I_a\sin\phi_a - KI_P)^2\right)^{\frac{1}{2}} \\
I_{Cb} &= \left((I_b\cos\phi_b - I_P)^2 + (I_b\sin\phi_b - KI_P)^2\right)^{\frac{1}{2}} \\
I_{Cc} &= \left((I_c\cos\phi_c - I_P)^2 + (I_c\sin\phi_c - KI_P)^2\right)^{\frac{1}{2}} \\
I_{Cn} &= \Big(\big(-I_a\cos\phi_a + \frac{1}{2}I_b\cos\phi_b + \frac{\sqrt{3}}{2}I_b\sin\phi_b + \frac{1}{2}I_c\cos\phi_c - \\
&\quad \frac{\sqrt{3}}{2}I_c\sin\phi_c\big)^2 + \big(-I_a\sin\phi_a - \frac{\sqrt{3}}{2}I_b\cos\phi_b + \frac{1}{2}I_b\sin\phi_b + \\
&\quad \frac{\sqrt{3}}{2}I_c\cos\phi_c + \frac{1}{2}I_c\sin\phi_c\big)^2\Big)^{\frac{1}{2}}.
\end{aligned} \tag{6.10}$$

The first square terms in the right hand side of (6.10) are the compensation currents for the active components and the second square terms are the compensation currents for the reactive

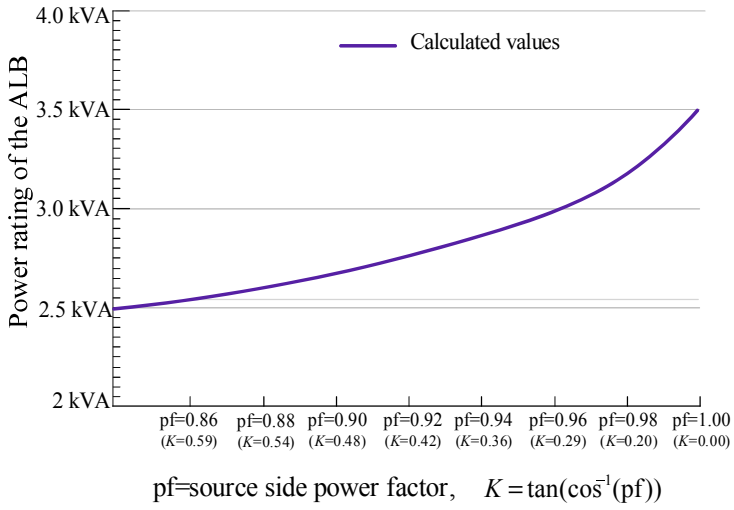

Figure 6.11: Relationship between power rating of the ALB, the value of K and source side power factor.

components. From (6.10), we can see that the amplitudes of I_{Ca}, I_{Cb} and I_{Cc} depend on value of K in the second square terms, which adjusts the amount of reactive compensation currents.

Fig. 6.11 shows the calculated results of the power rating of the ALB with various values of the source side power factors and K using the load condition in Table 6.2. The loads are 0.9 pu for a-phase, 0.5 pu for b-phase and 0.2 pu for c-phase in the 6 kVA transformer rating. The terminal voltage V_T of the transformer is 115 V in the calculation.

Fig. 6.12 shows a comparison of the experimental results using two source side power factors, 1.0 and 0.9, with the constant DC capacitor voltage control strategy and reactive power control strategy under the same load condition. Fig. 6.12(a) shows the experimental results with a unity power factor control. The compensation current flowing in each phase is I_{Ca} = 10.642 A, I_{Cb} = 6.113 A, I_{Cc} = 5.035 A and I_{Cn} = 8.712 A. Thus, the required power rating of the ALB is 3.5 kVA. Fig. 6.12(b) shows the experimental results with the power factor of 0.9. The compensation current flowing in each phase is I_{Ca} = 7.367 A, I_{Cb} = 2.356 A, I_{Cc} = 4.098 A and I_{Cn} = 8.970 A. The required power rating of the ALB is 2.6 kVA. Therefore, the proposed reactive power control strategy with power factor of 0.9 can reduce the required power rating of the ALB by 26% compared to the power rating obtained with the constant DC capacitor voltage control strategy.

Table 6.4. shows the required power rating of the ALB for the various source side power factors with the calculated results, simulation results and experimental results. The calculated

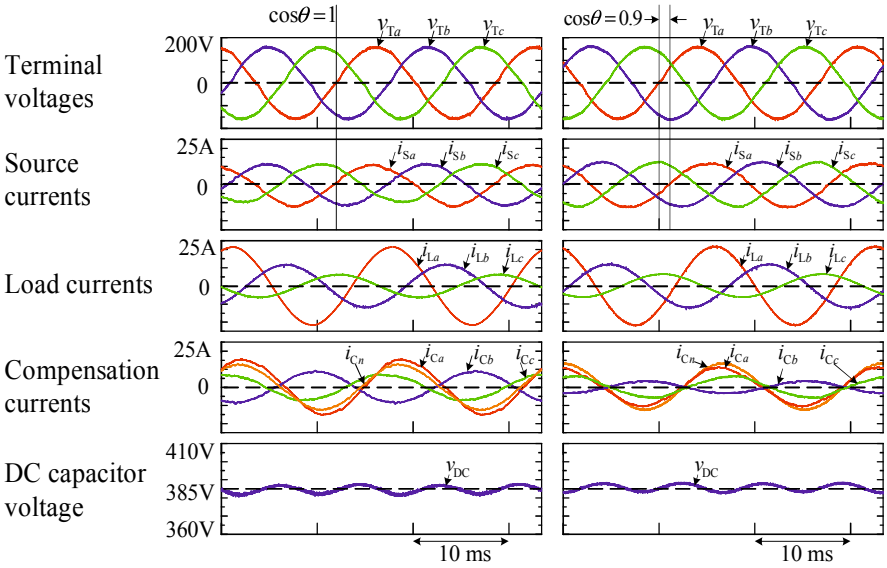

(a) Constant DC capacitor voltage control strategy for a unity power factor

(b) Reactive power control strategy for power factor of 0.9

Figure 6.12: Experimental waveforms of constant DC capacitor voltage control strategy for unity power factor and the reactive power control strategy with power factor of 0.9.

values well agree with the simulation results and the experimental results.

Table 6.4: Required power rating of the ALB with various source side power factors.

Source side power factor and (K)	Calculated power rating (kVA)	Simulation result (kVA)	Experimental result (kVA)
0.86 (K=0.59)	2.54 kVA	2.55 kVA	
0.88 (K=0.54)	2.59 kVA	2.59 kVA	
0.90 (K=0.48)	2.66 kVA	2.65 kVA	2.6 kVA
0.92 (K=0.42)	2.74 kVA	2.72 kVA	
0.94 (K=0.36)	2.83 kVA	2.81 kVA	
0.96 (K=0.29)	2.95 kVA	2.93 kVA	
0.98 (K=0.20)	3.11 kVA	3.10 kVA	
1.00 (K=0.00)	3.52 kVA	3.50 kVA	3.5 kVA
three-phase, 200 V, 60 Hz, 6 kVA distribution transformer base.			

6.6 Conclusion

In this chapter, the active load balancer with reactive power control strategy was discussed in three-phase four-wire distribution systems to reduce the power rating of the ALB. The proposed reactive power control strategy do not need any calculation blocks of the active and reactive of the load currents as in constant DC capacitor voltage control strategy in Chapter 5. However, the reference calculation method is different because the amount of reactive power for source side can be adjusted in this control strategy. The proposed reactive power control strategy is discussed in detail and then confirmed with simulation and experimental results. The relationships between the power rating of the ALB and the source side power factors, i.e., various amount of source side reactive power (the value of K) is theoretical analyzed. The simulation and experimental results well agree with the theoretical values. The theoretical values, the simulation and experimental results confirm that the constant DC capacitor voltage control strategy with a unity power factor requires 3.5 kVA capacity of the ALB, but the reactive power control strategy with power factor of 0.9 requires 2.6 kVA of the ALB in the 6 kVA distribution transformer rating. Therefore, the reactive power control strategy reduces the required power rating of the ALB by 26% compared to the power rating obtained with the constant DC capacitor voltage control. The proposed reactive power strategy for the ALB in three-phase four-wire distribuion system has been presented in IEEE energy conversion congress and expo and has been submitted and under revision in the Institute of Electrical Engineer of Japan (IEEJ) Journal of Industry Applications.

Chapter 7

Conclusions and Future Works

The electricity supply company generally try to limit energy losses in both transmission and distribution systems. The losses of transmission system between the power plant and the step-down substation should be within the range of 5%. The distribution system losses between the step-down substation and the consumer loads can be the same as in the transmission systems or even higher percentages in accordance with the international electrotechnical commission (IEC) [29]. Therefore, the distribution system losses takes an important part in the losses reduction of the power systems. The power quality of the distribution system and consumer load types greately affect on the losses of the distribution. Therefore, the utility try to improve the power quality by installing compensation devices, and limit the harmonic percentage and reactive power amount from the consumer.

7.1 Power Quality Problems and their Adverse Effects

This thesis deals with the power quality improving devices for the distribution level. The important of power quality improvement was discussed in the chapter 1. The standards, recommended practices, guidelines and requirements regarding the power quality improvement were presented for the economic operation of power system and greenhouse gas reduction. Then the power quality improving devices, passive power filters and power line conditioners, were reviewed with their advantages and drawbacks in chapter 1. The harmonic and three-phase unbalanced problems, which directly effect on the distribution equipments and the consumer loads, are described in chapter 2. The analysis methods, the adverse effects of harmonics and unbalanced condition were also discussed.

7.2 Active Power Quality Compensator in Electrified Railways

Chapter 3 discussed the power quality problems in electrified railways and reviewed the existing single-phase ALB for the electrified railways with the various power circuit topologies and different control designs. A half-bridge inverter based active power quality compensator (APQC), which is a single-phase active power line conditioner, for the electrified railways was proposed to reduce the power devices rating of third-leg in the three-leg based APQC topology. The new simple constant DC capacitor voltage control strategy with the DC voltage balancer was also discussed in detail in the chapter 4. The new control strategy can detect the active current by the constant DC capacitor voltage control and thus reduces the active current detection algorithm. Therefore, the execution time for the DSP is reduced using the simple constant DC capacitor voltage control strategy. Therefore, the proposed APQC topology and control strategy can reduce the size, weight, and cost of power conditioning devices.

7.3 Active Load Balancer in Three-Phase Four-Wire Distribution Feeders

In chapter 5, the world-wide distribution systems for the three-phase and single-phase consumer loads was introduced. Then the power quality problems of the three-phase four-wire distribution system was discussed. To solve the power quality problems, active load balancers (ALBs) were proposed in three-phase four-wire distribution feeders.

The power circuit topology of the various three-phase ALB with their compensation characteristic and various type of control strategies were examined for the three-phase four wire distribution systems. The instantaneous active, reactive power theory are widely used in the ALB control strategy for three-phase four-wire feeders. However, these control strategies require a significant amount of calculation steps because the active, reactive components are calculated from the instantaneous power. Therefore, a novel control strategy was proposed in the Chapter 5 to reduce active, reactive components calculation steps of the load currents. The proposed novel constant DC capacitor voltage control strategy was discussed in details using the power flow of the ALB. The simulation and experimental results confirm that the proposed novel control strat-

egy can operate the ALB without any active-reactive calculation blocks of the load currents in the control algorithm. Therefore a considerable amount of calculation steps are reduced in the ALB control strategy using our proposed method. In addition, the transformer loss of the distribution feeder with/without ALB are analyzed with experimental results. The results show that the transformer loss, which are caused by unbalanced and reactive components, can reduce using the ALB.

The relative power rating of the ALB with the distribution system is a key design factor, and therefore reduction of the ALB power rating is necessary in practical application. Reactive power control strategy based on DC capacitor voltage control was proposed to reduce the required power rating of the ALB in three-phase four-wire distribution systems in Chapter 6. The basic principle of reactive power control strategy was discussed in detail. The proposed reactive power control strategy is simple and does not require active, reactive components calculation blocks because it is also based on the DC capacitor voltage control. The validity of the proposed reactive power control strategy was confirmed by simulation and experiment. The relationship between the power rating of the ALB and various source side reactive power amounts (the various power factors of source side) is analyzed theoretically. The theoretical values, simulation and experimental results show that controlling the source-side reactive power with power factor of 0.9 can reduce the ALB power rating by 26% compared to that obtained with the constant DC capacitor voltage control with unity power factor. Therefore, this dissertation contributes the size and cost reduction of the practical ALB in three-phase four-wire distribution feeders.

7.4 Future Works

The active power filters for electrified railways and three-phase four-wire distribution systems were discussed in this dissertation. The ALB for three-phase four wire distribution system was verified under linear unbalanced load condition with the proposed control strategies. However, the real loads may contain harmonics in the distribution systems. Therefore, the proposed control strategies should be confirmed under non-linear loads conditions in the future. The loss analysis of distribution transformer was performed with experimental model. But the loss reduction in distribution lines and efficiency improvement of consumer loads were not performed with the

ALB operation in this dissertation. The overall improvement of distribution systems provided by the ALB should be studied in the future.

References

[1] J. Manson and R. Targosz (2008, November) *European power quality survey report* [Online]. Available: http://www.leonardo-energy.org/sites/leonardo-energy/files/root/pdf/2009/PQSurvey.pdf

[2] Standard of the Japanese Electrotechnical Committee, JEC-2200-1995, Dec. 1995.

[3] IEEE 519-1992, "Recommended Practices and Requirements for Harmonic Control in Electrical Power System,"1992.

[4] Y. Mochinaga, T. Uzuka, S. Hase, Y. Hisamizu, and Y. Ishizeki, "Development of Single Phase Feeding Power Conditioner for Shinkansen," *IEEJ Trans. on PE*, Vol. 120, No. 8/9, pp. 1084–1090, 2000. (in Japanese)

[5] Zhuo Sun, Xinjian Jiang, Dongqi Zhu, and Guixin Zhang, "A Novel Power Quality Compensator Topology for Electrified Railway," *IEEE Trans. on PE*, vol. 19, No. 4, pp. 1036-1042, July 2004.

[6] N. Ishikura, E. Hiraki, and T. Tanaka, "A Constant DC Voltage Control Based Strategy for an Active Power Quality Compensator in Electrified Railways with Improved Response, " *Conference of the IEEE Industrial Electronics Society*, PD-0008931, pp. 3199–3204, November 2008.

[7] H. Akagi, Y. Kanazawa,and A. Nabe, "Instantaneous reactive power compensators comprising switching devices without energy storage components, " *IEEE Trans. Ind. Appl.,* Vol. IA-20, No. 3 May/June 1984.

[8] F.Z. Peng, George W. Ott, Jr., and Donald J. Adams, "Harmonic and reactive power compensation based on the generalized instantaneous reactive power theory for three-phase four-wire systems, " *IEEE Trans. on Power Electron.,* Vol. 13, No. 6, November 1998.

[9] A. Nava-Segura and G. Mino-Aguilar, “Four-branches-inverter-based-active-filter for unbalanced 3-phase 4-wires electrical distribution systems ” *Proc. of IEEE Ind. Appl. Conf.,* Vol. 4, pp. 2503-2508, October 2000.

[10] A. Adya, A.P. Mittal, and J.R.P Gupta, “Modeling and control of DSTATCOM for three-phase, four-wire distribution systems ” *IEEE-IAS Ann. Meeting,* Vol. 4, pp. 2428-2434, October 2005.

[11] N. Geddada, S.B. Karanki, M.K. Mishra, and B.K. Kumar, “Modified four leg DSTATCOM topology for compensation of unbalanced and nonlinear loads in three phase four wire system, ” *Proc. of EPE’11,* pp. 1-10, September 2011.

[12] L.W. Dixon, J.J. Garcia, and L. Moran, “Control system for three-phase active power filter which simultaneously compensates power factor and unbalanced loads, ” *IEEE Trans. Ind. Electron.,* Vol. 42, pp. 636-641, December 1995.

[13] Energy Networks Association, ”Engineering Recommendation P29, Planning Limits for Voltage Unbalanced in the United Kingdom”, 1990.

[14] National Electrical Manufacturers Association (NEMA), ”NEMA Standards Publication MG 1-1998 (Revision 3, 2002) Interfiled Motors and Generators”, 1998.

[15] D. Rivas, L. Moran, J. Dixon, and J. Espinoza, “Improving passive filter compensation performance with active techniques, ”*IEEE Proc. Ninth Int. Conf. on Harmonics and Quality of Power* Vol. 1, 232-238, October 2000.

[16] H. Akagi, “Modern active filters and traditional passive filters, ”*Bulletin of the polish academy of science, technical science.* Vol.54, pp. 255-269, 2006.

[17] B.M. Bird, J.F. Marsh, and P.R. McLellan, “Harmonic reduction in multiple converters by triple-frequency current injection, ”*IEEE Proc.* 116(10), 1730-1734, 1969.

[18] H. Sasaki and T. Machida, “A new method to eliminate ac harmonic currents by magnetic compensation - considerations on basic design, ”*IEEE Trans. Power Appl. Syst.* 90(5), 2009-2019, 1971.

[19] A. Ametani, “Harmonic reduction in thyristor converters by harmonic current injection, ”*IEEE Trans. Power Appl. Syst.* 95(2), 441-449, 1976.

[20] H. Fujita and H. Akagi, “The unified power quality conditioner: The integration of series active filters and shunt active filters, ”*IEEE 27th Power Electron. Specialists Conf.* Vol.1, pp. 494-501, June 1996.

[21] Electric Railway Handbook 2007, CORONA PUBLISHING CO.,LTD (in Japanese).

[22] Journal of the Eastern Asia Society for Transportation Studies, *V*ol. 6, pp. 277-291, 2005.

[23] Martin J. Heathcote, “Special features of transformers for particular purposes”, *The J&P Transformer Handbook*, 13th Ed. Elsevier, pp. 743-745, 2007.

[24] Depenbrock, M., “The FBD-Method, a Generally Applicable Tool for Analyzing Power Relations, ” *IEEE Trans. on Power Syst.*, Vol. 8, No. 3, pp. 381-386, May 1993.

[25] L. N. Arruda, S. M. Silva, and B. J. C. Filho, “PLL Structure for Utility Connected Systems,” *in Conference Record of the* 36^{th} *IEEE-IAS Annual Meeting*, pp. 2655-2660, 2001.

[26] S.M. Silva, B.M. Lopes, B.J.C. Filho, R.P. Campana, W.C. Boaventura, “Performance Evaluation of PLL Algorithms for Single-phase Grid-connected Systems, ” *IEEE Industry Applications Society Annual Meeting,* pp. 2259-2263, October, 2004.

[27] F. S. Zhang,“Control of single phase power converter in D-Q rotating coordinates,” U.S Patent 6 621 252 B2, September, 2003.

[28] Japan Electric Association, Indoor Wiring Guidelines, JESC E0005, p. 32, 2005 (in Japanese).

[29] International electrotechnical commission (IEC 2007) *Efficient electrical energy transmission and distribution* [Online]. Available: http://www.iec.ch/about/brochures/pdf/technology/transmission.pdf

Papers published by author

Journal Papers

[1] Tint Soe Win, Y. Baba, M. Okamoto and E. Hiraki, and T. Tanaka, "A Half-bridge inverter based active power quality compensator for electrified railways", *Journal of the Japan Institute of Power Electronics* Vol.37, pp. 146-152, March 2012.

[2] Tint Soe Win, E. Hiraki, and T. Tanaka, "A novel active power quality compensator topology with DC voltage balancer for electrified railways", *IEEJ Trans. Electrical and Electronic Engineering* Vol. 8, Issue 6, pp. 634-639, 2013.

[3] Tint Soe Win, Toshihiko Tanaka, Eiji Hiraki and Masayuki Okamoto, and Seong Ryong Lee, "Constant DC capacitor voltage control based strategy for active load balancer in three-phase four-wire distribution systems", *J. of Int. Conf. on Elect. Mach. and Syst.* Vol. 3, No. 6, pp. 176-183, 2014.

[4] Tint Soe Win, Eiji Hiraki and Masayuki Okamoto, and Seong Ryong Lee and Toshihiko Tanaka, "Novel control algorithm for active load balancer in three-phase four-wire distribution systems", *IEEJ Journal of Industry Application* Vol. 3, No. 3, pp. 286-287, 2014.

[5] Tint Soe Win, Yoshihiro Hisada, Toshihiko Tanaka, Eiji Hiraki, Masayuki Okamoto and Seong Ryong Lee, "Reactive power control strategy based on DC capacitor voltage control for active load balancer in three-phase four-wire distribution systems", *IEEJ Journal of Industry Application* (Accepted).

International Conference Papers

[6] Tint Soe Win, Yusuke Baba, Masayuki Okamoto, Eiji Hiraki and Toshihiko Tanaka, "A half-bridge inverter based active power quality compensator with a DC voltage balancer for electrified railways", *Conf. Rec. IEEE-PEDS* pp. 185-190, December 2011.

[7] Tint Soe Win, Yusuke Baba, Eiji Hiraki, Toshihiko Tanaka and Masayuki Okamoto, “A half-bridge inverter based active power quality compensator using a constant DC capacitor voltage control for electrified railways”, *Conf. Rec. IEEE-IPEMC ECCE Asia* pp. 314-320, June 2012.

[8] Tint Soe Win, Eiji Hiraki, Masayuki Okamoto, Seong Ryong Lee and Toshihiko Tanaka, “Constant DC capacitor voltage control based strategy for active load balancer in three-phase four-wire distribution systems”, *Conf. Rec. IEEE-ICEMS* pp. 1560-1565, October 2013.

[9] Tint Soe Win, Yoshihiro Hisada, Toshihiko Tanaka, Eiji Hiraki, Masayuki Okamoto and Seong Ryong Lee, “Reactive power control strategy based on DC capacitor voltage control for active load balancer in three-phase four-wire distribution systems”, *Conf. Rec. IEEE-IPEC ECCE Asia* pp. 3292-3297, May 2014.

[10] Tint Soe Win, Yoshihiro Hisada, Toshihiko Tanaka, Eiji Hiraki, Masayuki Okamoto and Seong Ryong Lee, “Novel simple reactive power control strategy with DC capacitor voltage control for active load balancer in three-phase four-wire distribution systems”, *Conf. Rec. ECCE2014* pp. 3916-3921, September 2014.

[11] Yoshihiro Hisada, Tint Soe Win, Toshihiko Tanaka, Eiji Hiraki, Masayuki Okamoto and Seong Ryong Lee, “Active Load Balancer on Three-phase Four-wire Distribution System with Constant DC Capacitor Voltage Control for Multiple Loads”, *IEEE PEAC2014* pp. 782-787, November 2014.

Other Conference Papers

[12] Tint Soe Win, Eiji Hiraki, Masayuki Okamoto, Seong Ryong Lee and Toshihiko Tanaka, “Novel control algorithm for active load balancer in three-phase four-wire distribution systems”, *Proc. IEEJ Industry Application Conf.* pp. I225-I228, August 2013.

[13] Tint Soe Win, Yoshihiro Hisada, Toshihiko Tanaka, Eiji Hiraki, Masayuki Okamoto and

Seong Ryong Lee, “Novel reactive power control strategy for active load balancer in three-phase four-wire distribution systems”, *Rec. IEEJ Annu. meeting* pp. 260-261, March 2014.

[14] Tint Soe Win, Yoshihiro Hisada, Toshihiko Tanaka, Eiji Hiraki, Masayuki Okamoto and Seong Ryong Lee, “Reactive power control strategy under different source-side power factor for active load balancer in three-phase four-wire distribution systems”, *Rec. 65th Chugoku-brunch join convention 2014* pp. 388-389, October 2014.

[15] Yoshihiro Hisada, Tint Soe Win, Toshihiko Tanaka, Eiji Hiraki, Masayuki Okamoto and Seong Ryong Lee, “Ampere capacity of active load balancer in three-phase four-wire distribution systems”, *Rec. IEEJ Annu. meeting* pp. 240, March 2014 (in Japanese).

[16] Yoshihiro Hisada, Tint Soe Win, Hiroaki Yamada, Toshihiko Tanaka, Masayuki Okamoto and Seong Ryong Lee, “An active load balancer on three-phase four-wire distribution systems with constant DC capacitor voltage control for multiple loads”, *Proc. IEEJ Industry Application Conf.* pp. 90-89, August 2014 (in Japanese).